The *Myo*-inositol Biosynthesis Pathway and its Regulation by NFAT5 in Tilapia Salinity Tolerance Assessed by Genetic Manipulation of Cultured Cells

By

JENS HAMAR

DISSERTATION

Submitted in partial satisfaction of the requirements for the degree of

DOCTORATE OF PHILOSOPHY

in

Animal Biology

in the

OFFICE OF GRADUATE STUDIES

of the

UNIVERSITY OF CALIFORNIA

DAVIS

Approved:

Dietmar Kültz, Chair

Elizabeth Maga

Esteban Soto Martinez

Committee in Charge

2024

Acknowledgements

I would like to thank my PI, Dr. Dietmar Kültz, for ongoing mentorship and granting me the opportunity to pursue my academic interests and develop my scientific expertise. I would like to thank my other committee members, Dr. Elizabeth Maga and Dr. Esteban Soto Martinez, for their willingness to oversee this dissertation, guidance, and time. I want to extend my appreciation to several of my lab members; John Li, Leah MacNiven, and Tracy Le for not only their technical assistance in laboratory projects but also friendship and mental support during this challenge. I am also grateful to my family for their mental and financial support when times were hard. Last but not least, I extend my gratitude to the National Science Foundation (Grants IOS-1656371 and IOS- 2209383) and the US-Israel Binational Agricultural Research and Development Fund (Grants IS-4800-15 R and IS-5358-21) who's funding has made this dissertation project and my graduate student career possible.

Abstract

The constantly changing physical world subjects its inhabitants to variable abiotic conditions. Organisms function optimally within a range of abiotic parameters. Extreme divergence form that range due to conditions such as salinity fluctuations in some aquatic environments, imposes strain on their physiological systems such as hyper-osmotic (HO) stress. Persistence in such an environment is restricted to species capable of the necessary adaptive responses. The economically important Mozambique tilapia (*Oreochromis mossambicus*) is such a species, making it an ideal model for studying salinity stress tolerance. Previous work showed increased abundances of the myo-inositol biosynthesis (MIB) pathway enzymes myo-inositol phosphate synthase (MIPS) and inositol monophosphatase 1 (IMPA1.1) in tissues of *O. mossambicus* subjected to elevated salinity. Previous work also suggested an involvement of the transcription factor NFAT5 (nuclear factor of activated T-cells 5) in the osmotic regulation of the MIB pathway. However, the causality of these relationships with salinity tolerance phenotypes had yet to be established. The objective of this research was to test the overall hypothesis that upregulation of the MIB pathway enzymes contributes to salinity tolerance and is mediated by NFAT5 using CRISPR/Cas9 gene editing and synthetic biology approaches in a simplified but representative tilapia cell line model (OmB) to manipulate the genetic loci encoding these proteins.

Initial CRISPR/Cas9 editing attempts utilizing gRNA/Cas9 protein complexes and expression vectors optimized for zebrafish or mammalian cells failed to yield detectable gene edits. Therefore, a system customized for tilapia cells was developed using endogenous *O. mossambicus* EF1 alpha and U6 promoters to drive Cas9 and gRNA expression respectively. A version of the OmB cell line (Cas9-OmB1) was engineered to express the Cas9 protein by transposon mediated genomic integration of the Cas9 gene while different gRNAs are produced transiently by a plasmid vector with hygromycin resistance. Hygromycin selected Cas9-OmB1 cells transfected with this vector displayed high gene editing frequency(up to 81%). Substitution of the previously used U6 promoters into the new system yielded

negligible mutation frequency, thereby identifying heterologous U6 promoters as the primary cause for lack of gene edits in initial attempts.

This CRISPR/Cas9 system was then used to generate three knock-out (KO) clonal cell lines for MIPS, IMPA1.1, NFAT5 and a non-essential gene group as controls for any deleterious side effects of the gene editing and cell selection process. Measurement of metabolic activity and growth/survival of MIB KO and control cell lines exposed to both HO and basal iso-osmotic (IO) conditions were performed over a 288 hour period. The results show increased growth rates of both MIPS and IMPA1.1 KO lines over the control cells in basal IO conditions but decreased survival (although not significant) in HO conditions.

HO challenge of the NFAT5 KO and control lines followed by qRT-PCR targeting MIB enzyme transcripts showed a notable reduction of HO induced transcriptional upregulation in both IMPA1.1 (37-49%) and MIPS (6-37%). In wild-type (WT) OmB cells, co-transfection with vectors expressing dominant negative (DN) and WT versions of tilapia NFAT5 and a GFP reporter vector driven by the IMPA1.1 promoter caused statistically significant changes of reporter activity. Reporter activity was increased 5.1 fold by WT NFAT5 in basal iso-osmotic (IO) conditions and reduced ~45% by DN NFAT5 in HO conditions. These results provide evidence for an interaction between this transcription factor and the IMPA1.1 promoter regulatory elements.

In conclusion, a novel DNA vector-based CRISPR/Cas9 delivery platform can achieve high mutation rates when component expression is driven by tilapia endogenous promoters allowing proficient development of target gene KO cell lines. Inactivating the MIB pathway has moderate impact on survival of HO challenged OmB cells but has a growth promoting regulatory effect in IO conditions. We conclude that NFAT5 is an osmotic transcriptional regulator of the tilapia MIB pathway that is responsible for approximately 50% of IMPA1.1 and <37% of MIPS induction under the hyperosmotic stress conditions applied in this study.

Table of Contents

General Introduction

The focus of this dissertation is the cellular responses to hyper-osmotic (HO) stress in euryhaline fishes using a cell line model from the Mozambique tilapia (*Oreochromis mossambicus*). This is an economically important animal as *Oreochromis* species are some of the most widely used animals in aquaculture worldwide. *O.Oreochromis niloticus* is the predominant tilapia species used over other tilapia due to its superior growth rate and feed conversion characteristics. However, this species has only moderate salinity tolerance and thus the geographical range in which it can be cultured is limited by the availability of fresh water. Hyper salinization of ground and surface waters by anthropogenic and natural causes such as agricultural runoff, drought, or encroaching tidal influences by rising sea levels will make the freshwater resource even more limiting with time. For these reasons, increased salinity tolerance is a highly desirable trait in aquaculture stocks.

Elevated salinity imparts hyper-osmotic stress HO on an aquatic animal's cells and tissues through desiccation and excessive influx of ions. Systemic mechanisms integrate sensing of HO stress by the animal with signaling pathways (endocrine and paracrine) and specialized effector organs and tissues. In combination, the system works to maintain a relatively constant osmolality of the extracellular body fluids (ECF). Despite these mechanisms, in extreme salinities or during acute exposure to elevated salinity, the plasma and ECF osmolality rises significantly. This condition exposes internal cells to HO stress, which disturbs intracellular fluid (ICF) osmotic and ionic homeostasis, necessitating a compensatory cellular response. This cellular level of HO stress response must also be understood in attempts to discern whole animal salinity tolerance.

O. mossambicus is ideal to study these mechanisms as it is capable of tolerating an extreme range of osmotic environments from freshwater to salinities over three times that of seawater. Additionally, due to its close genetic relation to *O. niloticus*, findings in *O. mossambicus* are highly applicable to *O.*

niloticus and important genetic elements from *O.mossambicus* can be readily transferred into *O. niloticus* by the ability of the two species to interbreed.

Work in our lab and others show up-regulation and activation of effector proteins in tissues and cell cultures of tilapia and cells exposed to HO conditions. In *O. mossambicus*, among the highest of these include enzymes of the *myo*-inositol biosynthesis (MIB) pathway, *myo*-inositol phosphate synthase (MIPS) and inositol monophosphatase 1 (IMPA1.1) indicating the high importance of this pathway in HO stress response. This pattern is paralleled in an *O. mossambicus* brain fibroblast cell line (OmB) which can persist in salinity over double basal media levels, demonstrating its' utility as a representative model for these studies.

Of equal importance to effector protein abundance changes for HO stress response are the signaling networks that perceive the stress and regulate the changes. Investigation of *O. mossambicus* MIPS and IMPA1.1 promoter regions identified enhancer elements resembling the binding sequence of nuclear factor of activated T-cell (NFAT) transcription factors as responsible for the majority of transcriptional activation of these genes. The reputation of NFAT5 as the primary HO response transcription factor in mammals and that NFAT5 mRNA abundance increases in cells of HO challenged fish supports this transcription factor as a prominent regulator of the MIB pathway.

Despite the strong correlation of MIPS, IMPA1.1, and NFAT5 with HO stress treatment, causal relationships between these molecular changes and observed HO stress tolerance phenotypes of euryhaline fish cells have yet to be established. Gene knock-out (KO) is an effective strategy to evaluate causality between gene products and specific phenotypes. This has become a more accessible approach with the rise of CRISPR/Cas9 gene editing technology with successful platforms developed for multiple vertebrate cell lines, including initial progress in cultured fish cells.

In deciphering gene functions, genetic manipulation of cell culture models are an attractive alternative to genetically modified whole animals where applicable. Advantages of cell culture models include: isolation from systemic influence in studies of cellular mechanisms, reduction of animal welfare concerns, more cost effective maintenance, genetic manipulations are higher throughput, and reduction of the potential for expanded invasiveness into marine environment by accidental escape of genetically enhanced animals.

The objective of this dissertation project is to further characterize mechanisms of euryhaline fish salinity tolerance, specifically using molecular manipulations (predominantly CRISPR/Cas9 gene editing) and the *O. mossamicus* OmB cell line model to test the overall hypothesis that: **Upregulation of MIPS and IMPA1.1 is necessary for full wild-type hyper-osmotic stress tolerance at the cellular level, and their HO induced expression is regulated by NFAT5**. This objective was pursued through three primary aims: Aim 1) to develop a CRISPR/Cas9 system capable of generating gene KO versions of the OmB cell line for MIPS, IMPA1.1, and NFAT5; Aim 2) to perform assays quantifying physiological performance of MIPS and IMPA1.1 KO lines under HO challenge; and Aim 3) perform assays quantifying HO induced transcriptional regulation of *MIPS* and *IMPA1.1* genes by NFAT5 using NFAT5 KO lines and other synthetic biology techniques.

This chapter was published in *Scientific Reports* journal in April, 2021 (Volume 11, Article # 7854)

Aim 1: An Efficient Vector-based CRISPR/Cas9 System in an *Oreochromis mossambicus* Cell Line using Endogenous Promoters

Jens Hamar & Dietmar Kültz

Biochemical Evolution Laboratory, Department of Animal Science, University of California, Davis, CA 95616, USA. * email: dkueltz@ucdavis.edu

Abstract

CRISPR/Cas9 gene editing is effective in manipulating genetic loci in mammalian cell cultures and whole fish but efficient platforms applicable to fish cell lines are currently limited. Our initial attempts to employ this technology in fish cell lines using heterologous promoters or a ribonucleoprotein approach failed to indicate genomic alteration at targeted sites in a tilapia brain cell line (OmB). For potential use in a DNA vector approach, endogenous tilapia beta Actin (OmbAct), EF1 alpha (OmEF1a), and U6 (TU6) promoters were isolated. The strongest candidate promoter determined by EGFP reporter assay, OmEF1a, was used to drive constitutive Cas9 expression in a modified OmB cell line (Cas9-OmB1). Cas9-OmB1 cell transfection with vectors expressing gRNAs driven by the TU6 promoter achieved mutational efficiencies as high as 81% following hygromycin selection. Mutations were not detected using human and zebrafish U6 promoters demonstrating the phylogenetic proximity of U6 promoters as critical when used for gRNA expression. Sequence alteration to TU6 improved mutation rate and cloning efficiency. In conclusion, we report new tools for ectopic expression and a highly efficient, economical system for manipulation of genomic loci and evaluation of their causal relationship with adaptive cellular phenotypes by CRISPR/Cas9 gene editing in fish cells.

Introduction

Use of fish in physiology studies is widespread with purposes ranging from production enhancement of economically important species to models of basic vertebrate biology. Many of these studies have expanded into the use of cell cultures and there are now many fish cell lines available derived from various species and tissues[1,2], including an *Oreochromis mossambicus* brain cell line (OmB) generated in our lab[3]. Cell cultures have been used as early as 1910[4] as a simplified model to study molecular mechanisms and have been key in many important biological and medical discoveries since then[5–7]. Their use has many advantages including the ability to isolate cells from the influence of systemic factors such as hormones, facilitated control over the extracellular environment, proficient manipulation of intracellular systems through transfection of ectopic molecules (i.e. DNA, RNA, protein), minimization of genetic heterogeneity, and reduction in the costs and ethical concerns associated with the use of whole animals.

Targeted genetic manipulation of cell cultures has been an effective tool in deciphering specific functions of cellular components, which is enabled by applying CRISPR/Cas9 gene editing systems to cell culture models[8,9]. Compared to other gene targeting methods such as TALENS or zinc fingers that require complex assembly of many DNA binding domain coding sequences into a vector[10,11], the Cas9 nuclease can be directed to a specific locus of the genome by merely changing the 5' terminal ~20 bp of a 90 bp RNA molecule (guide RNA or gRNA) to be complementary to the target region adjacent to a genomic NGG Protospacer Adjacent Motif (PAM) sequence[12].

Utilization of this powerful tool has great potential to benefit cost-efficient and high-throughput mechanistic studies in fish cell lines. Implementation of CRISPR/Cas9 has been achieved in mammalian cell lines and in fish embryos, with consistent success in a wide variety of species such as zebrafish[13–16], medaka[17], killifish, carp[18], salmon[19], anchovy[20],catfish[21], and the economically important *Oreochromis*

species[22]. Methods for CRISPR/Cas9 gene editing in some fish cell lines have been pioneered[23,24] but only reported for a few lines and taxa so far. The methods employed with fish embryos utilized microinjection of either RNA or gRNA/Cas9 protein ribonucleoprotein (RNP) complexes. Microinjection is a suitable technique for the large cell size of the egg but not practical for high through-put application in cultured cells. A corresponding CRISPR/Cas9 system that works reliably and can be adopted in a high-throughput manner to enable efficient testing of causal relationships between many targets identified in systems biology approaches (transcriptomics or proteomics) and specific environmental contexts would be an invaluable complement to its use in fish embryos.

Using OmB cells, multiple attempts using DNA expression vector CRISPR/Cas9 delivery methods were made in our laboratory, all of which failed to yield evidence of sequence alteration at the targeted sites. Although no edits were observed, this work demonstrated efficient transfection of these constructs by using selectable markers and the ability to isolate transfected cells by growth on selective media. Consequently, we suspected that failure to observe CRISPR/Cas9 cleavage by this method was due to insufficient expression of the Cas9 enzyme by the polymerase II promoter, insufficient gRNA expression by the polymerase III U6 promoter, or both. These attempts used either the mammalian or zebrafish promoters for Cas9 and gRNA expression. However, Tilapia (percomorpha), are phylogenetically distant from zebrafish (otomorpha) and tetrapod vertebrates (tetrapodamorpha)[25–27], which may render the aforementioned promoters ineffective in cells derived from tilapia and other distantly related species.

Consequently, subsequent attempts should be precluded by evaluation of a set of known strong promoters including conventionally available viral and composite promoters, and multiple endogenous promoters known to be among the most efficient within their respective systems such as beta-Actin and elongation factor 1 (EF1) alpha. Other potential improvements that can be employed to increase editing efficiency in a vector-based system is constitutive expression of Cas9 and selectable marker systems built into the DNA vector. Constitutive Cas9 expression through genomic integration allows time for

accumulation and nuclear localization of Cas9 in addition to significantly reducing the vector size for subsequent transfection of the gRNA expressing constructs and permits testing many targets in a highly efficient manner. Selection systems allow for enrichment of cells that have at least obtained and are expressing the vector increasing the likelihood of isolating cells with targeted gene edits.

Another means to circumvent poor expression is to transfect cells directly with gRNA/Cas9 ribonucleoprotein complexes (RNPs). This approach can achieve high editing efficiency in cultured cells without relying on cellular mechanisms to recognize and produce the required CRISPR/Cas9 components from ectopic encoding molecules (ie DNA or RNA)[28].

In this work we sought to establish a highly efficient, high-throughput, and economical CRISPR/Cas9 gene editing system for the OmB cell line by testing direct transfection of gRNA/Cas9 RNPs and optimizing critical aspects of a DNA vector delivery approach.

Results

Lipid-based transfection of in vitro validated RNPs did not yield detectable gene edits in OmB cells

We chose the inositol monophosphatase 1.1 (*IMPA1.1*) gene as the target for optimization of gRNAs by *in vitro* cleavage assay. Of ten targets (T) within or adjacent to exons of the *IMPA1.1* coding sequence (Fig. 1a, b & c) screened by an *in vitro* cleavage assay, four targets (T1, T3, T7, and T10) showed the most thorough cleavage of the 1392 bp test amplicon containing all targets (Fig. 1d). Transfection of Cas9/gRNA RNPs using these targets was performed on wild-type OmB cells using a lipid-based transfection system specifically designed for delivery of Cas9/gRNA RNPs. PCR amplification of a 1392 bp amplicon containing the targeted region was performed on DNA harvested five days post transfection. Restriction site mutation (RSM) analysis, in which the occurrence of gene editing is

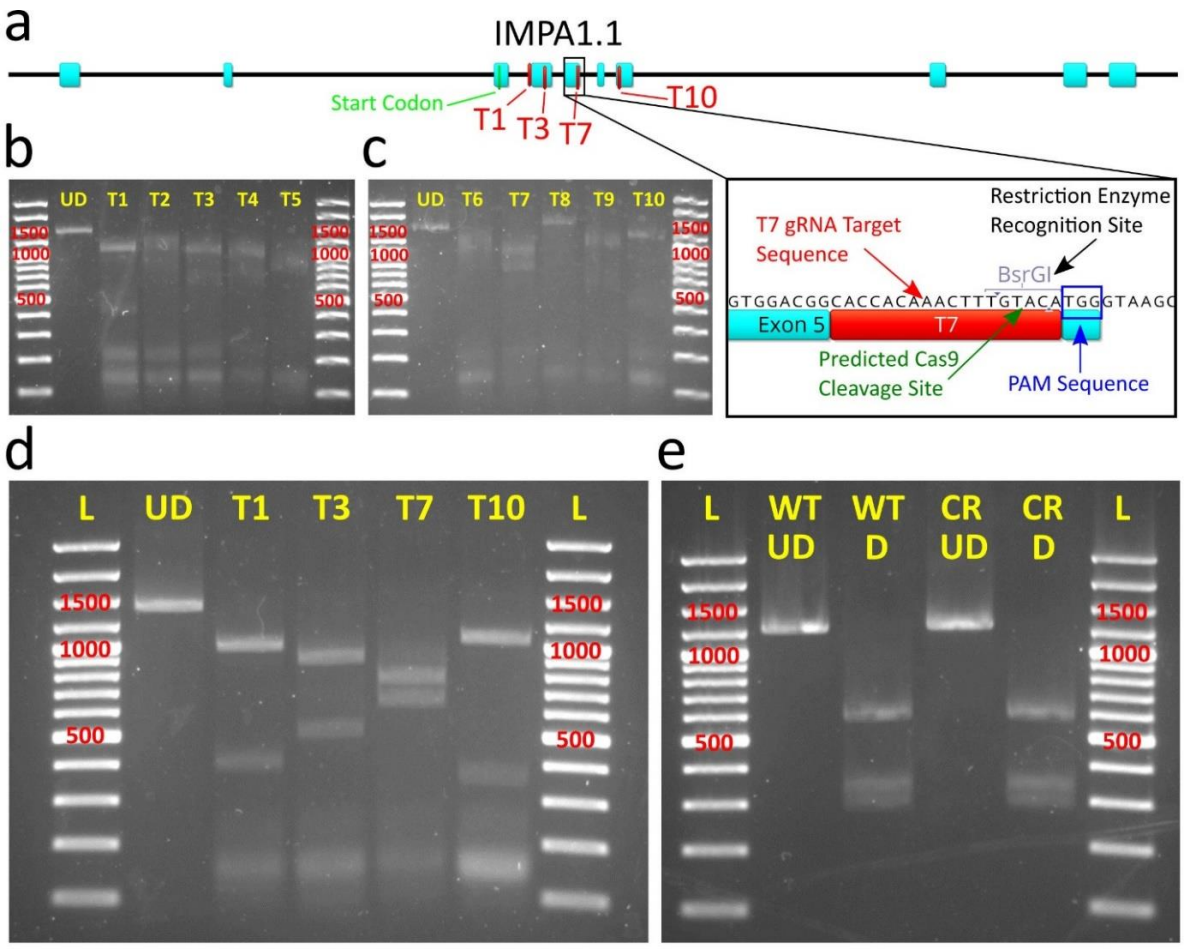

Figure 1. In vitro cleavage assay and OmB cell line gene targeting of *IMPA1.1* using Cas9/gRNA RNPs. (**a**) Gene map of Oreochromis *IMPA1.1* showing selected gRNA target sites and expanded view of T7 site containing BsrGI restriction site used for analysis of Cas9 cleavage. (**b-e**) Agarose gel images of with marker sizes (base pairs or bp) labeled in red (**b &c**) initial *in vitro* cleavage assay screen of ten target sites (T1-T10) and reference un-digested substrate amplicon (UD); (**d**) Follow up confirmatory *in vitro* cleavage assay results of the apparent most efficient cleaving gRNAs from the initial screen showing complete cleavage of substrate amplicon into expected fragments and (**e**) RSM analysis in which the BsrGI digested amplicon from *IMPA1.1* T7 CRISPR treated cells (CR D) shows the exact same band pattern as the BsrGI digested wild-type amplicon (WT D) indicating no detectable mutation at the target site. The un-digested amplicons were included for reference (WT UD = wild-type un-digested, CR UD = CRISPR treated un-digested). The gel images in this figure have been significantly cropped to conserve space and increase focus on relevant bands. Full-length gels are presented in Supplementary Figure S1. Gene map and sequence images were generated using Geneious 11.0.3 (Biomatters, https://www.geneious.com). Image editing and assembly into complete figures was performed using Inkscape 0.92 (https://www.inkscape.org).

evaluated by whether or not a restriction site overlapping with the potential Cas9 cleavage site is still able to be cleaved by the corresponding restriction enzyme, of the T7 amplicon was performed with BsrGI (Fig. 1e). RSM of the T7 treatment amplicon digested thoroughly by BsrGI yielded the identicalexpected band pattern (748 bp, 343 bp, and 301 bp) as the equivalent amplicon from control cells (Fig. 1e) indicating complete BsrGI digestion and lack of CRISPR induced mutation of the BsrGI restriction site. All target sequences and primers used for PCR amplification of test amplicons in the RNP experiments are listed in Supplementary Table S1.

Endogenous O. mossambicus promoters show greatest potential for maximal Cas9 expression in OmB cells

To maximize Cas9 expression from a DNA expression construct we cloned and screened a set of candidate Polymerase II promoters with documented strong expression in some fish or other vertebrate cells. These promoters include CAG (hybrid promoter consisting of CMV enhancer, chicken beta-Actin promoter, and rabbit beta-Globin intron), CMV (cytomegalovirus), SV40 (simian vacuolating virus 40), and the zebrafish *ubi* promoter[29] (Z*ubi*). Moreover, two *O. mossambicus* endogenous promoters, Beta-Actin (OmBAct) and EF1 alpha (OmEF1a) were cloned by PCR of genomic DNA (Fig. 2a) and sequenced (GenBank accession nos. MT791223 and MT791222 respectively). Expression strength of each promoter was compared by quantitation of relative enhanced green fluorescent protein (EGFP) fluorescent intensity (Fig. 2b) of cells transiently transfected with EGFP expression constructs driven by each of the promoters (n = 2 per promoter, SE = 2.1e+07, $\alpha = 0.05$). The *O. mossambicus* endogenous promoters showed the highest fluorescent intensity per cell with OmEF1a being significantly greater than CAG (>twofold, $p = 0.0485$) and SV40 (six-fold, $p = 0.0077$ respectively). Although not significant, the OmEF1a promoter gave higher fluorescence than the OmBAct promoter (1.53e+08 vs 1.50e+08). Qualitative visual assessment of the images was consistent with the quantitative data (Fig. 2c). Additionally, due to

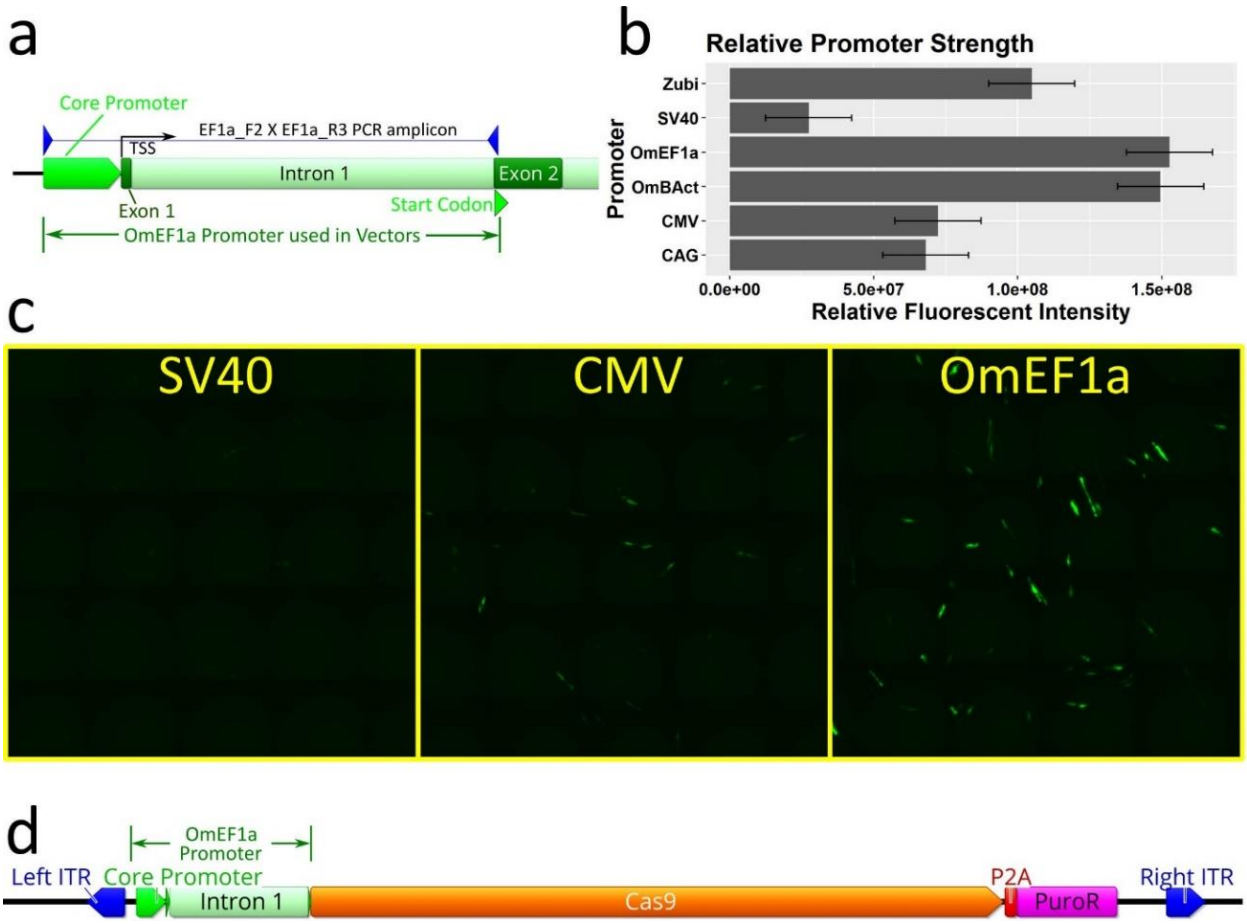

Figure 2. Isolation and selection of Polymerase II promoter for Cas9 expression in transposon plasmid vector. (**a**) PCR isolation of *O. mossambicus* endogenous promoters illustrated for EF1 alpha. The PCR amplicon spans ~150 bp upstream of the transcription start site, exon 1, intron 1, and part of exon 2 to the endogenous start codon. (**b**) Comparison of relative expression strength of candidate promoters for Cas9 quantified by fluorescent intensity of enhanced green fluorescent protein (EGFP). Data shown represent means ± SE (n = 2 per promoter) (**c**) Micrographs showing EGFP expression in OmB cells (green) from SV40, CMV, and OmEF1a EGFP vectors representative of those used for quantitative analysis (**d**) Plasmid map of transposon vector (OmEF1aCas9P2APuroSB) for generation of Cas9 cell line including OmEF1a promoter upstream of Cas9 and puromycin resistance coding sequences (separated by the P2A self-cleaving peptide sequence) in between the two Sleeping Beauty transposon internal terminal repeats (ITRs). Gene and vector maps were generated using Geneious 11.0.3 (Biomatters, https://www.geneious.com). Bar plot was generated using Rstudio 1.1.456 (https://rstudio.com). Image editing and assembly into complete figures was performed using Inkscape 0.92 (https://www.inkscape.org).

its more compact size (1039 bp vs 1643 bp) and lower frequency of common restriction enzyme sites, the OmEF1a promoter was selected for expression of Cas9. It was cloned into the OmEF1aCas9P2APuroSB Sleeping Beauty transposon vector (Fig. 2d) upstream of a single coding sequence including Cas9 and puromycin resistance genes separated by the P2A self-cleaving peptide. This construct was co-transfected into OmB cells with the Sleeping Beauty transposase expression plasmid. After three days of 2µg/ml puromycin treatment all un-transfected control cells had detached from the culture plate, but about 10% of the transfected cells persisted and proceeded to proliferate in the selection media indicating stable genomic integration of the transgene.

Identification of tilapia U6 promoters that contain vertebrate U6 consensus core elements

Because the endogenous OmBAct and OmEF1a promoters were substantially stronger in driving EGFP expression than commonly used heterologous polymerase II promoters, we presumed an endogenous *O. mossambicus* polymerase III promoter (U6) would be superior for driving gRNA expression than commonly used human or zebrafish U6 promoters. NCBI Blast searches of known fish U6 genes including promoters and approximately 100 bp of the transcribed region against the NCBI *O. niloticus* reference genome (taxid: 8128) yielded four unique candidate U6 promoters designated as TU6_1 (LOC112847594), TU6_2 (LOC112846585), TU6_3 (LOC112848092), and TU6_4 (LOC112841904). TU6_1, found by BLAST of a medaka U6 (taxid: 8090, LOC111948268), contained a well-defined TATA box at position -31 to -23 from the transcription start site (TSS +1) (Fig. 3a). Moreover, sequence alignments of the four candidate tilapia U6 promoters against each other identified regions of high identity between TU6_1 and TU6_4 (Fig. 3b) including a PSE like sequence with 60% pairwise identity to the vertebrate consensus PSE sequence [30] between positions -46 and -76, a SPH like sequence with 73.8% identity to the consensus SPH element [31] between positions -233 and -254, and a novel highly conserved sequence with 89.7% pairwise identity between the two promoters between positions -285 and -314, which we

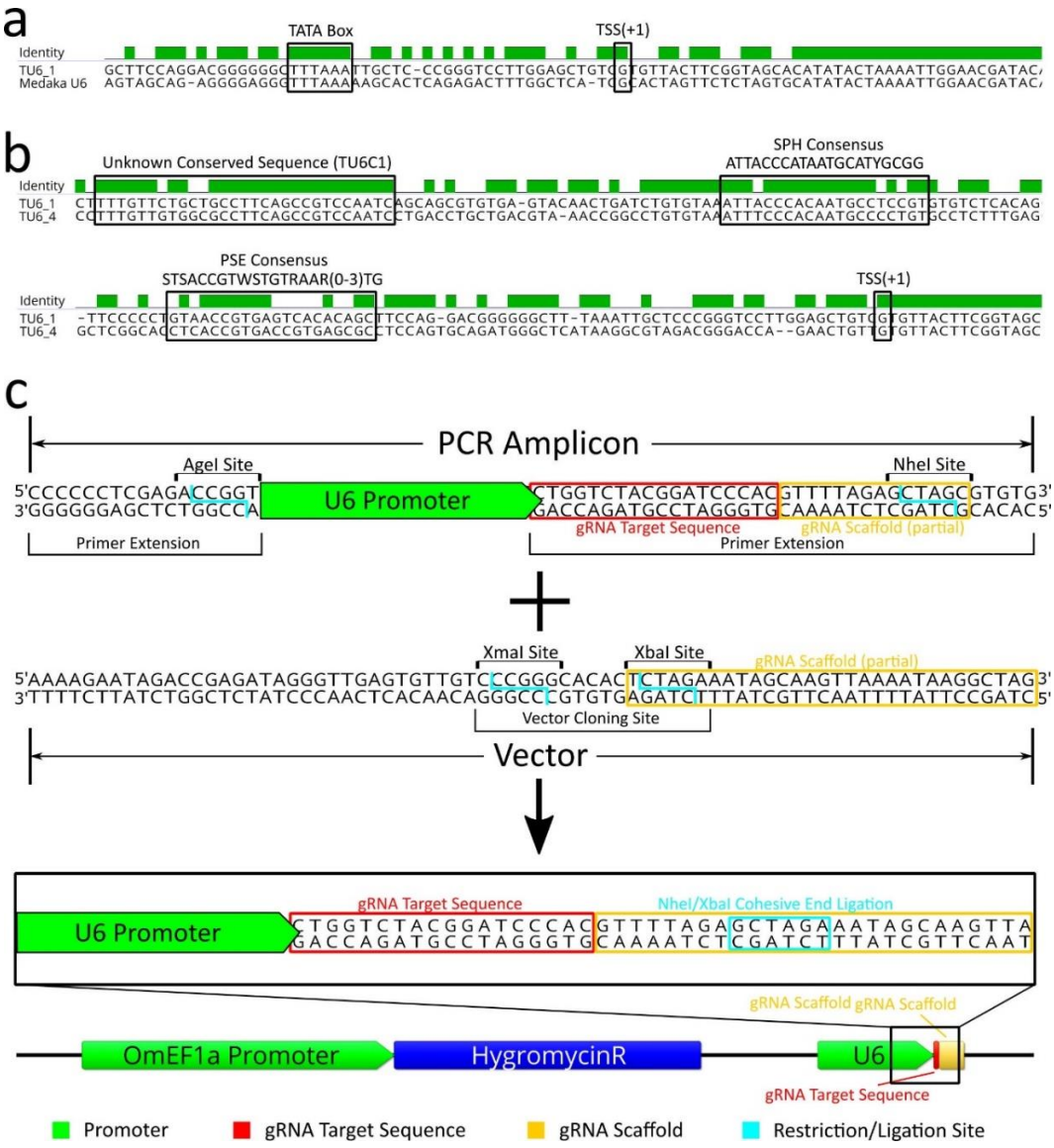

Figure 3. Identification/Characterization of *O. mossambicus* U6 promoter by BLAST/sequence alignment and cloning into gRNA expression vector. (**a**) Sequence alignment of the tilapia U6 and the Medaka U6 template used to identify it by BLAST search shows a highly conserved transcribed region and the TATA Box (-31 to -23 from transcription start site, TSS). (**b**) Sequence alignment of two candidate tilapia U6 promoters (1 and 4) identified by BLAST searches. Presumptive important U6 regulatory elements are highlighted, including a sequence that are similar to the vertebrate consensus PSE, vertebrate consensus SPH, and an unknown sequence that is highly conserved in the two tilapia U6 promoters (designated as TU6C1). (**c**) Schematic of the initial cloning strategy used to generate the U6 gRNA expression vectors. The base vector contains the gRNA scaffold sequence (yellow box) in which the 9th bp was changed from a G to a T to form a XbaI restriction site. Wild-type TU6, HU6, and ZU6 cassettes were generated by PCR amplification of the U6 promoter in which an extension of the reverse primer includes the gRNA target sequence (red box) and the 5' thirteen bases of the gRNA scaffold modified to form a NheI restriction site as an extension. Ligation of the amplicon into the vector by NheI/XbaI complimentary cohesive ends (blue box) forms the complete gRNA scaffold sequence of the final vector. DNA sequence alignments, sequence images, and vector map were generated using Geneious 11.0.3 (Biomatters, https://www.geneious.com). Image editing and assembly into complete figures was performed using Inkscape 0.92 (https://www.inkscape.org).

named the tilapia U6 consensus sequence 1 (TU6C1) . Compared to the other three candidate tilapia U6 promoters, TU6_1 contained the most identifiable known U6 regulatory elements and was selected to drive gRNA expression in an initial pilot experiment. Using PCR, the TU6_1 (designated as TU6 from this point forward) promoter was isolated from genomic DNA and sequenced (GenBank accession no. MT762368). The TU6 amplicon was subsequently cloned upstream of the same *IMPA1.1* T7 gRNA sequence (as a primer extension) used in the RNP experiment described above (Fig. 3c). This TU6-*IMPA1.1*-T7 construct was then cloned into the base plasmid vector (gRNAscaffHygroR) including the gRNA scaffold sequence a hygromycin resistance gene driven by the OmEF1a promoter to generate the final TU6 gRNA expression vector (Fig. 3c bottom).

Mutagenesis of IMPA1.1 by CRISPR in stable Cas9-OmB cells expressing gRNA from a tilapia U6 promoter

The TU6 *IMPA1.1* T7 gRNA vector was transfected into the presumed Cas9 expressing puromycin selected OmB cells (see above) followed by hygromycin B selection for 6 days. PCR targeting 780 bp of the *IMPA1.1* T7 targeted region was performed on DNA harvested from the remaining cells and untreated control cells. The PCR amplicons were subjected to RSM analysis using BsrGI with an expected band pattern of 136 bp, 301 bp, and 343 bp of fully digested amplicon (Fig. 4a). All of these bands were present in the gel resolving the products of the BsrGI digests for both PCR amplicons (Fig. 4b). However, an additional clear band of ~437 bp was present in the digest from the CRISPR treated cells representing the fragment generated if the BsrGI restriction site within the gRNA target sequence (between the 136 bp and 301 bp fragments) is mutated, indicating partial successful gene targeting.

Generation and Validation of a clonal Cas9 OmB Cell Line

To obtain a clonal Cas9 OmB cell line with a more consistent phenotype and limit variability between comparisons in high-throughput downstream studies, colonies derived from single cells plated at low

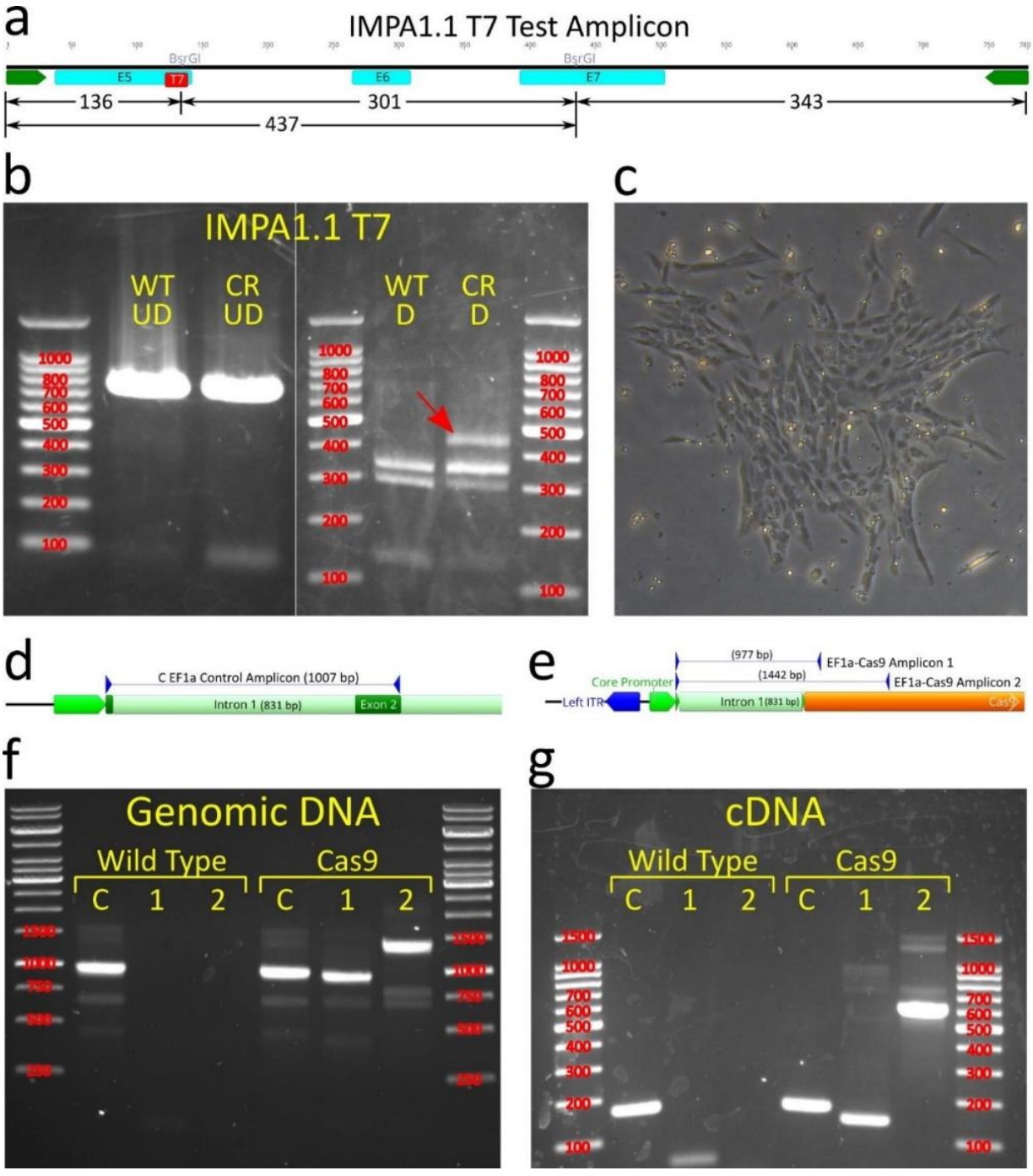

Figure 4. Pilot test of Cas9 expressing cells with isolation and validation of clonal Cas9 OmB cell line. (**a&b**) The first trial using TU6 gRNA vector with *IMPA1.1* T7 target sequence transfected into puromycin selected Cas9 expressing cells. (a) Schematic of the PCR generated test amplicon used to evaluate mutational efficiency at the IMPA1.1 T7 target including locations of the BsrGI restriction sites and predicted fragment lengths that would result from BsrGI digestion. (**b**) Agarose gels (marker sizes in bp labeled in red) of RSM analysis on IMPA1.1 T7. Left gel consists of un-digested test amplicons from wild-type (WT UD) and T7 CRISPR targeted (CR UD) cells. Right gel consists of BsrGI digested test amplicons from wild-type (WT D) and T7 CRISPR targeted cells (CR D) showing residual fragment length of ~ 437 bp (red arrow) indicative of incomplete digestion of BsrGI restriction site and alteration of the T7 target sequence by Cas9 cleavage. (**c**) Phase contrast image of colony formation of

OmEF1aCas9P2ApuroSB vector transfected, puromycin selected OmB cells. (**d&e**) Schematic of primer design for endogenous EF1 alpha control (**d**) and OmEF1a-Cas9 transgene (**e**) verification PCR reactions of presumed Cas9-OmB cell line. (**f&g**) Agarose gels of PCR amplicons (marker sizes in bp labeled in red) verifying genomic integration from genomic DNA template (**f**) and mRNA expression from cDNA template (**g**) of Cas9. Expected EF1 alpha positive control amplicon (C) was observed from both wild-type and presumptive Cas9 OmB cells from both DNA (1007 bp) and cDNA (176 bp) templates. Both of the two expected OmEF1a/Cas9 expression cassette amplicons (1 & 2) were only observed from the Cas9 OmB cells from both DNA (977 bp and 1442 bp) and cDNA (146 bp and 611 bp) templates. The gel images in this figure have been significantly cropped to conserve space and increase focus on relevant bands. Full-length gels are presented in Supplementary Figure S1. Gene and vector maps were generated using Geneious 11.0.3 (Biomatters, https://www.geneious.com). Image editing and assembly into complete figures was performed using Inkscape 0.92 (https://www.inkscape.org).

---

density (Fig. 4c) were isolated by passage into separate culture dishes. For the next phase of gRNA target testing, one clonal colony was selected and propagated due to morphology and proliferation phenotypes comparable to the founder OmB cell line and maintenance of robust puromycin resistance. To verify genomic presence and expression of the OmEF1aCas9 transgene, PCR was performed on genomic DNA and cDNA obtained from both wild-type OmB cells and the candidate Cas9 OmB clonal line. Three primer pairs were used on genomic DNA and cDNA for both cell types for a total of 12 reactions. All primer pairs were designed to flank the intron of the OmEF1a promoter with common forward primer in exon 1 of the promoter, a control reverse primer targeting the endogenous EF1 alpha exon 2 (Fig. 4d), and two different reverse primers in the Cas9 coding sequence (Fig. 4e). Expression of the genes would be indicated by a shorter amplicon using the same primer pairs on the cDNA from removal of the 831 bp intron between exons 1 and 2 of the OmEF1a promoter. The expected control amplicons had expected sizes of 1007 bp (endogenous EF1 alpha) and 176 bp (genomic DNA and cDNA) and were obtained for both wild type and Cas9 OmB cells. The two transgene target amplicons for genomic DNA (977 bp and 1442 bp) and cDNA (146 bp and 611 bp) were obtained only for the templates derived from Cas9 OmB cells verifyng both genomic integration (Fig. 4f) and active transcription of the EF1aCas9P2A-Puro expression cassette (Fig. 4g).

Clonal Cas9-OmB1 cells permit efficient high-throughput in vivo testing of multiple targets

To test the effectiveness and robustness of the clonal Cas9 OmB cell line (Cas9-OmB1), we manually designed 14 total gRNA sequences (Table 1), all containing a restriction enzyme site overlapping the potential Cas9 cleavage site. Of these, eight gRNAs target genes of interest included *IMPA1.1* (T7, T11, T12, and T13 target sites) and nuclear factor of activated T cells 5 (*NFAT5* T1, T7, T8, and T10 target sites). The other six target genes that are all presumed to be nonessential to OmB cells including glucocorticoid receptor (*NR3C1* T1 and T2), myostatin (*MSTN* T1 and T2), and two genes with previously validated gRNAs for tilapia from other labs, *WT1A*[32] and *NANOS3*[22]. Each target sequence was cloned downstream of the TU6 promoter into the gRNA expression vector and transfected into Cas9-OmB1 cells followed by hygromycin B selection as described above. PCR of hygromycin selected cells for gRNAs *IMPA1.1* T12, *NFAT5* T1, *NFAT5* T7, *MSTN* T2, and *WT1A* failed to yield an amplicon of the expected size and, therefore, these targets were excluded from further analysis (details of RSM reactions and expected band sizes are available in Supplementary Table S2).

Gel electrophoresis of restriction digests showed that *IMPA1.1* T7, all *NFAT5*, all *NR3C1*, and the *NANOS3* target amplicons yielded notable undigested bands indicating modification of the restriction enzyme recognition sequence (Fig. 5a-d). The *IMPA1.1* T11 and T13 targets yielded little detectable full-length bands indicating near complete digestion and inefficient gene targeting. Not enough substrate DNA was available for the *MSTN* target to obtain clear bands and the results for this target are, thus, inclusive. Sanger sequencing was also performed on the PCR amplicons from the treated cells and equivalent wild-type control amplicons. To obtain percent indel mutation frequencies, chromatogram sequence files were loaded to the online quantitative assessment of genome editing TIDE (Tracking of Indels by Decomposition) webtool. This was also performed on test PCR amplicons from the *IMPA1.1* targeting RNP treated cells (see previous section) for comparison. For the gRNA vector treated cells only

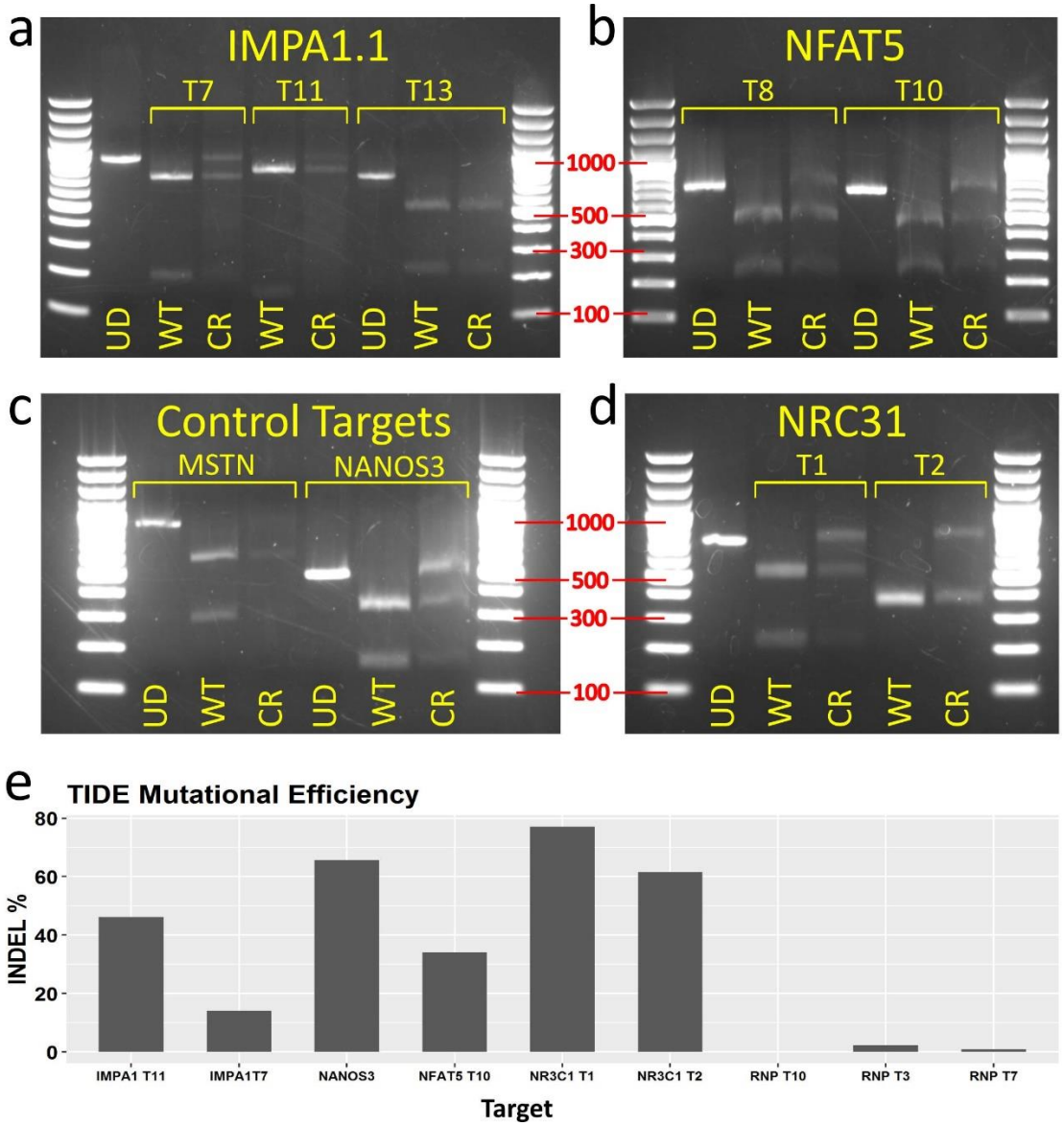

Figure 5. Mutation analysis from TU6 gRNA expression vector transfected Cas9 OmB cell line treated cells testing multiple targets of different genes. (**a-d**) Agarose gel electrophoresis of RSM analysis of TU6 gRNA expression vector treated Cas9-OmB1 cells targeting diverse loci (marker sizes in bp labeled in red). Except *IMPA1.1* T13 and *MSTN*, nearly all targets showed clear residual undigested amplicon from CRISPR treated cells (CR) relative to equivalent digested amplicon from un-treated OmB cells (WT) indicating at least some successful Cas9 cleavage. For each target, an un-digested control amplicon was included for reference (UD). (**a**) *IMPA1.1* targets T7 and T11 shared the same un-digested control (far left lane). (**b**) NFAT5, the two target regions were amplified by different primer pairs and thus have separate un-digested controls. (**c**) Presumed non-essential gene control targets. Clear residual un-digested amplicon from *NANOS3* target but lack of conclusive results from *MSTN* target due to low quantity of DNA. (**d**) The *NR3C1* targets T1 and T2 shared the same un-digested control (far left lane). (**e**) TIDE indel analysis of amplicons from TU6 vector treated Cas9-OmB cells and from previous *IMPA1.1* targeting Cas9/gRNA RNP treated cells. Note the common target between the two approaches (IMPA1.1 T7), 14.1% from the vector versus 0.9% from the RNP methods. Bar plot was generated using Rstudio 1.1.456 (https://rstudio.com). Image editing and assembly into complete figures was performed using Inkscape 0.92 (https://www.inkscape.org).

the *NR3C1* T1, *NR3C1* T2, *IMPA1.1* T7, *IMPA1.1* T11, *NANOS3*, and *NFAT5* T10 targets yielded sufficient quality reads for analysis for which the indel % values were 77.1, 61.6, 14.1, 46.1, 65.7, and 34.1 respectively. The indel % values obtained from the *IMPA1.1* RNPs cells were 2.2, 0.9, and 0.0 for T3, T7, and T10 respectively (Fig. 5e). Note the common target between the two approaches (IMPA1.1 T7), 14.1% using the vector method versus 0.9% using the RNP method. The average value for gRNA vector targeted cells (49.8%) was significantly greater than the average value from the RNP treated cells (1.03%, p-value = 0.0096).

Verification of mutagenesis of NANOS3 and NFAT5 genes and characterization of indel properties

Sequence analysis of individual mutation events was performed to confirm the observations from RSM are due to mutations of the target sequence, obtain quantitative information on the frequency of mutation in the form of indels (insertion or deletion of genomic sequence that occurs when a cell repairs breaks in DNA), and obtain qualitative information on the typical mutations that can occur. *NFAT5* T10 and *NANOS3* PCR amplicons from gRNA expression plasmid treated Cas9 cells were cloned into pBluescript II SK(+) vectors, transformed into competent *E. coli* followed by PCR and sequencing of the plasmids from clonal bacterial colonies. For *NANOS3*, 21 of the 24 *E. coli* clones analyzed yielded a band of sufficient sequence match to be identified as the targeted amplicon. Of these, 17 sequences showed alteration of the target site while 4 were identical to wildtype (Fig. 6a). Most alterations were deletions ranging in size from 1 to 50 bp. For *NFAT5*, 19 of the 24 *E. coli* clones analyzed yielded a band of sufficient sequence match to be identified as the targeted amplicon. Of these, only 3 sequences showed alteration of the target site while 16 were identical to wildtype (Fig. 6b). Compared to the *O. niloticus* reference sequence, a consistent additional T nucleotide (position 5 from the gRNA scaffold in the target sequence) was detected in *the O. mossambicus* PCR amplicons. Therefore, the gRNA used for *NFAT5*

T10 had a single base pair mismatch between the substrate genomic DNA, which likely contributed to the lower efficiency of this target.

Gene Target	Target Sequence 5′ to 3′	Test Amplicon Primers 5′ to 3′		
		Forward	Reverse	Size (bp)
IMPA1.1 T7	CACCACAAACTTTGTACA	ACTCGTCGACATTGTTGCAT	GTAGCTTCATTTGACGTACCTCC	867
IMPA1.1 T11	AAGCAAAATGGAAGATCCA			
IMPA1.1 T12	GGGTCTCTTAAAGAGGAATT			
IMPA1.1 T13	GTGACGACGAACCCATTC	TGCAGATTCCCATTTGTGGC	CCCGATAGCTCAGCAACACT	705
NFAT5 T1	ATGCCTCTTCTCTGACCA	TGGCCTGCTCAACTTTTGTC	AGTTGCCTCAAGGTGCTACA	1099
NFAT5 T7	TACCCCTCGTCAAAGGCC			
NFAT5 T8	CTGCAGCTCTGATGAACCT	ATGTACTGCAGCAAACCCCA	GTGAACACAGTCCAGACCCC	708
NFAT5 T10	GGTTTTACCAAGCCTGCA	CAGAGCCCAGGAATGACAGG	AGGTGCAGTGTTAACTTGGGT	651
NR3C1 T1	ATAGACGGTCCAGAGCCCC	CTACACTGAAAGCCCCGAGG	ATTGGTCACACTGCTGCCAT	709
NR3C1 T2	ACATCACCCAGTCCTCCA			
MSTN T1	CAAATCTCCCGGCTTATAC	TGAGACATGGTGTTTGGGCA	CGCTTGTCCAAATGCAGGTG	858
MSTN T2	GCAAGATCCCCTCCATGG	TCAGCAACCGTTCATGGAGG	CAGCTGTGTTTTTCCGAGCC	938
NANOS3	GCTGGTCTACGGATCCCAC	GCAAACGAACCAAAGCATGC	AATTGATGCAAAACCCGCCG	466
WT1A	GGGTTGCTGAACATCCTGGT	CCAGAGAAGGAGCACGTCAG	CCCACCACCATGATGCAGAT	549

Table 1. Target sequences, primer pairs used to generate test amplicons by PCR, and sizes of un-digested test amplicons used in RSM analysis of diverse gRNA target testing of the Cas9-OmB1 cell line.

Improved gRNA vector construction proficiency by modification of the TU6 promoter

To facilitate more rapid and economical production of gRNA expression vectors, the TU6 promoter was modified to accommodate direct cloning of annealed oligos containing new target sequences (Fig. 6c). This was achieved by a single nucleotide change adjacent to the TSS generating a ClaI resitriction site. This mutated version of the TU6 (TU6m) was included in the base vector upstream of the modified XbaI site containing gRNA scaffold sequence. This resulted in reduced time and resources used to generate a gRNA vector with a new target sequence by elimination of the PCR step used in the previous cloning strategy.

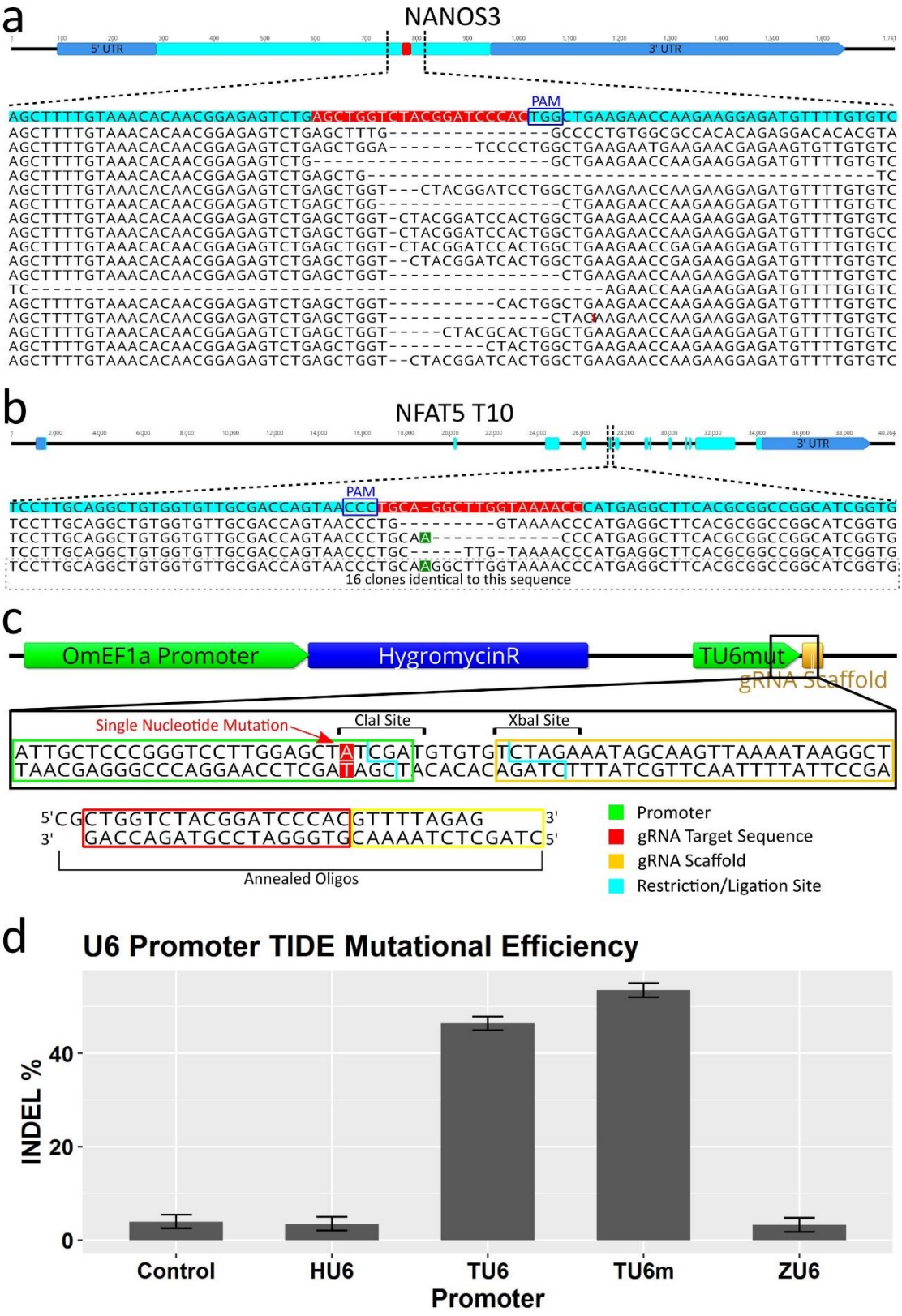

Figure 6. CRISPR/Cas9 editing confirmation and efficiency comparisons of different U6 promoters by analysis of *NANOS3* gRNA target. (**a&b**) Sequencing results of individual alleles from plasmid sub-cloned test amplicons. (**a**)

For the *NANOS3* target, 17 out of 21 amplicons (81%) were altered at the target site (4 wild-type sequences not shown). (**b**) For the *NFAT5* T10 target, 3 out of 19 amplicons (16%) were altered at the target site. The remaining 16 sequences were identical to the *O. niloticus* reference sequence except for an extra nucleotide (an A when reading the gene sequence 5' to 3', a T when reading the gRNA sequence 5' to 3') 5 base pairs from the PAM sequence (highlighted in green). (**c**) Alternate cloning strategy for changing gRNA target sequence in expression vector illustrated. Utilizes a mutated TU6 (TU6m) in which a single nucleotide was changed adjacent to the TSS generating a ClaI restriction site. The TU6m is included in the base vector in which new gRNA target sequences can be added by annealed oligos. (**d**) Mutational efficiency quantified by TIDE indel% analysis of four different U6 promoters using the same gRNA target (*NANOS3*) showing superior editing obtained from both versions of the tilapia U6 promoters (over 5 fold over all others). The Human and Zebrafish U6 promoters were not statistically significant from the no U6 control. Gene maps and DNA sequence images were generated using Geneious 11.0.3 (Biomatters, https://www.geneious.com). Bar plot was generated using Rstudio version 1.1.456 (https://rstudio.com). Image editing and assembly into complete figures was performed using Inkscape version 0.92 (https://www.inkscape.org).

Confirmation of superiority of endogenous tilapia U6 Promoters for gRNA expression in OmB cells

To evaluate what influence the specific U6 promoter had on the efficiency of CRISPR/Cas9 induced gene edits in this system, the human and zebrafish U6 promoters (HU6 and ZU6 respectively) from previous work, TU6, and TU6m from this report were cloned upstream of a common gRNA sequence (*NANOS3*). Cas9-OmB1 cells were treated with the gRNA expression plasmids followed by hygromycin selection and PCR as described previously in replicates of four for each U6 type. The control was a gRNA expression plasmid with no target sequence or U6 transfected into Cas9 OmB cells. The *NANOS3* gRNA sequence was chosen for this analysis because of the high mutation rate observed in previous analysis and thus a wide dynamic range to measure differences in mutation frequency between different promoters. This time Sanger sequencing was performed directly on the original PCR amplicon from the treated cells. Mutation efficiencies were quantified using the TIDE webtool[33]. TIDE analysis of *NANOS3* target amplicon chromatograms yielded mean indel efficiencies of 3.98, 3.48, 3.27, 46.40, and 53.52 percent for the control, HU6, ZU6, TU6, and TU6m, respectively (Fig. 6d). The TU6 and TU6m target efficiencies were significantly greater than all others (n = 4 per promoter, SE = 2.09, α= 0.05, p-value < 0.001, Tukey multiple comparison statistical analysis). The TU6m was significantly greater than the TU6 (p-value =

0.0271). The control, HU6, and ZU6 efficiencies were not statistically different from each other (p-value > 0.996) indicating no or negligible editing obtained by use of these promoters.

Discussion

In this work we developed an efficient CRISPR/Cas9 system for the OmB tilapia cell line. We identified inadequate expression strength in OmB cells when using heterologous promoters as the cause of previous failures to achieve detectable gene edits. The first attempt to circumvent this issue was direct transfection of gRNA/Cas9 protein RNP complexes. Since the efficiency of RNPs was *in-vitro* validated, the lack of observed gene edits indicated poor delivery using the transfection reagent method described. Due to previous success with DNA transfection and plasmid based antibiotic selection in OmB cells, a DNA expression vector method of CRISPR/Cas9 delivery was the most practical platform to pursue. Other factors, in addition to high transfection efficiency in OmB cells, make DNA vectors an attractive platform to implement CRISPR/Cas9 gene targeting. Even if alternative modes of delivery of RNPs (e.g. electroporation) elevate transfection efficiency to equal or greater than that achieved with DNA transfection, the plasmid based delivery system has the distinct advantage of being able to select for only the cells that have acquired all the CRISPR/Cas9 components through antibiotic/resistance gene systems, thus compensating for any deficiencies in delivery. This approach significantly reduces the amount of clonal screening to find the desired gene edits. It also eliminates the need for time consuming *in vitro* transcription or purchase of expensive synthetic RNA or Cas9 protein.

Success of the DNA vector method is dependent on sufficient promoter strength in the cell line being used. Identification of the most appropriate Pol II promoter was initiated by evaluating a set of rational options for screening. Several viral and engineered Pol II promoter options exist such as the SV40, CMV, and CAG which are among the most universally used promoters across diverse vertebrate taxa and have shown effective expression in fish cells[34–36], which render them reasonable options for this application.

Successful CRISPR/Cas9 gene editing in fish cells lines was reported using the CAG promoter (as part of the pX458 vector) in Grass Carp (*Ctenopharyngodon idellus)* cells[37]and the CMV promoter in a species salmon (CHSE) cell line[23] for transient and constitutive Cas9 expression, respectively. However, the relative expression strength of these heterologous promoters in fish cells can vary greatly with species[38] and cell type[39,40] and their use , thus, produces uncertain outcomes in novel cell lines.

Strong species-specific endogenous promoters such as beta-actin and EF1-alpha represent viable alternatives that can equal or exceed SV40, CMV or CAG in promoting expression in some cells[41]. Fish beta-actin has shown superior expression strength over conventional promoters such as CMV, for example in Fathead Minnow (*Pimephales promelas*) cells[42]. However, the relative effectiveness of these promoters can be unpredictable as seen in Japanese Flounder (*Paralichthys olivaceus*) cells, in which CMV has been reported as stronger than endogenous beta-actin[43]. Also, the tilapia beta-actin promoter outperformed the equivalent carp beta-actin promoter in reporter gene expression in tilapia cells[44], supporting species specificity as an important factor for promoter efficiency. Considering this uncertainty of Pol II promoter function in a given fish cell type, evaluation of potential Pol II promoters represents a prudent optimization step before investing in downstream applications. In this study, we used fluorescent microscopic analysis of OmB cells transfected with different candidate promoters driving EGFP expression vectors to assist with the Pol II promoter selection. The SV40 promoter showed nearly negligible expression in this study. Moreover, the CMV and CAG promoters were notably, although not significantly, weaker than the two endogenous tilapia promoters.

Another consideration, in cases of stable integration of transgenes, endogenous promoters such as EF1-alpha are known to sustain expression longer than viral promoters such as CMV which have a tendency to be silenced over time[45]. The OmEF1a promoter (1039 bp) is more compact and showed slightly higher EGFP reporter intensity than the OmBAct promoter (1643 bp). Therefore, OmEF1a represented the strongest choice for Cas9 expression in this project. Based on these factors, the OmEF1a promoter

is likely to have improved the editing efficiency, but since the difference in promoter strength was moderate (just over two-fold greater than CMV and CAG) it did not constitute the primary cause for the success of this system over our previous attempts.

Optimized expression of the gRNA component represented an equally valuable node to improve CRISPR/Cas9 gene editing efficiency in fish cells. Numerous studies have demonstrated efficient CRISPR/Cas9 gene editing through the use of a human U6 promoter in mammalian cells[8,46] and at least some level of effectiveness in phylogenetically distant cell cultures, such as chicken[47], mouse[48], and even carp cells[37]. However, a species-specific U6 promoter can have significantly greater expression as seen in a study comparing human U6 to chicken U6 promoters by quantitative RT-PCR. Such a comparison revealed a four-fold greater RNA abundance in a chicken fibroblast cell line when using the chicken U6 promoter compared to the human U6 promoter[49].

A limited number of teleost U6 promoters have been isolated and characterized for small gRNA expression in fish cells. Confirmed expression from a pufferfish (*Takifugu rubripes*) U6 promoter was achieved in cell lines of different fish species, grunt (*Haemulon sciurus*) and salmon (*Oncorhynchus tshawytscha*), and found to be more effective than mouse U6 promoter in driving shRNA based knock-down[50]. Evidence supporting the expression of zebrafish U6 promoters (including the one utilized in this study) in tilapia (*Oreochromis* spec.) cells has been obtained by northern blot analysis[51]. Our work has isolated an additional fish U6 promoter, the *O. mossambicus* TU6, and demonstrated its superior effectiveness in driving sufficient gRNA expression to achieve reliable CRISPR/Cas9 gene editing in OmB cells.

Despite this wide variety in the effectiveness of different U6 promoters, a systematic comparison of phylogenetically diverse U6 promoters in the context of CRISPR/Cas9 gene editing had not been reported for fish cell lines. The direct comparison of the efficiencies of candidate U6 promoters in the

present study resulted in the identification of the TU6 and TU6mut promoters as efficient tools for transcription of small RNAs in tilapia cells. Furthermore, our systematic comparison of U6 promoter efficiencies highlights the critical importance of a suitable polymerase III promoter for efficient gRNA expression. The lack of gene edits (indicated by TIDE analysis) resulting from the use of gRNA expression constructs driven by HU6 and ZU6 heterologous promoters explains the failure of our previous attempts to perform gene editing in OmB cells and establishes the U6 promoter as a critical element of gene targeting systems in fish cell lines. Despite reports of interspecies U6 promoter function, the expression levels for both the human and zebrafish U6 promoters were insufficient to achieve even low levels of Cas9 induced gene editing in OmB cells. Collectively, our experiments demonstrate the necessity of identification and validation of an efficient polymerase III promoter for DNA vector gRNA expression based approaches for CRISPR/Cas9 gene targeting in a given cell line model. Our work further illustrates that phylogenetic proximity represents a key consideration in selecting promoters for gRNA transcription.

In addition to optimizing promoter strengths, we incorporated stable genomic integration of the Cas9 gene into the cell line to elevate Cas9 protein levels available for gene editing at the targeted sites. This approach provides more time for Cas9 protein to accumulate and localize to the nucleus. Direct comparisons have shown superior gene editing efficiency in cells stably expressing Cas9 over transient expression of Cas9, e.g. in Drosphila[52] and human[53] cell lines. Stable Cas9 expression has also been reported for the very few fish cell lines that have been successfully gene edited using CRISPR/Cas9. The first reported success of CRISPR/Cas9 in fish cell culture was achieved using stable genomic integration of Cas9 into the Chinook Salmon Embryo (CHSE) cell line[23] and was subsequently used to generate a targeted gene knock-out cell line[54].

The effectiveness of the new CRISPR/Cas9 gene editing system generated in this study was evaluated using multiple targets and by multiple means of mutational analysis. These means included RSM,

sequencing of individual cloned amplicons and TIDE analysis of the PCR reaction Sanger sequencing reads, which provided key information on the potential overall mutation rate and the relative frequency of specific types of mutations that occur. The RSM analysis was used strictly for method development purposes as it was a rapid way to visually indicate the presence or absence of mutations. However, this method limits gRNA target selection to the fraction of candidate sequences that have a restriction site overlapping with the potential Cas9 cleavage site and provides little information on the frequency and type of mutations.

The approach of sequencing the cloned amplicons, which can be employed on any target, provided more quantitative data and, as seen with the *Nanos3* target, indicated that a mutation efficiency of at least 81% is possible with our system. This number is likely an under-estimate as the amplicon was gel extracted, which biased for fragments with lengths that are similar to that of the un-mutated wildtype while Sanger sequencing revealed individual amplicons with large deletions of up to 50 bp. Larger deletions or insertions would have been missed because of the bias towards expected wild-type length during gel extraction and, therefore, a subset of gene edits may not be accounted for in the determination of overall mutation efficiency. Our results inform future studies by demonstrating the existence of large deletions, which should be accounted for by increasing the width of bands that are gel-extracted and prepared for Sanger sequencing in future studies. Despite possibly underestimating gene editing efficiency in this study, the Sanger sequencing method provided a wealth of information with estimates of mutation frequency and identification of specific sequence changes resulting from mutagenesis. This approach represents the strongest confirmation of the presence and specific nature of mutations. However, it is also the most labor intensive and not appropriate for high-throughput screening of candidate gRNAs.

TIDE mutation detection analysis represents an appropriate compromise as it can be performed on any target using a sequencing read of a PCR amplicon directly from the genomic DNA without the need of

cloning individual mutants. The TIDE results of this study were consistent with the qualitative restriction site mutation analysis and clonal sequencing detection results, which demonstrates that TIDE represents a reliable and high-throughput approach to evaluate specific gRNA efficiency. With the *NANOS3* target, TIDE analysis yielded a smaller mutation estimate than the sequencing of mutant clones (~65.7% vs 81% respectively). This discrepancy between analyses is important to take into consideration as the actual mutation rate in cells induced by CRISPR/Cas9 gene editing may be higher than estimates obtained from TIDE. Further replicates are needed to see if this relationship is consistent.

Our study establishes an efficient system for generating and analyzing CRISPR/Cas9 induced mutations. This technology can be utilized to investigate molecular mechanisms of interest and causality of gene-environment interactions in the OmB cell model. However, despite the significant advantages of the DNA vector method presented here, some limitations of this type of approach must be considered in the experimental design and interpretation of results to minimize their impact. One concern associated with constitutive expression of Cas9 in cell lines is the potential for erroneous side effects on cellular growth and phenotype that can occur from excessive stress on protein production/turnover mechanisms or non-physiological interactions with sustained high levels of a foreign protein[55]. Nevertheless, in our study no noticeable differences in growth or morphology were observed between the new Cas9 OmB cell line and the parent cell line from which it was derived. It is important, however, to include appropriate controls to account for this issue and understand the limitations of phenotype interpretations. Follow up experiments utilizing CRISPR/Cas9 methods with less side effects to confirm results obtained from stable Cas9 cell lines may be warranted. Despite the disadvantages, stable Cas9 cell lines have been effectively used to identify genes responsible for specific phenotypes in other vertebrate cell lines[54,56] and are a valuable model of choice for initial high-throughput screens to identify the most suitable targets. Using this approach, key information such as cellular phenotype and gRNA

efficiency can be obtained in a high-throughput manner to inform subsequent experiments that validate specific targets are associated with phenotypes of interest.

Prolonged expression of Cas9 and gRNAs as in this plasmid based system can also result in increased off-target effects[57]. This side-effect was clearly demonstrated by the sequencing results from the NFAT5 T10 target in which an editing efficiency of 15.7% was observed despite a single-nucleotide difference between the gRNA and the substrate DNA. Selection of gRNA target sequences with the fewest potential off-target cleavage sites is one way to minimize this effect. However, without in-depth analysis of whole genome sequencing, off-target effects cannot be completely predicted or quantified. Among experimental controls that account for potential off-target effects, using multiple target sequences on the same gene represents one way to support that effects are limited to the targeted gene if a consistent phenotype is observed.

Direct delivery of pre-complexed gRNA/Cas9 RNPs is a preferred method to minimize side effects attributed to the prolonged presence of active Cas9. This would be a suitable approach for development of clonal knock-out cell lines and subsequent analysis of phenotypes associated with the manipulated locus. Although no detected edits at the targeted loci were observed using RNPs, we only attempted one RNP delivery method and thus should not be dismissed. Other RNP delivery methods exist including electroporation which was demonstrated as an efficient tool in fish cells. This method achieved efficient results in Medaka (*Oryzias latipes*) cell lines while not relying on species-specific promoters and circumventing inefficient RNA/protein complex transfection procedures [24]. However, this approach required electroporation, careful optimization of cell type-specific electroporation parameters and equipment, *in vitro* production or purchase of gRNA, and purchase of Cas9 protein making it less practical for low-cost, high-throughput projects. A practical workflow for the OmB cell line would be to use the vector approach described here in high-throughput screening of candidate gRNAs for mutational efficiency and preliminary phenotype information. From this, gRNAs could still be

selected and used with more invested RNP based CRISPR/Cas9 gene editing in cell lines and embryos for more in-depth phenotype analyses. Electroporation or other delivery methods may need to be explored to support efficient delivery of RNP complexes into the OmB cell line.

In summary, we report a robust, efficient, and economical approach that uses novel promoters and an expression plasmid optimized for economical and efficient screening of gRNAs and phenotypes for CRISPR/Cas9 gene targeting in fish cell lines. This approach is well-suited for high-throughput screening of targets that cause phenotypes of interest while relying on only having to vary small, target-specific DNA oligos for PCR at very low cost. Our approach reduces the amount of screening of cells with desired gene edits by utilizing antibiotic selection. It requires only basic cell culture and DNA cloning methods without the need for complicated vector production such as lentiviral systems or specialized equipment for electroporation or microinjection.

Materials and Methods

Primers and Oligonucleotides

All DNA primers and oligos mentioned in the materials and methods section are listed in Table 2. Additional oligos not mentioned in the main text are listed in Supplementary Table S3.

In vitro cleavage assay and transfection with gRNA/Cas9 ribonucleoprotein complexes

Guide RNAs were *in vitro* transcribed using New England Biolabs HiScribe T7 High Yield RNA Synthesis kit (cat # E2040S) according to manufacturer's protocol. PCR amplicons were produced using a forward primer with the T7 promoter sequence (TAATACGACTCACTATAGG) as a 5' extension followed by the target sequences listed in Supplementary Table S1 and a 3' binding region to the gRNA scaffold (GTTTTAGAGCTAGAAATAGCAAG). Approximately 400 ng gRNAs were complexed with 500 ng PNA Bio Cas9 protein (cat # CP01-50) and incubated with 100 ng of a 1392 bp test amplicon produced using

Name	Sequence 5' to 3'
ActinProm_F1	CCCCCGTCGACGTGAGTGACGCCGGACCAATC
ActinProm_R1	CCCCCTCTAGACCATGTCATCCCAGTTGGTCACAAT
Ef1a_F2	CCCCCGGTACCGTTGCAGGGTTTCATTCGGC
Ef1a_R3	CCCCCTCATGATTTTAGTTTCTGTGGCCAAGATT
EF1aCas9RT_F	GCCGTGAAAACCCAGAAACA
EF1aCas9RT_R	CGGAATTGTCGGGGTTCAGA
EF1aCas9RT_R3	AGTCGTCTGTAATCACTGCCC
EF1aX2RT_R	CGGCTTCCTTCTCAAACTTC
EF1aX2RT_R2	CAGCGGCTTCCTTCTCAAAC
HU6(AgeI)_F	CACACACCGGTAAGGTCGGGCAGGAAGAG
HU6_Nanos3gRNA(NheI)_R	CCCCCGCTAGCTCTAAAACGTGGGATCCGTAGACCAGCGGTGTTTCGTCCTTTCCACA
Nanos3target	CGCTGGTCTACGGATCCCACGTTTTAGAG
Nanos3targetCompl	CTAGCTCTAAAACGTGGGATCCGTAGACCAG
TU6_1_F	CTGAAGTATACTATGTGCCGAAT
TU6_1_Fb	CCCCCCTCGAGACCGGTCTGAAGTATACTATGTGCCGAAT
TU6_1_R	AACACGACAGCTCCAAGGAC
TU6_ClaI_XbaI_R	GGGTCCTTGGAGCTATCGATGTGTGTCTAGAGTGTG
ZU6_F1	CCCCCCTCGAGACCGGTATGCGTCTTTTGTTCTGGTCATC
ZU6_Nanos3gRNA(NheI)_R	CACACGCTAGCTCTAAAACGTGGGATCCGTAGACCAGCGAACCAAGAGCTGGAGGGA

Table 2. Sequences of all primers and oligos mentioned in the Materials and Methods.

IMPA1RegStart_F and IMPA1X1RAR primers. Four selected RNPs (2.5µg Cas9/1.2µg gRNA) were transfected into 35 mm wells of 90% confluent OmB cells (one 6-well plate well per target) using Invitrogen Lipofectamine CRISPRMAX transfection reagent system (ref #MAX00001) according to manufacturer's protocol. Genomic DNA was harvested 5 days post transfection using Invitrogen Purelink Genomic DNA Mini Kit (cat # K1820-01). Test amplicons and expected cleavage products (by either Cas9 or restriction enzyme) for in vitro cleavage assay, RSM, and TIDE analysis were PCR amplified using primers listed in Supplementary Table S1.

EGFP Fluorescence Microscope Evaluation of Promoter Strength

The endogenous *O. mossambicus* promoters were PCR amplified from genomic DNA using ActinProm_F1 and ActinProm_R1 primers (modeled after those used in Hwang et al[44] for original isolation of the equivalent promoter in *O. niloticus*) for OmBAct and EF1a_F2 and EF1a_R3 primers for OmEF1a. The CAG, CMV, SV40, and Zubi promoters were obtained from pSpCas9(BB)-2A-Puro (Addgene # 48139), pCS2-nCas9n (Addgene # 47929), pBABE-hygro-hTERT (Addgene # 1773), and pENTR5'_ubi:loxP-EGFP-

loxP (Addgene #27322) plasmids, respectively. Prospective polymerase II promoters were cloned into the base EGFP expression vector (EGFP_SV40PA, See Supplementary Fig. S2) using standard restriction enzyme cloning techniques. The constructs were transfected into separate wells of a 12-well plate. A tile scan of the center 10% of each well was imaged after 18 hours with a Leica DMi8 microscope using the GFP filter cube and an exposure time of 250 ms. LASX software (Leica) was used to calculate fluorescent intensity per cell.

Selection of gRNA Target Sequences

Sequences were manually designed to be within exons in the 5 prime half of the coding sequence but 3 prime of the start codon by scanning specific annotated genes of the *O. niloticus* reference genome (taxid: 8128). For all gRNAs beyond the RNP experiment, only candidate target sequences containing a restriction enzyme recognition site overlapping the predicted Cas9 cleavage site were selected to facilitate an additional downstream analysis of Cas9 target cleavage.

Identification of O. mossambicus U6 Promoter

NCBI nucleotide blast searches using known fish U6 promoters, including approximately 100 bp of the transcribed region, were performed against the *O. niloticus* reference genome to identify candidate tilapia U6 genes. The query fish promoters included Medaka (geneID LOC111948268), Fugu (geneID LOC115246710) from Zenke and Kim[50] and zebrafish U6-2 (described in Boonanuntanasarn et al[58]). Sequence alignments using Geneious 11.0.3 (Biomatters, https://www.geneious.com) of the known U6 genes against the candidate tilapia U6 genes and the candidate tilapia U6 genes against each other were performed to identify conserved U6 promoter regulatory sequence elements. The selected TU6 was PCR amplified from genomic DNA with TU6_1_F and TU6_1_R primers.

Construction of CRISPR DNA expression plasmids

All plasmid vectors were constructed using standard cloning techniques using New England Biolabs enzymes and Promega T4 DNA Ligase (ref# M180A). A more detailed description of plasmid construction of all vectors used in this experiment is available in the Supplementary Methods. The OmEF1aCas9P2ApuroSB vector was constructed using the pSBbi-GP (Addgene # 60511) plasmid as the base vector. The zebrafish codon optimized Cas9 coding sequence from the pCS2-nCas9n (Addgene # 47929) plasmid and a puromycin resistance gene were cloned downstream of the OmEF1a promoter PCR amplicon separated by a P2A self-cleaving peptide into the base vector between the ITRs to complete the construct.

The gRNAscaffHygroR vector was constructed by PCR amplification of the Hygromycin resistance gene from pBABE-hygro-hTERT (Addgene # 1773) plasmid and cloning into the EGFP_SV40PA vector downstream of the OmEF1a promoter followed by the modified guide RNA scaffold sequence PCR amplified from gRNA_GFP-T2 (Addgene # 41820).

The template TU6 promoter was PCR amplified with TU6_F1b primer at the 5' end and a reverse primer (reverse compliment) with a CACACGCTAGCTCTAAAAC TU6 binding region followed by the specific gRNA target sequence (Table 1) and the first 13 bp of the gRNA scaffold sequence modified to be an NheI restriction site (CGACAGCTCCAAGGACCC) at the terminal end. Final gRNA expression vectors were constructed by cloning these U6/gRNA PCR amplicons into the gRNAscaffHygroR vector digested with XmaI and XbaI restriction enzymes, which, upon ligation of the complimentary NheI and XbaI cohesive ends, generates the original guide RNA scaffold sequence reported by Jinek et al[12]. The *NANOS3* gRNA expression cassettes driven by HU6 and ZU6 promoters were generated in the same manner using primer pair HU6(AgeI)_F and HU6_Nanos3gRNA(NheI)_R with gRNA_GFP-T2 (Addgene # 41820) plasmid

as template DNA and primer ZU6_F1 and ZU6_Nanos3gRNA(NheI)_R with pDestTol2pA2-U6:gRNA (Addgene # 63157) plasmid as template DNA respectively.

The TU6m promoter was generated by PCR with a reverse primer (TU6_ClaI_XbaI_R) with an extension changing G to A at the -4 site resulting in a ClaI restriction site at the TSS. The resulting sequence was cloned together with the truncated gRNA scaffold sequence containing a terminal XbaI site to generate the TU6m-gRNAscaffHygroR base vector. Complimentary oligos containing the *NANOS3* gRNA target (Nanos3Target and Nanos3TargetCompl) were annealed to generate a 5' CG single-stranded overhang complimentary to the ClaI overhang, the gRNA target sequence, and the initial gRNA scaffold sequence with a terminal CTAG overhang complimentary to the XbaI overhang capable of constituting the complete gRNA scaffold sequence upon ligation.

Cell Culture Maintenance

Cells were maintained at ambient CO_2 and 26˚ C in L-15 medium containing 10% fetal bovine serum, 100 U/ml penicillin, and 100 mg/ml streptomycin. When plates reached a confluency of ~90%, they were passaged at 1:6 ratio by trypsinization (0.25% trypsin EDTA).

Generation of the Cas9-OmB1 cell line

OmB cells were co-transfected with the new OmEF1aCas9P2ApuroSB vector and the pCMV(CAT)T7-SB100 (Addgene # 34879) transposase expression vector into a 90% confluent, 10 cm cell culture plate of passage # 37 OmB cells. Ten µg total DNA [20:1 OmEF1aCas9P2ApuroSB: pCMV(CAT)T7-SB100] was first mixed with 940 µl Gibco Opti-MEM I Reduced Serum Media (ref # 31985-070) and then mixed with 30 µl Promega ViaFect (ref # E4982). This solution was incubated for 15 minutes and pipetted evenly over the 10 cm plate of cells. After 24 hours of incubation with the transfection complex solution, along with one confluent 10 cm plate of un-transfected Cas9 OmB cells as a control, all media was removed

from the plate and replaced with 8 ml of 2 µg/ml puromycin (Santa Cruz Biotech cat # sc-108071) L-15 selection media. The transfected cells were maintained on selection media for 25 days. At this point, colonies derived from single cells were isolated with 1 cm cloning disks and transferred to separated plates.

To test for genomic integration and transcription of the Cas9 transgene in one selected clone, DNA and RNA were isolated from 10 cm plates of both wild-type and Cas9 OmB cells using Invitrogen Purelink Genomic DNA Mini Kit (cat # K1820-01) and RNA Mini Kit (cat # 12183018A) respectively according to manufacturer provided protocols. Synthesis of cDNA from this RNA was performed using Invitrogen SuperScript IV First Strand Synthesis kit (ref # 18091050) with both random hexamer and oligoDT(20) primers. PCR reactions with a control primer pair (EF1aCas9RT_F X EF1aX2_R2) targeting endogenous EF1 alpha and two transgene targeting primer pairs of different lengths (EF1aCas9RT_F X EF1aCas9RT_R3 and EF1aCas9RT_F X EF1aCas9RT_R3) were performed on both genomic DNA and cDNA from wild-type and Cas9 OmB cells.

Selection of Cas9-OmB1 cells transfected with gRNA expression plasmid

Transfection complexes of each gRNA expression vector (10 µg plasmid DNA in 1 ml solution) were prepared and applied to nearly confluent 10 cm plates of Cas9-OmB1 cells as described in the previous section. After 2 days, all medium was removed from transfected plates and one un-transfected control plate of Cas9-OmB1 cells. Medium was replaced with 8 ml 500 µg/ml Hygromycin B (EMD Millipore cat# 400050) L-15 selection media in which plates were maintained for 7 days until all cells had detached from the surface of the control plate.

Template DNA Preparation for PCR of CRISPR treated cells

Due to the low quantity of cells remaining after hygromycin selection, the following cell lysis approach was used to obtain template DNA for subsequent PCR reactions. Each 10 cm plate of selected cells was rinsed with 3 ml PBS after all media was removed. Cells were scraped from the surface of the dish in fresh 1.5 ml PBS, transferred to a 1.5 ml tube and centrifuged for 5 minutes at 14000 rpm followed by removal of supernatant. Initially, cell pellets were re-suspended in 50 µl of distilled water followed by heat treatment in a boiling water bath for 10 minutes, centrifugation at 14000 rpm for 5 minutes and collection of supernatant which contained the template DNA. Due to inconsistent success of PCR reactions by this method, subsequently cell pellets were treated by incubation at 95˚C in 50 µl 25 mM NaOH followed by addition of 50 µl 40 mM Tris-HCL after which the resulting solution was used directly as a PCR template to generate test amplicons.

RSM analysis of Cas9 target cleavage

For each test amplicon from targeted cells and the corresponding control cell test amplicon, equivalent amounts of substrate DNA was prepared in 20.5 µl solution. These amplicon pairs were subjected to identical digestions with 2 µl of the NEB restriction enzyme matching recognition site with each specific amplicon and 2.5 µl of restriction enzyme buffer according to Supplementary Table S2. After 1 to 4 hour incubation time (each amplicon pair was incubated the same duration), digestions were loaded to 1.5% agarose gels, run at 200 V for 25 minutes and imaged.

Sequence analysis of individual amplicons

To validate and characterize individual mutation events, the *NANOS3* control target amplicon was selected for more detailed confirmatory analysis due to its high target cleavage efficiency by gel analysis and that it contained convenient SpeI and XmaI restriction sites near the 5’ and 3’ ends of the amplicon

respectively. The amplicon was digested with these two enzymes and ligated into pBluescript II SK(+) digested with XbaI and XmaI. New England Biolabs DH5 alpha competent *E. coli* (cat # C2987H) were transformed with 2 µl of the ligation reaction according to manufacturer's protocol. Each transformation reaction was plated onto 100 µg/ml carbencillin LB agar plates. From the resulting colonies, PCR was performed on 24 individual colonies using M13 forward and M13 reverse primers. Gel electrophoresis was performed on samples from each reaction to identify amplicons near the expected length which were purified and sent for Sanger sequencing.

TIDE analysis

Quantitative INDEL mutation frequency data was assessed using the TIDE webtool version 2.0.1[33]. Purified PCR amplicons encompassing the targeted sequence from control and CRISPR/Cas9 treated cell DNA were sent to the UC Davis core facility for Sanger sequencing. Resulting chromatogram sequence files (abi1) were uploaded to the TIDE website and analyzed using default settings except that the INDEL size range was set to + or – 25 bp.

Statistical analysis

All analysis was performed using Rstudio version 1.1.456. Relative Polymerase II promoter strength (2 replicates) and U6 promoter TIDE INDEL mutation percent (4 replicates) were analyzed by Tukey multiple comparisons test. TIDE INDEL mutation percent comparison between RNP and stable Cas9 methods was performed by standard student t-test.

Acknowledgements

This investigation was supported by the National Science Foundation (NSF) Grant IOS-1656371 and the US-Israel Binational Agricultural Research and Development Fund (BARD) Grant (IS-4800-15 R).

Author contributions statement

D.K. and J.H. conceived the experiments. J.H. conducted the experiments. J.H. analyzed the results. All authors reviewed the manuscript.

References

1. Hightower, L. E. & Renfro, J. L. Recent applications of fish cell culture to biomedical research. *J Exp Zool* **248**, 290–302 (1988).
2. Lakra, W. S., Swaminathan, T. R. & Joy, K. P. Development, characterization, conservation and storage of fish cell lines: a review. *Fish Physiol Biochem* **37**, 1–20 (2011).
3. Gardell, A. M., Qin, Q., Rice, R. H., Li, J. & Kultz, D. Derivation and osmotolerance characterization of three immortalized tilapia (Oreochromis mossambicus) cell lines. *PLoS One* **9**, e95919 (2014).
4. Carrel, A. & Burrows, M. T. CULTIVATION OF TISSUES IN VITRO AND ITS TECHNIQUE. *J. Exp. Med.* **13**, 387–396 (1911).
5. Okamoto, T., Sato, J. D., Barnes, D. W. & Sato, G. H. Biomedical advances from tissue culture. *Cytotechnology* **65**, 967–971 (2013).
6. Pitcher, J. A., Freedman, N. J. & Lefkowitz, R. J. G protein-coupled receptor kinases. *Annu Rev Biochem* **67**, 653–92 (1998).
7. Barretina, J. *et al.* The Cancer Cell Line Encyclopedia enables predictive modelling of anticancer drug sensitivity. *Nature* **483**, 603–607 (2012).
8. Mali, P. *et al.* RNA-guided human genome engineering via Cas9. *Science* **339**, 823–6 (2013).
9. Cong, L. *et al.* Multiplex genome engineering using CRISPR/Cas systems. *Science* **339**, 819–23 (2013).

10. Bogdanove, A. J. & Voytas, D. F. TAL effectors: customizable proteins for DNA targeting. *Science* **333**, 1843–1846 (2011).

11. Gaj, T., Gersbach, C. A. & Barbas, C. F. 3rd. ZFN, TALEN, and CRISPR/Cas-based methods for genome engineering. *Trends Biotechnol.* **31**, 397–405 (2013).

12. Jinek, M. *et al.* A programmable dual-RNA-guided DNA endonuclease in adaptive bacterial immunity. *Science* **337**, 816–21 (2012).

13. Chang, N. *et al.* Genome editing with RNA-guided Cas9 nuclease in zebrafish embryos. *Cell Res* **23**, 465–72 (2013).

14. Jao, L. E., Wente, S. R. & Chen, W. Efficient multiplex biallelic zebrafish genome editing using a CRISPR nuclease system. *Proc Natl Acad Sci U A* **110**, 13904–9 (2013).

15. Hisano, Y. *et al.* Precise in-frame integration of exogenous DNA mediated by CRISPR/Cas9 system in zebrafish. *Sci Rep* **5**, 8841 (2015).

16. Hoshijima, K., Jurynec, M. J. & Grunwald, D. J. Precise Editing of the Zebrafish Genome Made Simple and Efficient. *Dev Cell* **36**, 654–67 (2016).

17. Yeh, Y.-C. *et al.* Using CRISPR/Cas9-mediated gene editing to further explore growth and trade-off effects in myostatin-mutated F4 medaka (Oryzias latipes). *Sci. Rep.* **7**, 11435 (2017).

18. Chakrapani, V. *et al.* Establishing targeted carp TLR22 gene disruption via homologous recombination using CRISPR/Cas9. *Dev Comp Immunol* **61**, 242–7 (2016).

19. Edvardsen, R. B., Leininger, S., Kleppe, L., Skaftnesmo, K. O. & Wargelius, A. Targeted mutagenesis in Atlantic salmon (Salmo salar L.) using the CRISPR/Cas9 system induces complete knockout individuals in the F0 generation. *PLoS One* **9**, e108622 (2014).

20. Sakaguchi, K. *et al.* Comprehensive Experimental System for a Promising Model Organism Candidate for Marine Teleosts. *Sci. Rep.* **9**, 4948 (2019).

21. Elaswad, A. *et al.* Effects of CRISPR/Cas9 dosage on TICAM1 and RBL gene mutation rate, embryonic development, hatchability and fry survival in channel catfish. *Sci. Rep.* **8**, 16499 (2018).

22. Li, M. *et al.* Efficient and heritable gene targeting in tilapia by CRISPR/Cas9. *Genetics* **197**, 591–9 (2014).

23. Dehler, C. E., Boudinot, P., Martin, S. A. & Collet, B. Development of an Efficient Genome Editing Method by CRISPR/Cas9 in a Fish Cell Line. *Mar Biotechnol NY* **18**, 449–52 (2016).

24. Liu, Q., Yuan, Y., Zhu, F., Hong, Y. & Ge, R. Efficient genome editing using CRISPR/Cas9 ribonucleoprotein approach in cultured Medaka fish cells. *Biol. Open* **7**, (2018).

25. Schwarzer, J., Misof, B., Tautz, D. & Schliewen, U. K. The root of the East African cichlid radiations. *BMC Evol. Biol.* **9**, 186 (2009).

26. Betancur-R, R. *et al.* Phylogenetic classification of bony fishes. *BMC Evol. Biol.* **17**, 162 (2017).

27. Robinson-Rechavi, M. *et al.* Euteleost fish genomes are characterized by expansion of gene families. *Genome Res.* **11**, 781–788 (2001).

28. DeWitt, M. A., Corn, J. E. & Carroll, D. Genome editing via delivery of Cas9 ribonucleoprotein. *Methods San Diego Calif* **121–122**, 9–15 (2017).

29. Mosimann, C. *et al.* Ubiquitous transgene expression and Cre-based recombination driven by the ubiquitin promoter in zebrafish. *Development* **138**, 169–77 (2011).

30. Dahlberg, J. E. & Lund, E. The Genes and Transcription of the Major Small Nuclear RNAs. in *Structure and Function of Major and Minor Small Nuclear Ribonucleoprotein Particles* (ed. Birnstiel, M. L.) 38–70 (Springer Berlin Heidelberg, 1988). doi:10.1007/978-3-642-73020-7_2.

31. Schaub, M., Krol, A. & Carbon, P. Flexible zinc finger requirement for binding of the transcriptional activator staf to U6 small nuclear RNA and tRNA(Sec) promoters. *J. Biol. Chem.* **274**, 24241–24249 (1999).

32. Jiang, D. *et al.* CRISPR/Cas9-induced disruption of wt1a and wt1b reveals their different roles in kidney and gonad development in Nile tilapia. *Dev. Biol.* **428**, 63–73 (2017).

33. Brinkman, E. K., Chen, T., Amendola, M. & van Steensel, B. Easy quantitative assessment of genome editing by sequence trace decomposition. *Nucleic Acids Res.* **42**, e168–e168 (2014).

34. Helmrich, A., Bailey, G. S. & Barnes, D. W. Transfection of cultured fish cells with exogenous DNA. *Cytotechnology* **1**, 215–221 (1988).

35. Leisy, D. J., Lewis, T. D., Leong, J.-A. C. & Rohrmann, G. F. Transduction of cultured fish cells with recombinant baculoviruses. *J. Gen. Virol.* **84**, 1173–1178 (2003).

36. Friedenreich, H. & Schartl, M. Transient expression directed by homologous and heterologous promoter and enhancer sequences in fish cells. *Nucleic Acids Res.* **18**, 3299–3305 (1990).

37. Ma, J. *et al.* Efficient resistance to grass carp reovirus infection in JAM-A knockout cells using CRISPR/Cas9. *Fish Shellfish Immunol.* **76**, 206–215 (2018).

38. Bearzotti, M. *et al.* Gene expression following transfection of fish cells. *J. Biotechnol.* **26**, 315–325 (1992).

39. Iwai, T., Inoue, S., Kotani, T. & Yamashita, M. Production of transgenic medaka fish carrying fluorescent nuclei and chromosomes. *Zool. Sci* **26**, 9–16 (2009).

40. Mella-Alvarado, V., Gautier, A., Le Gac, F. & Lareyre, J. J. Tissue and cell-specific transcriptional activity of the human cytomegalovirus immediate early gene promoter (UL123) in zebrafish. *Gene Expr Patterns* **13**, 91–103 (2013).

41. Damdindorj, L. *et al.* A comparative analysis of constitutive promoters located in adeno-associated viral vectors. *PloS One* **9**, e106472 (2014).

42. Ruiz, S., Tafalla, C., Cuesta, A., Estepa, A. & Coll, J. M. In vitro search for alternative promoters to the human immediate early cytomegalovirus (IE-cMV) to express the G gene of viral haemorrhagic septicemia virus (VHSV) in fish epithelial cells. *Vaccine* **26**, 6620–6629 (2008).

43. Wang, B. *et al.* Functional Analysis of the Promoter Region of Japanese Flounder (Paralichthys olivaceus) β-actin Gene: A Useful Tool for Gene Research in Marine Fish. *Int. J. Mol. Sci.* **19**, (2018).

44. Hwang, G. L. *et al.* Isolation and characterisation of tilapia beta-actin promoter and comparison of its activity with carp beta-actin promoter. *Biochim Biophys Acta* **1625**, 11–8 (2003).

45. Hsu, C.-C. *et al.* Targeted methylation of CMV and E1A viral promoters. *Biochem. Biophys. Res. Commun.* **402**, 228–234 (2010).

46. Ran, F. A. *et al.* Genome engineering using the CRISPR-Cas9 system. *Nat Protoc* **8**, 2281–2308 (2013).

47. Zou, Z. *et al.* Construction of a highly efficient CRISPR/Cas9-mediated duck enteritis virus-based vaccine against H5N1 avian influenza virus and duck Tembusu virus infection. *Sci. Rep.* **7**, 1478 (2017).

48. Mehravar, M., Shirazi, A., Mehrazar, M. M., Nazari, M. & Banan, M. CRISPR/Cas9 System for Efficient Genome Editing and Targeting in the Mouse NIH/3T3 Cells. *Avicenna J. Med. Biotechnol.* **11**, 149–155 (2019).

49. Gandhi, S., Piacentino, M. L., Vieceli, F. M. & Bronner, M. E. Optimization of CRISPR/Cas9 genome editing for loss-of-function in the early chick embryo. *Dev. Biol.* **432**, 86–97 (2017).

50. Zenke, K. & Kim, K. H. Novel fugu U6 promoter driven shRNA expression vector for efficient vector based RNAi in fish cell lines. *Biochem Biophys Res Commun* **371**, 480–3 (2008).

51. Boonanuntanasarn, S., Panyim, S. & Yoshizaki, G. Usage of putative zebrafish U6 promoters to express shRNA in Nile tilapia and shrimp cell extracts. *Transgenic Res* **18**, 323–325 (2009).

52. Viswanatha, R., Li, Z., Hu, Y. & Perrimon, N. Pooled genome-wide CRISPR screening for basal and context-specific fitness gene essentiality in Drosophila cells. *eLife* **7**, (2018).

53. Munoz, I. M., Szyniarowski, P., Toth, R., Rouse, J. & Lachaud, C. Improved genome editing in human cell lines using the CRISPR method. *PloS One* **9**, e109752 (2014).

54. Dehler, C. E. *et al.* Viral Resistance and IFN Signaling in STAT2 Knockout Fish Cells. *J. Immunol. Baltim. Md 1950* **203**, 465–475 (2019).

55. Moriya, H. Quantitative nature of overexpression experiments. *Mol. Biol. Cell* **26**, 3932–3939 (2015).

56. Prolo, L. M. *et al.* Targeted genomic CRISPR-Cas9 screen identifies MAP4K4 as essential for glioblastoma invasion. *Sci. Rep.* **9**, 14020 (2019).

57. Liang, X. *et al.* Rapid and highly efficient mammalian cell engineering via Cas9 protein transfection. *J. Biotechnol.* **208**, 44–53 (2015).

58. Boonanuntanasarn, S., Panyim, S. & Yoshizaki, G. Characterization and organization of the U6 snRNA gene in zebrafish and usage of their promoters to express short hairpin RNA. *Mar. Genomics* **1**, 115–121 (2008).

This chapter has been submitted to *Genomics* journal and is currently under review.

Aim 2: Effects of CRISPR/Cas9 targeting of the *myo*-inositol biosynthesis pathway on hyper-osmotic tolerance of tilapia cells

Jens Hamar[a, 1], Avner Cnaani[b], Dietmar Kültz[a,*]

a Department of Animal Sciences, University of California Davis, Meyer Hall, One Shields Avenue, Davis, CA 95616, USA
b Department of Poultry and Aquaculture, Institute of Animal Sciences, Agricultural Research Organization, Volcani Center, P.O. Box 15159, Rishon LeZion 7528809, Israel

Keywords: CRISPR/Cas9, osmoregulation, salinity, myo-inositol, Oreochromis tilapia

Abstract

Myo-inositol is an important compatible osmolyte in vertebrates. This osmolyte is produced by the myo-inositol biosynthesis (MIB) pathway composed of myo-inositol phosphate synthase and inositol monophosphatase. These enzymes are among the highest upregulated proteins in tissues and cell cultures from teleost fish exposed to hyperosmotic conditions indicating high importance of this pathway for tolerating this type of stress. CRISPR/Cas9 gene editing of tilapia cells produced knockout lines of MIB enzymes and control genes. Metabolic activity decreased significantly for both MIB KO lines in hyperosmotic media. Trends of faster growth of the MIB knockout lines in isosmotic media and faster decline of MIB knockout lines in hyperosmotic media were also observed. These results indicate a decline in metabolic fitness but only moderate effects on cell survival when tilapia cells with disrupted MIB genes are exposed to hyperosmolality. Therefore MIB genes are required for full osmotolerance of tilapia cells.

1. Introduction

Aquatic animals are common subjects of scientific study with utility ranging from comparative models for fundamental biological processes to advancement of aquaculture expertise and technique. Euryhaline fishes are of exceptional interest due to their unique physiologies allowing them to adapt to a wide range of environmental salinities. These include tilapia of the economically important *Oreochromis* genus, which are some of the most commonly used animals in aquaculture worldwide. *Oreochromis niloticus* is the predominant tilapia aquaculture species due to its superior growth rate and feed conversion characteristics over other tilapia species. However, this species has only moderate salinity tolerance (0 to 40 ppt)[1,2] and an ideal growth rate between 0 and 8 ppt[3–5] making the geographical range in which it can be cultured limited by the availability of freshwater. In contrast, *O. mossambicus* has a much wider salinity tolerance (0 to 120 ppt)[6] and greater growth performance in salinities ranging from 14 to 35 ppt compared to freshwater[7,8]. Besides the potential for *O. mossambicus* use in brackish and seawater aquaculture, the high salinity tolerance of this species also makes it an ideal model organism for revealing the mechanisms of teleost salinity tolerance.

Overall salinity tolerance of vertebrates is a combination of multiple levels of hyper-osmotic (HO) responses. Systemic mechanisms integrate sensing of HO stress by the animal with extracellular signaling (endocrine and paracrine) and specialized epithelial effector organs and tissues[9] working collaboratively to maintain a relatively constant osmolality of the extracellular body fluids (ECF)[10–12]. This reduces the burden on cellular iono- and osmoregulatory mechanisms in support of protein and cellular mechanism function which is optimal within a narrow range of intracellular osmotic and ionic conditions[13]. Despite these systemic mechanisms, in extreme salinities or during acute exposure to elevated salinity, the plasma and ECF osmolality rises significantly[14–18]. This condition exposes all internal cells to HO stress, which disturbs intracellular fluid (ICF) osmotic and ionic homeostasis, necessitating a

compensatory cellular homeostasis response (CHR) [19]. This cellular level of osmoregulation is achieved by transport of ions in both directions to maintain optimal gradients across the cell membrane and avoid changes in cell volume[20].

HO ECF results in temporary cell shrinkage causing cytoskeletal, protein and DNA damage, cell cycle arrest, macromolecular crowding, and an elevated suboptimal inorganic ion concentration[19,21–24]. Cells quickly counteract this loss of cell volume by active uptake of inorganic ions in a process referred to as regulatory volume increase (RVI)[22,25] which alleviates the volume and crowding issues. However, the problem of elevated inorganic ion strength still persists requiring a secondary response to replace excessive inorganic ions with neutrally charged organic solutes referred to as compatible osmolytes[26,27]. Tilapia and many other vertebrate cells, such as cells of the mammalian kidney inner medulla, use *myo*-inositol (MI) as the primary compatible osmolyte[14,27,28]. MI can be obtained by either import from the ECF[29,30] or *de novo* synthesis through the *myo*-inositol biosynthesis pathway (MIB).

MIB is a two enzyme pathway originally characterized in yeast[31] and rat testis[32] in which glucose-6-phosphate is catalyzed by *myo*-inositol phosphate synthase (MIPS)[33] to *myo*-inositol-1-phosphate which is further metabolized to *myo*-inositol by inositol monophosphatase 1 (IMPA1)[34]. Subsequently this pathway has been found in a variety of eukaryotic taxa and cell types[27,35]. In multiple tissues of tilapia and European eel (*Anguilla anguilla*) exposed to hyper-osmotic conditions, MIPS and IMPA1.1 are among the highest upregulated proteins during HO indicating the high importance of this pathway for salinity acclimation[14,36,37]. This pattern is paralleled in an *O. mossambicus* brain cell line (OmB) demonstrating its' utility as a representative model for these studies[38,39]. Despite the strong correlation of MIPS and IMPA1.1 with hyper-osmotic stress treatment, causal relationships between these molecular changes and observed hyper-osmotic stress tolerance phenotypes have yet to be established. Alteration of genetic loci, such as by CRISPR/Cas9 gene targeting results in functional disruption of gene products in question and allows for evaluation of causal links to phenotypes of interest.

Since its initial characterization[40] and subsequent adaptation to use in eukaryotic cells[41,42] CRISPR/Cas9 gene targeting has emerged as a more robust tool for generating specific mutations in cultured cells compared to previous approaches[43,44]. By merely changing the variable ~20 base pair region of the guide RNA (gRNA) to be complimentary to the genomic DNA target sequence, the gRNA can complex with Cas9 nuclease and guide it to cleave that site. The repaired break from the cell's non-homologous end joining mechanism is often altered from the original sequence due to insertions or deletions of DNA fragments (INDELs) of varying nucleotide number and composition. With properly designed gRNAs this can result in disabled gene products through deletion of essential coding sequence or translation reading frameshift mutations. We previously developed a comprehensive CRISPR/Cas9 tool set customized to the tilapia cell culture model including a constitutive Cas9 expressing version of the OmB cell line (Cas9-OmB1) and gRNA expression/selection vectors using species specific promoters capable of disrupting targeted gene sequences with high efficiency[45]. Using this system, single CRISPR treated and selected cells can be propagated into *MIPS* and *IMPA1.1* mutant cell lines. If cell lines can be obtained with functional disruption of the target gene in at least one allele, the relationship between osmo-tolerance phenotypes and MIB enzymes can be evaluated. The objective of this study was to establish MIB enzyme mutant cell lines using CRISPR/Cas9 gene targeting with the hypothesis that complete knock-out (KO) or partial disruption of *MIPS* or *IMPA1.1* genetic loci will result in reduced tolerance of OmB cells to hyper-osmotic conditions.

2. Results

2.1. Guide RNA design and selection

Guide RNAs were designed and selected for the two genes of interests (*MIPS* and *IMPA1.1*) and three non-essential (NE) genes to be used as controls for any deleterious side effects of the general CRISPR/Cas9 process. The genes nanos C2HC-type zinc finger 3 (*NANOS3*), myostatin (*MSTN*), and

tyrosinase (*TYR*) were selected as the controls based on no expected physiological effect at the cellular level relevant to this study. Documented reports exist for each control gene in which CRISPR/Cas9 deletion was not lethal in tilapia at the whole organism level and were involved in pathways unimportant to cultured cells and unrelated to osmoregulation (ie fertility, muscle development, and pigmentation, respectively)[46–48]. To find highly conserved regions (assumed to be essential domains) the predicted amino acid (aa) sequence of each target gene product from Nile tilapia (*Oreochromis niloticus*, taxid:8128), Japanese medaka (*Oryzias latipes,* taxid:8090), and mummichog (*Fundulus heteroclitus*, taxid:8078) were aligned. The multi-species alignments yielded two conserved regions in the first third of the coding sequence. These motifs had lengths of 32 aa and 19 aa for MIPS (Fig. 1a) and 19 aa and 33 aa for IMPA1.1 (Fig. 1b). For myostatin and tyrosinase only one sufficient conserved region within the first third of the coding sequence was found. Therefore, an additional conserved region found downstream was used to increase the pool of candidate gRNAs. The genetic sequences corresponding to the conserved regions were input into the CRISPOR gRNA selection algorithm[49,50] to identify potential gRNA target sites with associated MIT specificity[51] and Doench efficiency scores[52]. For both *MIPS* and *IMPA1.1* the conserved regions corresponded to exons 3 and 4 of their respective genes (Fig. 1c and 1d) in which 8 distinct candidate gRNAs were identified with MIT specificity scores above 90 (a criteria chosen to minimize off-target effects). For both *MSTN* and *TYR* the two conserved regions were also located in exons 3 and 4 but only 6 suitable candidate gRNAs for found for myostatin and 5 for tyrosinase. Only one *TYR* (T1) and all 6 *MSTN* candidate gRNAs had MIT specificity scores above 90. For in vitro empirical testing of these candidates, the gRNA sequences were cloned into gRNA expression plasmids and used to treat Cas9-OmB cells followed by Sanger sequencing and TIDE analysis of PCR test amplicons from the targeted regions. The gRNAs selected for downstream KO protocols with the highest mutational efficiency (INDEL%) quantified by TIDE analysis are listed in Table 1. The top scoring gRNAs for *MIPS* were T1, T3, and T4 (TIDE scores

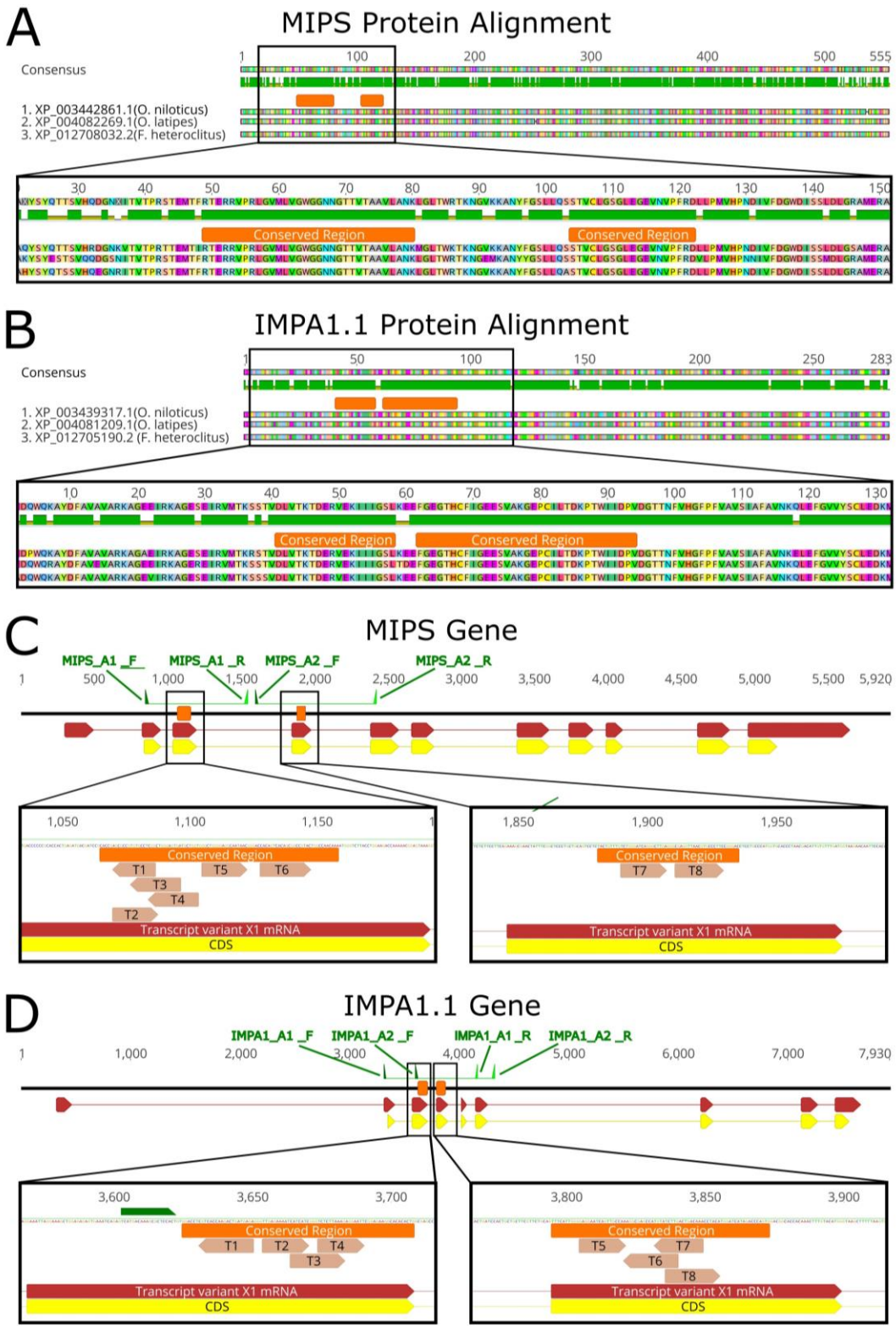

Fig. 1. Sequence maps and alignments used in the gRNA selection/screening process for MIPS and IMPA1.1. (A & B) Protein amino acid sequence alignments used to identify conserved regions for CRISPR/Cas9 targeting. (C & D) gene maps indicating genomic regions corresponding to protein conserved regions, locations of the eight candidate gRNAs screened for each gene, and PCR primer binding sites of test amplicons.

52.3, 50.3, 49.3, respectively). The top scoring gRNAs for *IMPA1.1* were T5, T6, and T7 (TIDE scores 33.7, 20.2, 40.2, respectively). The most efficient gRNAs for *MSTN* and *TYR* controls were T5 and T1 (TIDE scores 50.3 and 74.6, respectively). The previously validated *NANOS3* gRNA[45,47] was used as the third NE control gene target (TIDE score 53.5).

Gene Target	Target #	gRNA Sequence	Test Amplicon (Primers and Length)			Potential Off Targets	MIT Spec. Score	TIDE INDEL%
			Forward Primer	Reverse Primer	Size (bp)			
MIPS	T1	CCGAGGCACACGGCGCT	AACGTTCACATCAACAGCCC	AGTGGTAGTTTTCACATCCCGT	699	12	98	52.3
	T2	AGCGCCGTGTGCCTCGGC				17	96	32.9
	T3	TCACTCCCAGCCGAGGCACA				31	94	50.3
	T4	CCAGCATCACTCCCAGCCG				37	92	49.3
	T5	GGCTGGGGAGGCAATAAC				27	95	9.1
	T6	CACAGTCACAGCGGCCGTAC				19	97	27.4
	T7	TCTGGGATCAGGGCTTGA	GTATGTCCCCTGCTGCAGAA	GCTCCATTGCACTGCCTAGA	828	41	92	33.3
	T8	CGAGGTGAACGTGCCCTTC				9	97	9.4
IMPA1	T1	TCTCATCAGTCTTGGTGACG	GACTCTCCTAAGCAAGCCCC	CCACACCAAACTCCAGCTGA	854	53	92	9
	T2	GTTGAGAAAATCATCATC				45	91	4.6
	T3	CATCATCGGGTCTCTTAAAG				33	94	11.8
	T4	GTCTCTTAAAGAGGAATT				37	93	2.3
	T5	GAGGAGTCAGTTGCCAA	TCATGACAAAGCGCTCCACT	TACGGTGTCCATTTGCCAGT	721	20	96	33.7
	T6	CAAGATACATGGCTCGCCTT				10	97	20.2
	T7	TTTGTCAGTCAAGATACA				42	91	40.2
	T8	TCTTGACTGACAAACCTACA				40	92	19.5
Myostatin	T1	GGATCAGTACGACGTGCT	TGCGTTGGGTCCAGTAGTTC	TACGCGACTGGCTTGAAACT	723	15	98	38.8
	T2	GTGCTGGGAGATGACAAC				29	92	25.8
	T3	TATTGCACCAAAACGCTACA	GCAGGGCAGCGGATTAAAAG	TTCTTGCATCCACCTGGCTT	732	32	96	0
	T4	GTTGGCCTTGTAGCGTTT				16	96	0.1
	T5	CAAGGCCAACTATTGCTCTG				23	95	50.3
	T6	ACACTCCCCAGAGCAATAGT				24	95	45.1
Tyrosinase	T1	AGGCAGGGCTGATGAGGT	GGCACAGAGTCTTCCTGCTT	TGCCTCTCACTCCTACCCTC	828	85	91	74.6
	T2	CCTCTGTCTTCTCATCA				94	85	14.1
	T3	CTTCCATGATGAGAAGACAG				80	83	58.7
	T4	CATGATGTAGCAGGAATATT	TGTTCCACCAAGCTCACGTT	TGCCAGATCTCTTGTGCCTG	818	41	89	5.8
	T5	TACATCATGCTTTCATTGAC				53	89	5.2
Nanos3	NA	GCTGGTCTACGGATCCCAC	GCAAACGAACCAAAGCATGC	AATTGATGCAAAACCCGCCG	466	15	97	53.5

Table 1. Final gRNA sequences selected for downstream gene targeting experiments including test amplicon sizes with associated primer pairs, CRISPOR MIT specificity scores, and TIDE INDEL%.

2.2. KO clonal cell line genotyping

Treatment of Cas9-OmB1 cells was repeated with the selected gRNAs followed by low-density seeding into 96-well plates to isolate different genotypes which were propagated into clonal lines, defined in this context as an isolated cell pool with a single cell genotype or at least a stable dominant cell genotype. For each candidate clone, Sanger sequencing chromatograms were generated from PCR produced test

Clone ID	INDEL IDs	Net Δ	Allele Sequence	Freq (%)	Model R^2
MIPS T1		WT	ATCCGCACCGAGCGCCGTGTGCCTCGGCTGGGAGTGATGCTGGCGGGCTGGGGAGGCAAT		
Init.	(+1)	+1	ATCCGCACCGAGCAGCCGTGTGCCTCGGCTGGGAGTGATGCTGGCGGGCTGGGGAGGCAA	100.0	0.99
Post	(+1)	+1	ATCCGCACCGAGCAGCCGTGTGCCTCGGCTGGGAGTGATGCTGGCGGGCTGGGGAGGCAA	100.0	1.00
MIPS T3		WT	ATCCGCACCGAGCGCCGTGTGCCTCGGCTGGGAGTGATGCTGGCGGGCTGGGGAGGCAAT		
Init.	(+1)	+1	ATCCGCACCGAGCGCCGTGTGGCCTCGGCTGGGAGTGATGCTGGCGGGCTGGGGAGGCAA	92.2	0.98
	(-1)	-1	ATCCGCACCGAGCGCCGTGT-CCTCGGCTGGGAGTGATGCTGGCGGGCTGGGGAGGCAAT	07.8	
Post	(+1)	+1	ATCCGCACCGAGCGCCGTGTGGCCTCGGCTGGGAGTGATGCTGGCGGGCTGGGGAGGCAA	68.2	0.95
	(-1)	-1	ATCCGCACCGAGCGCCGTG-CGCTCGGCTGGGAGTGATGCTGGCGGGCTGGGGAGGCAAT	12.5	
	(-10)	-10	ATCCGCACCGAGCGCCGTGT----------GGAGTGATGCTGGCGGGCTGGGGAGGCAAT	09.8	
	(-4)	-4	ATCCGCACCGAGCGCCGTG----TCGGCTGGGAGTGATGCTGGCGGGCTGGGGAGGCAAT	09.5	
MIPS T4		WT	ATCCGCACCGAGCGCCGTGTGCCTCGGCTGGGAGTGATGCTGGCGGGCTGGGGAGGCAAT		
Init.	(-1)	-1	ATCCGCACCGAGCGCCGTGTGCCTCGG-TGGGAGTGATGCTGGCGGGCTGGGGAGGCAAT	100.0	1.00
Post	(-1)	-1	ATCCGCACCGAGCGCCGTGTGCCTCGG-TGGGAGTGATGCTGGCGGGCTGGGGAGGCAAT	100.0	0.77
IMPA1.1 T5		WT	GGGGAGGAGTCAGTTGCCAAAGGCGAGCCATGTATCTTGACTGACAAACCTACATGGATC		
Init.	(-2)	-2	GGGGAGGAGTCAGTT--CAAAGGCGAGCCATGTATCTTGACTGACAAACCTACATGGATC	100.0	1.00
Post	(-2)	-2	GGGGAGGAGTCAGTT--CAAAGGCGAGCCATGTATCTTGACTGACAAACCTACATGGATC	100.0	1.00
IMPA1.1 T6		WT	GGGGAGGAGTCAGTTGCCAAAGGCGAGCCATGTATCTTGACTGACAAACCTACATGGATC		
Init.	(-11)	-11	GGGGAGGAGTCAGTT----------GCCATGTATCTTGACTGACAAACCTACATGGATC	46.2	0.64
	(+25)	+25	GGGGAGGAGTCAGTTGCCAAAGTGATGTGAAAGGTACTATGTCCTCAGCGAGCCATGTAT	35.8	
	(-111)	-111	GGGGAGGAGTCAGTTGCCAAAG----------(-111)----------TAACT	10.1	
	(WT)	0	GGGGAGGAGTCAGTTGCCAAAGGCGAGCCATGTATCTTGACTGACAAACCTACATGGATC	07.9	
Post	(-11)	-11	GGGGAGGAGTCAGTT----------GCCATGTATCTTGACTGACAAACCTACATGGATC	55.2	0.89
	(+25)	+25	GGGGAGGAGTCAGTTGCCAAAGAGCAACTTTGGGAACTGTGTCCTCAGCGAGCCATGTAT	36.3	
	(-6)	-6	GGGGAGGAGTCAGTTGCCAA------GCCATGTATCTTGACTGACAAACCTACATGGATC	05.8	
	(WT)	0	GGGGAGGAGTCAGTTGCCAAAGGCGAGCCATGTATCTTGACTGACAAACCTACATGGATC	13.8	
IMPA1.1 T7		WT	GGGGAGGAGTCAGTTGCCAAAGGCGAGCCATGTATCTTGACTGACAAACCTACATGGATC		
Init.	(+1)	+1	GGGGAGGAGTCAGTTGCCAAAGGCGAGCCATGTAATCTTGACTGACAAACCTACATGGAT	50.6	0.98
	(-14)	-14	GGGGAGGAGTCAGTTGCCAAAGGCGAGCCATGT----------ACCTACATGGATC	49.4	
Post	(+1)	+1	GGGGAGGAGTCAGTTGCCAAAGGCGAGCCATGTAATCTTGACTGACAAACCTACATGGAT	48.2	0.96
	(-14)	-14	GGGGAGGAGTCAGTTGCCAAAGGCGAGCCATGT----------ACCTACATGGATC	51.8	
NANOS3		WT	GAAAGGGACACAAAACATCTCCTTCTTGGTTCTTCAGCCAGTGGGATCCGTAGACCAGCT		
Init.	(-1)	-1	GAAAGGGACACAAAACATCTCCTTCTTGGTTCTTCAGCCAGT-GGATCCGTAGACCAGCT	100.0	1.00
Post	(-1)	-1	GAAAGGGACACAAAACATCTCCTTCTTGGTTCTTCAGCCAGT-GGATCCGTAGACCAGCT	100.0	1.00
MSTN T5		WT	GGACTGGATTATTGCACCAAAACGCTACAAGGCCAACTATTGCTCTGGGGAGTGTGAGTA		
Init.	(-155,+1)	-154	GGACTGGATTATTGCACCAAAACGCTACA----------(-154)----------CGAGC	62.6	0.92
	(-41)	-41	GGA----------CTGGGGAGTGTGAGTA	18.4	
	(-21)	-21	GGACTGGATTATTGCACCAAAACGCTACAAGGCCAAC----------TA	10.3	
	(-29,+7)	-22	GGACTGGATTATTGCACCAAAACGCTACAAGGCCAACTATTGCTACTTGCC-(-22)-AA	08.8	
Post	(-154)	-154	GGACTGGATTATTGCACCAAAACGCTACAA----------(-154)----------GAGC	52.0	0.84
	(-41)	-41	GGA----------CTGGGGAGTGTGAGTA	24.9	
	(-21)	-21	GGACTGGATTATTGCACCAAAACGCTACAAGGCCAAC----------TA	15.6	
	(-22)	-22	GGACTGGATTATTGCACCAAAACGCTACA----------GTGTGAGTA	07.6	
TYR T1		WT	GATGGGTGGACGCAACTCCCTTAATCCCAACCTCATCAGCCCTGCCTCTGTCTTCTCATC		
Init.	(-83,+2)	-81	GATGGGTGGACGCAACTCCCTTAATCCCATT---------(-81)----------AGTGG	59.4	0.97
	(-1)	-1	GATGGGTGGACGCAACTCCCTTAATCCCAACC-CATCAGCCCTGCCTCTGTCTTCTCATC	40.6	
Post	(-81)	-81	GATGGGTGGACGCAACTCCCTTAATCCCA----------(-81)--------TCAGTGG	52.1	0.95
	(-1)	-1	GATGGGTGGACGCAACTCCCTTAATCCCAACC-CATCAGCCCTGCCTCTGTCTTCTCATC	47.9	

PAM Target Sequence Insertion - Deletion

Fig. 2. DECODR initial (Init.) and post experiment genotype output for each clone used in this study including the specific predicted INDELs present in each allele (INDEL ID), net bp change (Net Δ) , calculated relative allele frequency (Freq %), the R^2 model fit for each output and location relative to wild-type sequence (WT): PAM sequence (highlighted in red); gRNA sequence (highlighted in green); insertions (highlighted in blue); deletions (indicated by -).

amplicons encompassing the gRNA target site and initial genotyping was obtained by analysis of each chromatogram using the online DECODR algorithm[53]. Two clones from each gRNA were selected based on highest frameshift mutation%, purity of genotype (% composed of two or less predicted alleles), and model R^2 values for exposure to osmotic treatments. To ensure appropriate genotypes for the experimental design were maintained from initial screening throughout the duration of the experiment, including a cell line expansion process requiring several passages, genotyping was repeated post osmotic treatments. For each gRNA, the clone that maintained the highest percentage of frameshift knockout and most stable genotype was selected for downstream phenotyping analysis to form the MIPS KO, IMPA1.1 KO, and NE KO control experimental groups (for a total of 3 clones per group). Initial and post treatment genotypes of the selected clones are summarized in Fig. 2. The representative clone for MIPS T1, MIPS T4, IMPA1.1 T5, IMPA1.1 T7, and Nanos3 maintained the same clonal genotype without any detected wild-type (WT) or non-frameshift mutations. Clone MIPS T3 showed 1 bp shift in it's initial -1 INDEL and two additional minor alleles with -10 and -4 INDELS but still maintained 100% frameshift status. Clone IMPA1.1 T6 showed an initial dominant genotype consisting of -11 and +25 frameshift INDELs and two minor alleles of -111 INDEL and WT (frequency of 10.9% and 7.9% respectively). Post analysis showed the predicted genotype stayed mostly stable except the sequence of the +25 bp insertion changed and the -111 bp INDEL was replaced by a -6 INDEL. Clones MSTN T5 and TYR T1 yielded the same deletion INDEL sizes in both initial and post analysis (with only one -21 bp INDEL in MSTN T5 being non-frameshift) with minor shifts in predicted location and insertion sequence in some alleles.

2.3. Cell morphology

Phase contrast imaging was used to qualitatively assess morphology of clones from different target gene groups. Representative images of one clone from each experimental group in both hyper-osmotic and iso-osmotic media after 48 hours are shown in Fig. 3. In general MIPS (Fig. 3a) and IMPA1.1 KO cells

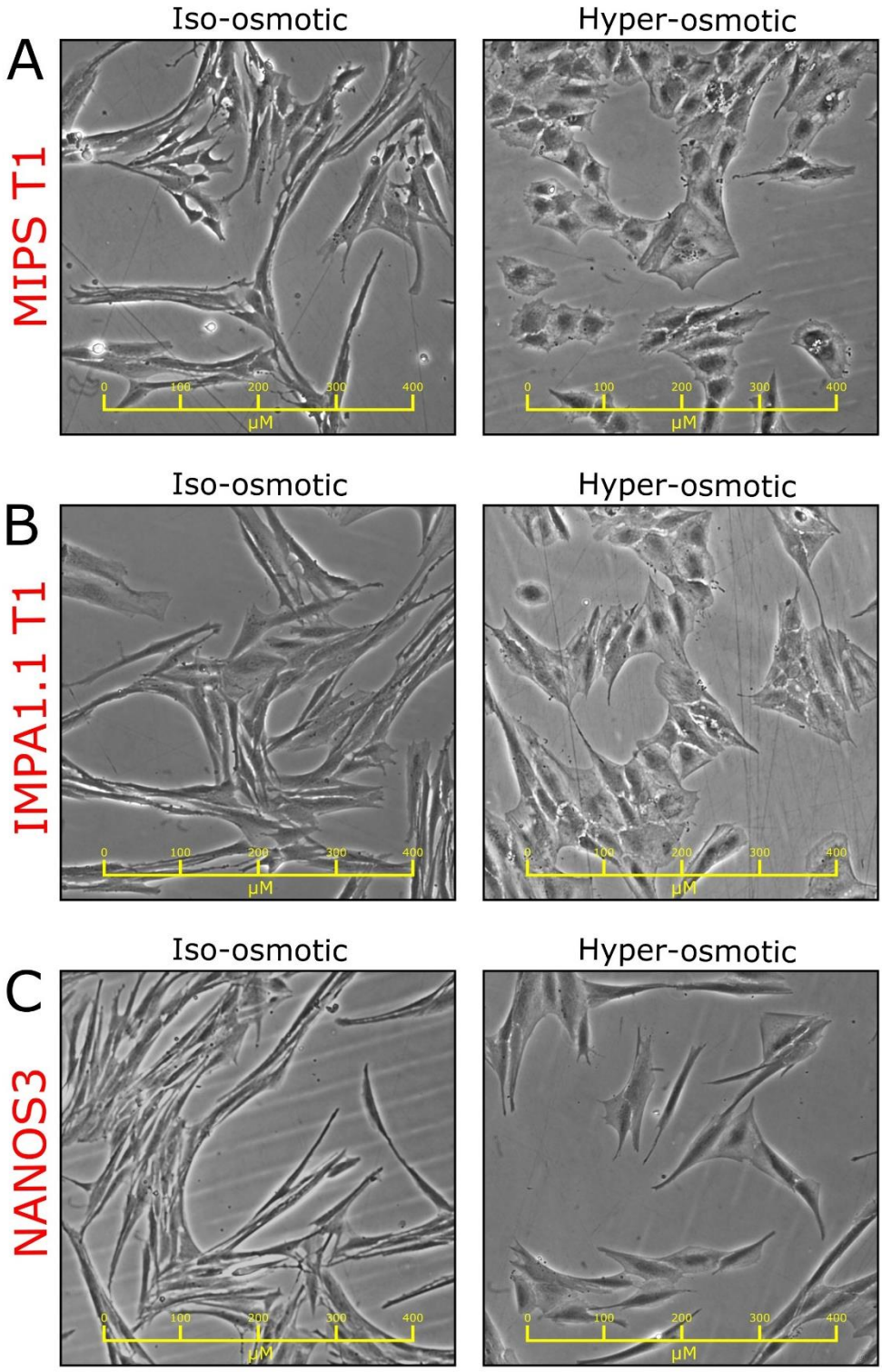

Fig. 3. Representative images of one clone from each experimental group: MIPS KO (A), IMPA1.1 KO (B), and NE KO control (C) in both iso-osmotic (315 mOsm) control and hyper-osmotic (650 mOsm) treatment conditions 96 hours after seeding.

(Fig. 3b) had a higher prevalence of cuboidal morphologies in HO media than the NE control group (Fig. 3c). This trend was more extreme in MIPS KO cells especially in clonal line MIPS T1.*2.4.*

2.4 Cell coverage area change over time

To assess the effect of MIB enzyme KO on HO tolerance, growth and/or survival was quantified by measurement of the 2-dimensional culture vessel sampling surface area covered by cells, or cell coverage area (CCA), of the same cell populations at different time intervals. Phase contrast tile scan images were generated for all target gene groups in both HO and iso-osmotic (IO) control media at each time interval. From these images, accurate CCA quantification was achieved using LASX software (Leica, see example in Fig. 4a and 4b). All replicates for all groups were counted and seeded at the same cell number but notable disparities in area were present at the first measurement (time point 0, 3 days after seeding) in both IO and HO experiments. This is likely due to a faster growth rate of the MIPS and IMPA1.1 KO groups over the controls in the 3 days between seeding and time point 0 when the first measurement and initiation of treatments was performed. Growth kinetics of the cell lines were modeled using the Verhults logistic growth equation due its utility in estimating growth parameters of cultured cells[54,55] and the resemblance of the plotted data (Fig. 4c and 4d) to this type of curve. R was used to generate non-linear logistic growth models with the coefficients K (carrying capacity) and r (intrinsic growth rate) that could be compared. In this context, carrying capacity (K) represents the maximum CCA that can be achieved based on density dependent factors such as limited resources (ie substrate, nutrients), inhibitory paracrine factors, and contact inhibition[56,57]. The MIPS KO group had the highest growth rate at 2.94e-02 with a 95% confidence interval (CI) of [5.00e-03, 5.73e-02], followed by IMPA1.1 KO at 2.91e-02 (95% CI [1.55e-02, 4.27e-02]) and NE control group at 2.11e-02 (95% CI [1.03e-02, 3.19e-02]). The NE control group had the highest maximum CCA at 1.93e+07 (95% CI [1.66e+07, 2.20e+07]) followed by IMPA1.1 KO at 1.84e+07 (95% CI [1.66e+07, 2.01e+07]), and MIPS KO at 1.51e+07 (95% CI [1.30e+07, 1.72e+07]). In the HO experiment, CCA of all groups gradually declined

in a linear pattern so survival was quantified by R generated linear regression models for each group where the model regression slopes represents change in CCA over time (ΔCCA/t). The NE control group had the highest ΔCCA/t (-3932 μm^2/hour) followed by IMPA1.1 KO (-5414 μm^2/hour) and MIPS KO (-5867 μm^2/hour). Although the ΔCCA/t slopes for MIPS KO and IMPA1.1 KO groups were notable steeper than controls, the difference for neither IMPA1.1 or MIPS KO group was statistically significant by ANOVA F-test at alpha level 0.05 with p-values of 0.8971 and 0.4250 respectively.

2.5. Viability and Metabolism

To assess the effect of MIPS and IMPA KO relative to NE KO control on metabolic activity during HO challenge, we quantified metabolism as relative luciferase units (RLU) using a 96-well plate metabolism-based viability assay of cells in either HO or IO conditions for different durations of 72 hour increments up to 288 hours. The metabolic assay was performed on live cells without requirement of cell harvest allowing a subsequent DNA content assay to be performed on the same cells. The metabolic activity values (RLU) were divided by the DNA concentrations of the same adherent cells normalizing RLU to the amount of cells present and decreasing variability caused by differences in cell content per well. This normalized data is reported as relative metabolic activity (RMA). In IO control conditions, mean IMPA1.1 RMA was notably lower than the other groups at the 216 and 288 hour time points (Fig. 4e) but repeated measures ANOVA yielded no significant difference between control and IMPA1.1 KO RMA ($p = 0.123$) and between control and MIPS KO RMA ($p = 0.896$). Under HO conditions and for all time points both MIPS KO and IMPA1.1 KO mean RMA was substantially lower than the NE KO control group (Fig. 4f). The overall difference was highly significant by repeated measures ANOVA; between control and IMPA1.1 KO groups ($p = 9.09e-06$), and between control and MIPS KO groups ($p = 8.08e-06$).

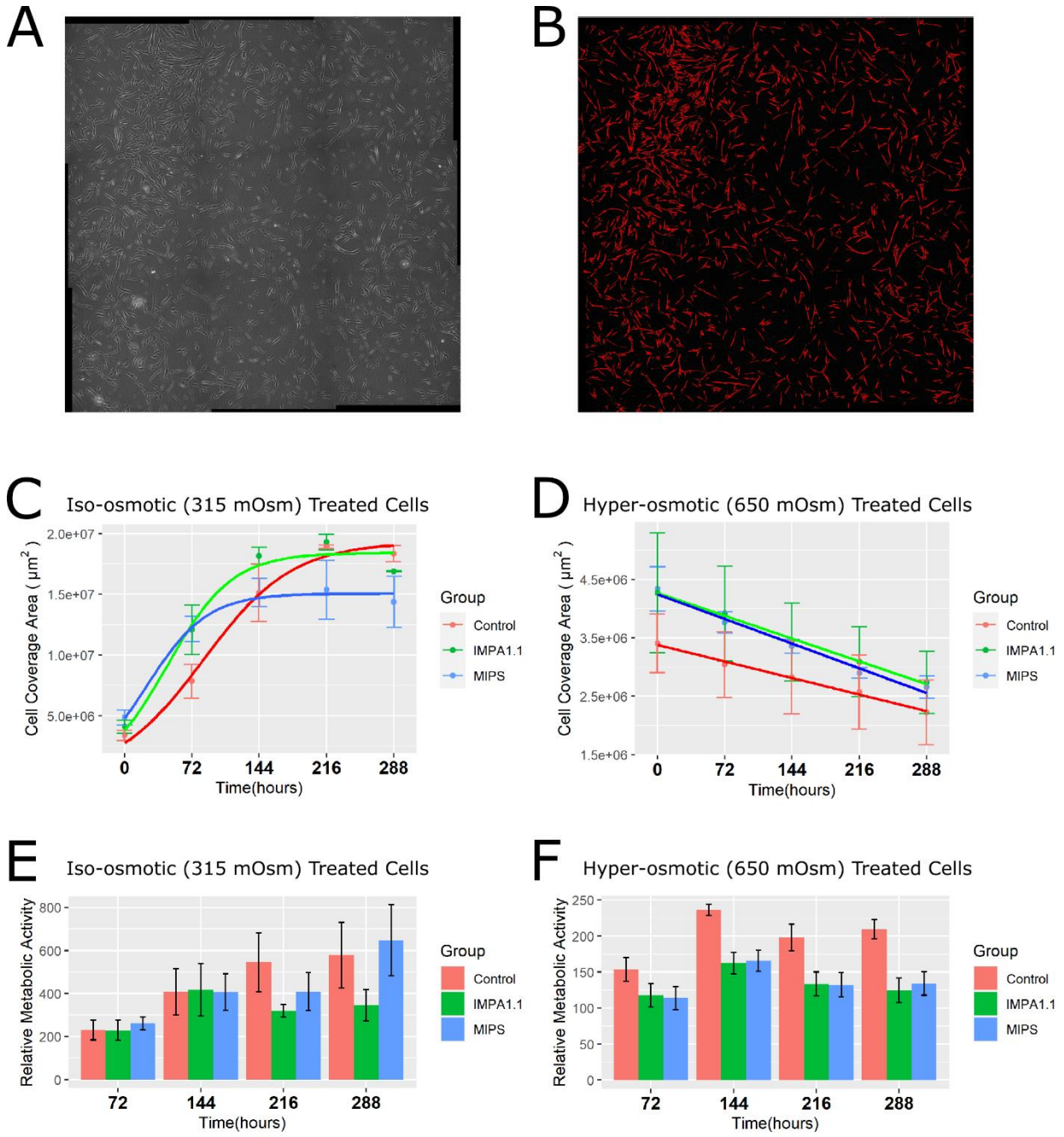

Fig. 4. Cell coverage area and relative metabolic activity phenotypes of clones in both iso-osmotic (315 mOsm) control and hyper-osmotic (650 mOsm) treatment conditions measured over time at 72 hour increments. (A & B) Representative images of automated image processing used to measure cell area of phase contrast image (A) with area automatically assigned and measured as cell shown in red (B). (C & D) Mean total area with standard error bars measured for each gene target group at each interval (points) with R generated regression lines representing ΔCCA/t (solid lines) for (C) cells in iso-osmotic media and (D) cells in hyper-osmotic media. (E & F) Mean relative metabolic activity (relative luciferase units/[DNA]) calculated for each gene target group at each interval for (E) cells in iso-osmotic media and (F) cells in hyper-osmotic media (both MIPS and IMPA1.1 KO groups were significantly different than control group by repeated measures ANOVA, with p values of 8.08e-06 and 9.09e-06 respectively).

3. Discussion

This study aimed to establish causality between the MIB pathway and cellular hyper-osmotic stress tolerance using CRISPR/Cas9 KO of the MIB enzymes and three control genes in the tilapia OmB cell line model. Calculated CRISPR/Cas9 gRNA selection and experimental design was optimized to account for potential weaknesses of this approach.

The wild-type CRISPR/Cas9 system used in this study has high mutational efficiency and thus, has the potential for off-target effects and erroneous phenotypes. This was evident in the considerable variation in growth rates and HO survival observed in this study between clones of the same target gene. Each gRNA has its own set of potential off-target effects so it is important to use multiple gRNAs to control for this variable. This enables dissection of common phenotypes that are independent of unknown off-target effects, which could be falsely attributed to target gene function. To account for these factors, we used an experimental design including clones from three different gRNA sequences for each group as replicates. Additionally, the transfection/antibiotic selection and general CRISPR/Cas9 process imposes significant stress and thus it was considered critical that the controls underwent the same processes. Multiple control genes were chosen to reduce the possibility that an unknown effect on osmotolerance of any particular control gene or gRNA skews the results of the study.

Using a high-throughput approach, this study was successful in obtaining many stable genotype clones with a single initial seeding per gRNA without repeated rounds of purification. For one gRNA per experimental group the best available clone did not possess the desired criteria of a single genotype with 100% frameshift mutation and had a minor contaminating genotype, some with non-frameshift or wildtype alleles. However, the gRNA selection process was restricted to highly conserved areas of the amino acid coding sequence (cds) maximizing the potential of a disrupted gene product even if the INDELs were non-frameshift. We are confident the frequency of wild-type alleles is low enough to not

affect the study outcome and adhering to the experimental design of higher replication from different gRNAs had greater value than removal of these isolates from the experiment.

Despite the weaknesses of CRISPR/Cas9 systems, through targeting of both *MIPS* and *IMPA1.1* with this stringent experimental design we were able to 1) detect consistent metabolic perturbance in HO conditions 2) establish that loss of either enzyme is not lethal and 3) disruption of the MIB pathway only minimally reduces osmotolerance of tilapia OmB cells in terms of survival.

The primary finding of this study is the effect on RMA by disruption of either IMPA1.1 or MIPS in HO conditions relative to the NE control lines. The RealTime-Glo assay used in this study quantifies metabolism indirectly through Luciferase catalysis of NanoLuc substrate which is only made available by reduction of the NanoLuc pre-substrate in metabolically active cells[58]. In this study, RMA was quantified based on the ability to metabolically reduce the presubstrate, which was diminished to a highly significant degree in both MIB KO groups. This effect is consistent with the viewpoint that intracellular MI accumulation is a primary mechanism to maintain a suitable ICF osmolyte milieu for cellular function during exposure to HO ECF. Loss of either enzyme would slow or limit this process impairing protein and enzyme function such as those involved in cellular metabolism. Correlation between robust induction of the MIB pathway and HO stress has been well established at both the cellular and whole animal levels with fold increases up to three orders of magnitude for mRNA[14,38] and two orders of magnitude for protein [39,59]. The RMA results from this study strongly support causality between the MIB enzymes and tolerance to HO exposure.

The results from the other metric used to assess HO tolerance (ΔCCA/t) followed the same trend with a faster rate of decline in the MIB KO lines than the control group. The MIPS KO group declined the fastest suggesting the loss of MIPS is more detrimental than IMPA1.1. A minor difference in contribution to HO tolerance between MIPS and IMPA1.1 could be due to the existence of other IMPA

isoforms. IMPA1.1 was selected for manipulation in this experiment because it is the predominant HO regulated IMPA isoform[14,36,38], but three other IMPA1 isoforms and IMPA2 exist in the *Oreochromis* tilapia genome[36]. These would be much less abundant in HO conditions but may impart some level of protection with what MI they can synthesize. Another possible contributor to a slight advantage to the IMPA1.1 KO lines is that the product of MIPS, inositol-3-phosphate, has some degree of compatible osmolyte function. Inositol phosphates are used as osmolytes in bacteria and archaea[60,61] for some of which the precursor is also inositol-3-phosphate[62] making this molecule a plausible early ancestral osmolyte to broad phylogenetic lineages. MIPS only has one isoform and thus loss of MIPS would result in reduction of both inositol-3-phosphate and myo-inositol.

Despite the predicted trend and considering how differentially regulated the MIB enzymes are in response to HO treatment, the magnitude of ΔCCA/t differences was much less than anticipated and not enough to yield statistical significance. The treatment of 650 mOsm was selected as a pre-determined near maximum but non-lethal tolerance threshold for OmB cells having the highest potential to detect differences in HO tolerance between the MIB KO and control cell lines with the expectation of immediate impact on cell survival. However, severe acute cell death exceeding the background in controls was not observed in MIB and IMPA1.1 KO clones of OmB cells. This indicates the ability to survive this condition is retained in the absence of an intact MIB pathway due to parallel and compensatory mechanisms. Similar to what had been observed previously in wildtype OmB cells[38] after exposure to 650 mOsm HO media, growth arrest was induced at the start of HO treatment followed by a gradual decline in CCA over time in all experimental groups. The results of the metabolic assays assures the methodology was effective in disrupting the pathway providing confidence in the experimental design and that the MIB pathway was not critical in cell survival in the study HO treatment conditions. Alternatively, conservation of strong HO regulated MIB may be due other selective advantages it imparts, such as improved metabolic efficiency under more moderate HO conditions. A less severe

osmotic stress such as 450 mOsm in which wild-type OmB cells are able to proliferate indefinitely, may improve the resolution of this method by allowing differences between MIB KO clones and controls to increase with time.

Many mechanisms could potentially contribute to compensate for a disrupted MIB pathway and survival in such an extreme level of HO challenge. In addition to alternative enzyme isoforms, we would expect transport from other MI reserves to buffer the deleterious effects of disrupted de novo MI synthesis. In mammalian cells, HO induced accumulation of MI relies on import of myo-inositol from the blood[29,30] through transporters such as the sodium/myo-inositol co-transporter (SMIT) [63,64] in contrast to tilapia cells in which the MIB pathway is highly differentially regulated dependent on the extracellular conditions. The *SMIT* gene is typically not present in stenohaline freshwater fish such as *Danio rerio* but has been identified in euryhaline fish genomes such as *Neogobius melanostomus* and *O. niloticus* tilapia[65]. OmB cells are thus potentially capable of upregulated de novo synthesis and import depending on the presence and activity of the enzyme and provided the ECF has sufficient MI to support it. The OmB cell culture media is supplemented with FBS which has a typical MI concentration in the range of 0.9-1 mM[66,67] (or 0.18 g/L). At 10% of the media combined with the 0.002 g/L of MI present in the base L-15 media would give a final MI concentration of about 0.02 g/L. This is in the same range of serum MI concentration that has been reported for Nile tilapia between 0.017 and 0.022 g/L[68,69] indicating sufficient MI for partial compensation of MIB disruption through transport. The ability to assimilate extracellular sources of MI into hyper-osmotic stress response systems is supported enhanced performance of Nile tilapia subjected to high salinities after dietary supplementation of myo-inositol [69,70] and *O. mossambicus* under long term salinity stress[71]. Development of defined media for fish cell lines that enable control of MI concentrations would facilitate evaluating the contribution of such extracellular solutes.

We must also consider that, although MI is the most prominent compatible osmolyte used by tilapia, it is but one component of a complex mixture of suitable osmolytes. A wide variety of osmolyte systems are used by fishes[26,72,73] exposed to osmotically challenging environments, often consisting of other sugars (e.g. sorbitol) and specific amino acids acids[74–77]. Utilization of taurine and glycine as compatible osmolytes have been reported in tissues of salinity challenged tilapia[78,79]. Strong upregulation of glutamine synthesis has been demonstrated in OmB cells treated with hyper-osmotic media[80]. OmB cells may be able to compensate for reduced availability of MI by increased utilization of alternative osmolytes.

In addition to the effects of MIB KO on HO response, prominent observations were made from the IO exposures as well. Despite steady growth equal to or exceeding the MIPS and Control groups, a near significant substantial reduction in the IMPA1.1 KO group metabolic activity was observed in the last two time points relative to the other groups. Why this effect was more severe compared to the MIPS KO group may be due to myo-inositol being the primary route for recycling this pathway. MI is catalyzed to glucuronic acid by myo-Inositol oxygenase (MIOX)[81,82] which was found to be present and differentially regulated in tilapia tissues under hyper-osmotic stress[83]. Glucuronic acid can be converted to available energy stores in the form of NADPH and sugars such as ribose-5-phosphate through the glucuronate-xylulose and pentose phosphate pathways (PPP)[84,85]. Ribose-5-phosphate, a product of the PPP, can enter glycolysis in the form fructose-6-phosphate through the actions of transketolase and transaldolase[86]. Since there is no known alternative for inositol-3-phosphate recycling back into energy utilization pathways other than through IMPA, a portion of glucose-6-phosphate may be made unavailable through conversion to inositol-3-phosphate by functional MIPS but disrupted/reduced IMPA activity. Even though there are multiple other IMPA variants potentially present and IMPA1.1 is known as the HO induced isoform, the significant metabolic perturbation by IMPA1.1 KO in IO conditions observed in this study indicates it is responsible for a large fraction of basal IMPA activity as well at least

in the OmB cell line. This seems inconsistent to that reported in Kalujnaia et al 2013[36], in which IMPA1.3 was the predominantly expressed isoform in tissues from freshwater acclimated tilapia. Nutritional importance of MI to fish is supported by numerous reports in which dietary supplementation with MI improves growth and metabolic activities in fish[87–90], so abnormalities from MIB enzyme KO in IO conditions would also be expected. In combination with the observation that the maximum CCA achieved by the MIPS KO group was much lower than that of the IMPA1.1 group, it appears the MIPS KO group has more accessible energy but is eventually limited by the availability of MI. Another noteworthy result from the earlier time points of IO conditions (before density dependent growth inhibition was a factor) is the apparent increased growth rate of both MIB KO groups compared to controls. This initially seems counterintuitive especially considering the metabolic impairment in the IMPA1.1 KO group. However, in addition to its role as a primary compatible osmolyte MI is active in intracellular signaling pathways. There is a minimum requirement for MI in animal cells[27,91], but elevated MI can act as a growth and cell-cycle suppressor. Exogenous application of MI or overexpression of MIB enzymes can have inhibitory effects on in vitro cultured cells[92–94]. Additionally, MI and it's derivative inositol hexaphosphate have well documented suppressive effects on cancer cell proliferation[95,96]. The pro-proliferative signaling pathways negatively affected by these molecules include PI3K/Akt, Wnt/β-catenin, and Notch1[97,98]. This would explain how a reduction in MI in the MIB KO groups would lead to increased growth rates in IO conditions and suggests a similar role for MI of cell cycle suppression in tilapia cells during HO stress.

The ability of the cells to survive in extreme osmolality despite disruption of such a major pathway illustrates the combinatorial nature of the osmotic stress response. The complexity of the compatible osmolyte systems, CHR, and CSR in general provides many ways the cells can compensate for the loss of one gene. Much work has been done investigating the relationship between salinity tolerance and growth in tilapia and strains with high salinity tolerance and economic traits are in high demand in the

aquaculture industry. Compatible osmolytes, the CHR, and CSR are critical components of whole animal salinity tolerance. Understanding how major pathways such as MIB contribute and interact with the overall response network will identify key gene targets to help guide selective breeding or gene-editing approaches in the production of improved genetics stocks of this economically important animal.

In conclusion, the current study demonstrates that loss of MIB pathway function causes significant metabolic disruption specific to HO response but can be effectively compensated by tilapia cells. Although changes in phenotype are evident, the effect of functional MIB pathway KO on cell survival is much smaller than originally hypothesized when considering the large magnitude of HO induction of the MIB enzymes. These results indicate, at least in the cell culture model described in this study, that the MIB pathway has a moderate impact on HO survival and the ability to persist in severe and/or prolonged osmotic stress is imparted by not just a single pathway but buffered robustly by other compensatory pathways. The loss of MIPS is likely the most detrimental of the two MIB enzymes despite greater metabolic perturbance shown by IMPA1.1 KO in IO conditions. Considering MIPS KO has apparently less routes for compensation and the specific effect of IMPA1.1 KO on HO response may be difficult to discern from its general metabolic effects, MIPS KO may also make a better model for overall MIB KO disruption. Our study provides the groundwork for future research aimed at identifying more specifics on the role of MI and other compensatory mechanisms utilized for osmotolerance in the IMPA1.1 and MIPS KO lines, including the roles of SMIT and MIOX, alternative compatible osmolyte systems (such as taurine import or glutamine synthesis), and the effects of HO conditions below 650 mOsm and defined media (such as inositol free media).

4. Materials and Methods

4.1. Guide RNA design and selection

For each target gene, the amino acid sequence of the corresponding protein for *Oreochromis niloticus* (MIPS XP_003442861.1, IMPA1.1 XP_003439317.1, MSTN XP_003458880.1, TYR XP_003441635.1), *Oryzias latipes* (MIPS XP_004082269.1, IMPA1.1 XP_004081209.1, MSTN NP_001188428.1, TYR XP_020564474.1), and *Fundulus heteroclitus* (MIPS XP_012708032.2, IMPA1.1 XP_012705190.2, MSTN XP_012736594.1, TYR XP_036005521.1), were aligned using global alignment with free end gaps in Genious 11.0.3 (Biomatters, https://www.geneious.com). Conserved protein regions were selected with a preference to those within the first 3rd of the amino acids sequence to maximize the effect of frameshift mutations. The corresponding nucleotide sequences of the selected conserved regions were copied into the online CRISPOR (version 5.01)[49] gRNA selection tool using *O. niloticus* as the reference genome. The generated gRNA sequences and corresponding scores for all conserved regions were copied into a single spreadsheet and sorted by MIT specificity score from highest to lowest. Up to 8 of the highest scoring gRNAs were selected for in vitro mutational efficiency testing excluding those with Doench efficiency scores less than 30. When possible, selected gRNAs were trimmed to no lower than 18 bp to make the initial G from the TU6m transcription start site (TSS) match the substrate DNA sequence to decrease target sequence/substrate DNA mismatch and potential associated off-target effects[99,100].

4.2. Cell culture maintenance

Unless otherwise stated, cells were maintained at standard OmB cell maintenance conditions consisting of ambient CO_2 and 26˚C in OmB culture medium (L-15 medium containing 10% fetal bovine serum, 100 U/ml penicillin, and 100 mg/ml streptomycin). When plates reached a confluency of ~ 90%, they were passaged by trypsinization with 1 ml (0.25% trypsin EDTA).

4.3. Cloning and gene targeting

Selected candidate gRNAs for each target were cloned into TU6m-gRNAscaffHygroR (Addgene# 165485) plasmid, transfected into Cas9-OmB1 tilapia cells, followed by hygromycin B selection and template DNA preparation as described previously[45]. Slight modifications were made as follows: 1.2 µg plasmid DNA in 10 µl Qiagen EB buffer and 116 µl of serum free L-15 media was mixed with 4 µl Promega ViaFect according to manufacturer's protocol; the resulting transfection solution was pipetted into 3.5 cm wells confluent with Cas9-OmB1 cells of a 6-well plate; two days after transfection, wells were treated with 2 ml 500 µg/ml Hygromycin selective media for 6 days.

4.3. Candidate gRNA mutation efficiency screening

Template DNA from CRISPR treated wells was prepared according to the NaOH extraction method described previously[45] except cells were scraped into 1 ml of PBS. For each DNA isolate PCR reactions were prepared by mixing 20 µl template DNA with 25 µl Promega PCR Master Mix and 2.5 µl of each primer according to Table 1. Primers were designed to produce amplicons of 600-800 base pairs (bp) with the forward primer ~200 bp from target sequence. Amplicons from CRISPR treated cells and control wild-type OmB DNA were sequenced from the forward primer at the UC Davis core facility for Sanger sequencing. Quantitative INDEL efficiencies were obtained by upload of the resulting chromatogram sequence files (ab1) to TIDE webtool version 2.0.1.

4.4. Generation and genotyping of KO clonal cell lines

The three gRNAs for each treatment group were selected for generation of target gene KO clonal cell lines: the three highest TIDE INDEL efficiency scoring gRNAs for IMPA1.1 and MIPS, the single gRNA with the highest TIDE INDEL efficiency scores for myostatin and tyrosinase, and the nanos3 target used previously[45]. The procedure for gene targeting from section 4.3 was repeated using these gRNA targeting plasmids. For each well, the cells remaining after hygromycin selection were rinsed with 1 ml

PBS then trypsinized for 5 minutes with 500 µl 0.25% trypsin EDTA at 26°C. Trypsin was neutralized with 1.5 ml culture followed by addition of 48 ml media to make a dilute 50 ml cell suspension. Cell suspension was distributed to five 96-well plates, 100 µl per well. Over the course of 6 weeks, visual screening was performed to identify wells containing only one colony derived from one central site (referred to as candidate clones at this point). Once identified wells had reached at least 25% confluency, the well was split into two new wells (the same well location of two separate 96-well plates, one for propagation and one for genotyping) by removing media and rinsing with 200 µl PBS, trypsinization for 10 minutes with 20 µl 0.25% trypsin EDTA at 26°C, then addition of 180 µl culture media in which the resulting 200 µl was pipette mixed and transferred 100 µl each to the two new wells. When wells of the genotyping 96-well plate reached a confluency of at least 25% they were harvested for template DNA using a modified version of the NaOH method: media was removed from each well followed by a rinse with 100 µl 25 mM NaOH; another 50 µl 25 mM NaOH was added to each well and incubated for 5 minutes at room temperature; this 50 µl solution was pipette mixed in the well and transferred to a 1.5 ml tube followed by incubation at 95°C for 30 minutes; final template DNA was obtained by neutralization with addition of 50 µl 40 mM Tris-HCl to each solution. For each template, PCR and sequencing were performed as described in section 4.3. Allele sequence and relative frequency present in each candidate clone were estimated by upload of the chromatograms and gRNA sequences to DECODR version 3.0[53]. For downstream phenotyping experiments, clones were selected with priority based on KO due to frameshift mutation in all alleles, purity of clone (2 or less alleles present), and highest R^2 value for DECODR model fit.

4.5. Propagation and maintenance of KO clonal cell lines

Once selected wells from genotyping screen were near 100% confluent, the trypsinization procedure for 96-well plate wells described above was repeated except the entire 200 µl cell suspension was transferred to a 2.5 cm well of a 12-well plate followed by addition of 1 ml culture media. Once a 12-

well plate well was near 100% confluent, the well was rinsed with PBS and trypsinized for 10 minutes with 200 µl 0.25% trypsin EDTA at 26°C followed by addition of 1.8 ml culture media. The resulting 2 ml cell suspensions were transferred to 10 cm culture dishes with 6 ml culture media to bring final volume to 8 ml. At this point clonal lines were propagated using standard OmB cell maintenance procedures.

4.6. Hyper-osmotic stress treatments

Each genotype was passaged, counted using Hausser Scientific Hemacytometer (cat#1483) and plated into 12-well plates (2 wells each, 10000 cells per well), 6-well plates (2 wells each, 37500 cells per well) and five replicate white opaque walled imaging 96-well plates (four wells per genotype, 1500 cells per well). Treatment media, 650 mOsm hyper-osmotic media or 315 mOsm iso-osmotic control media, were prepared by addition of NaCl to OmB culture media. Three days after plating, media was removed from all wells and replaced with treatment media, one well per treatment per genotype for 6-well plates and two wells per treatment per genotype for each replicate 96-well plate.

4.7. Morphology and area quantification

All images were acquired using a Leica DMi8 inverted microscope in phase contrast mode. For morphology assessment 12-well plates were imaged every 24 hours at 20X magnification for the first 3 days of treatment, then every 48 hours. For area quantification, the center 20% of the same 6-well plates was imaged as a composite tile scan immediately before (time point 0) and every 3 days after for a total duration of 12 days. Media was filtered and returned to wells before imaging to remove interference by detached cells and debris. Individual tiles were imaged at 5X magnification with an exposure duration of 50.14 ms and intensity of 89. Total cell area was quantified using LASX Navigator analysis tool (Leica Application Suite X Version 3.0.4 software) with Find black detail Image Processing Pre-filter (size setting 10 and Auto Contrast selected) and Otsu global threshold.

4.8. Relative metabolic activity quantification

At each of the above time points, two plate assays were performed on one of the replicate 96-well plates. Cellular metabolic activity was quantified as luminescence (RLU) using the non-cytotoxic Promega RealTime-Glo MT Cell Viability Assay (Ref# G9711) and Promega GloMax Navigator luminometer (after 30 minutes incubation) according to manufacturer's protocol which allowed measurement with cells left in adherent state. After completion of the first assay, media was removed from all wells and plates were frozen in -80°C freezer for at least 24 hours. DNA concentration was determined on the same wells using Invitrogen CyQUANT Cell Proliferation Assay Kit (Cat #C7026) according to manufacturer's protocol (with individual standard curve performed on each plate) and measured on Biotek Synergy HT plate reader using Gen5 Version 2.03.1 software with 485/528 excitation/emission wavelength settings. Relative metabolic activity for each well was calculated by dividing the luminescence (RLU) by the DNA concentration (ng/ml).

4.9. Statistical Analysis

All mathematical modelling and statistical analysis were performed using Rstudio version 2021.09.1. Individual comparisons of change in relative metabolic activity over time between MIPS KO or IMPA1.1 KO and the NE control KO group were made using repeated measures ANOVA. Comparisons of ΔCCA/t between groups in IO conditions was performed by non-linear modeling using the Verhults logistic growth equation[54] except substituting A for N (population):

$$A(t) = \frac{K}{1 + \left(\frac{K - A_0}{A_0}\right) e^{-rt}}$$

Where a = CCA (μm^2), t = time (hours), K = carrying capacity (μm^2), A_0 = initial CCA (μm^2) at time point zero, and r = intrinsic growth rate (μm^2/hour). For each experimental group, the nls() function was used to fit a model to the data set and calculate coefficients. The 95% confidence intervals for each

coefficient were calculated using the confint2() function from the "nlstools" package. For the HO experiments, the lm() function was used to fit linear models and calculate regression slopes. Statistical significance (F-test) of differences in regression slopes (the group and time interaction effect) between groups was evaluated by ANOVA performed on combined data sets of each MIB group and the control group. R code and details in model calculation available in supplemental material. All data reported and shown in figures are represented as means ± standard errors.

Acknowledgements

This study was funded by National Science Foundation Grant IOS- 2209383 and BARD grant IS-5358-21

References

1. Al-Amoudi, M. M. Acclimation of commercially cultured *Oreochromis* species to sea water — an experimental study. *Aquaculture* **65**, 333–342 (1987).
2. Schofield, P. J., Peterson, M. S., Lowe, M. R., Brown-Peterson, N. J. & Slack, W. T. Survival, growth and reproduction of non-indigenous Nile tilapia, *Oreochromis niloticus* (Linnaeus 1758). I. Physiological capabilities in various temperatures and salinities. *Mar. Freshw. Res.* **62**, 439–449 (2011).
3. Likongwe, J. S., Stecko, T. D., Stauffer Jr, J. R. & Carline, R. F. Combined effects of water temperature and salinity on growth and feed utilization of juvenile Nile tilapia *Oreochromis niloticus* (Linneaus). *Aquaculture* **146**, 37–46 (1996).
4. de Alvarenga, E. R. *et al.* Moderate salinities enhance growth performance of Nile tilapia (*Oreochromis niloticus*) fingerlings in the biofloc system. *Aquac. Res.* **49**, 2919–2926 (2018).
5. Azevedo, R. V. de *et al.* Responses of Nile tilapia to different levels of water salinity. *Lat. Am. J. Aquat. Res.* **43**, 828–835 (2015).

6. Stickney, R. R. Tilapia tolerance of saline waters: a review. *Progress. Fish-Cult.* **48**, 161–167 (1986).
7. Payne, A. L., Ridgway, J. & Hamer, J. L. The influence of salt (NaCl) concentration and temperature on the growth of *Oreochromis spilurus spilurus*, *O. mossambicus* and a red tilapia hybrid. in *The Second International Symposium on Tilapia in Aquaculture* vol. 15 481–487 (ICLARM Conference Proceeding, 1988).
8. Sparks, R. T. *et al.* Effects of environmental salinity and 17α-methyltestosterone on growth and oxygen consumption in the tilapia, *Oreochromis mossambicus*. *Comp. Biochem. Physiol. B Biochem. Mol. Biol.* **136**, 657–665 (2003).
9. Takei, Y. & McCormick, S. D. 3 - Hormonal Control of Fish Euryhalinity. in *Fish Physiology* (eds. McCormick, S. D., Farrell, A. P. & Brauner, C. J.) vol. 32 69–123 (Academic Press, 2012).
10. Beaufrère, H. *et al.* Plasma osmolality reference values in African grey parrots (*Psittacus erithacus erithacus*), Hispaniolan Amazon Parrots (*Amazona ventralis*), and Red-fronted Macaws (*Ara rubrogenys*). *J. Avian Med. Surg.* **25**, 91–96 (2011).
11. Larsen, E. H. *et al.* Osmoregulation and excretion. *Compr. Physiol.* **4**, 405–573 (2014).
12. Waymouth, C. Osmolality of mammalian blood and of media for culture of mammalian cells. *In Vitro* **6**, 109–127 (1970).
13. Somero, G. N. Protons, osmolytes, and fitness of internal milieu for protein function. *Am. J. Physiol.* **251**, R197-213 (1986).
14. Gardell, A. M. *et al.* Tilapia (*Oreochromis mossambicus*) brain cells respond to hyperosmotic challenge by inducing *myo*-inositol biosynthesis. *J. Exp. Biol.* **216**, 4615–4625 (2013).
15. Lema, S. C., Carvalho, P. G., Egelston, J. N., Kelly, J. T. & McCormick, S. D. Dynamics of gene expression responses for ion transport proteins and aquaporins in the gill of a euryhaline pupfish during freshwater and high-salinity acclimation. *Physiol. Biochem. Zool. PBZ* **91**, 1148–1171 (2018).

16. Christensen, E. A. F., Svendsen, M. B. S. & Steffensen, J. F. Plasma osmolality and oxygen consumption of perch *Perca fluviatilis* in response to different salinities and temperatures. *J. Fish Biol.* **90**, 819–833 (2017).

17. Yamaguchi, Y. *et al.* Acute salinity tolerance and the control of two prolactins and their receptors in the Nile tilapia (*Oreochromis niloticus*) and Mozambique tilapia (*O. mossambicus*): A comparative study. *Gen. Comp. Endocrinol.* **257**, 168–176 (2018).

18. Root, L. *et al.* Nonlinear effects of environmental salinity on the gill transcriptome versus proteome of *Oreochromis niloticus* modulate epithelial cell turnover. *Genomics* **113**, 3235–3249 (2021).

19. Kültz, D. The combinatorial nature of osmosensing in fishes. *Physiol. Bethesda Md* **27**, 259–275 (2012).

20. Hoffmann, E. K., Lambert, I. H. & Pedersen, S. F. Physiology of cell Volume regulation in vertebrates. *Physiol. Rev.* **89**, 193–277 (2009).

21. Di Ciano-Oliveira, C., Thirone, A. C. P., Szászi, K. & Kapus, A. Osmotic stress and the cytoskeleton: the R(h)ole of Rho GTPases. *Acta Physiol.* **187**, 257–272 (2006).

22. Lang, F. *et al.* Functional significance of cell volume regulatory mechanisms. *Physiol. Rev.* **78**, 247–306 (1998).

23. Dmitrieva, N. I., Michea, L. F., Rocha, G. M. & Burg, M. B. Cell cycle delay and apoptosis in response to osmotic stress. *Comp. Biochem. Physiol. A. Mol. Integr. Physiol.* **130**, 411–420 (2001).

24. Dmitrieva, N. I., Cai, Q. & Burg, M. B. Cells adapted to high NaCl have many DNA breaks and impaired DNA repair both in cell culture and in vivo. *Proc. Natl. Acad. Sci. U. S. A.* **101**, 2317–2322 (2004).

25. Chamberlin, M. E. & Strange, K. Anisosmotic cell volume regulation: a comparative view. *Am. J. Physiol.* **257**, C159-173 (1989).

26. Yancey, P. H., Clark, M. E., Hand, S. C., Bowlus, R. D. & Somero, G. N. Living with water stress: evolution of osmolyte systems. *Science* **217**, 1214–1222 (1982).

27. Michell, R. H. Inositol derivatives: evolution and functions. *Nat. Rev. Mol. Cell Biol.* **9**, 151–161 (2008).

28. Bagnasco, S., Balaban, R., Fales, H. M., Yang, Y. M. & Burg, M. Predominant osmotically active organic solutes in rat and rabbit renal medullas. *J. Biol. Chem.* **261**, 5872–5877 (1986).

29. Nakanishi, T., Turner, R. J. & Burg, M. B. Osmoregulatory changes in myo-inositol transport by renal cells. *Proc. Natl. Acad. Sci. U. S. A.* **86**, 6002–6006 (1989).

30. Su, X. B., Ko, A.-L. A. & Saiardi, A. Regulations of *myo*-inositol homeostasis: Mechanisms, implications, and perspectives. *Symp. Issue 2022* **87**, 100921 (2023).

31. Chen, I. W. & Charalampous, F. C. Biochemical studies on inositol. 8. Purification and properties of the enzyme system which converts glucose 6-phosphate to inositol. *J. Biol. Chem.* **240**, 3507–3512 (1965).

32. Eisenberg, F. J. D-myoinositol 1-phosphate as product of cyclization of glucose 6-phosphate and substrate for a specific phosphatase in rat testis. *J. Biol. Chem.* **242**, 1375–1382 (1967).

33. Maeda, T. & Eisenberg, F. J. Purification, structure, and catalytic properties of L-*myo*-inositol-1-phosphate synthase from rat testis. *J. Biol. Chem.* **255**, 8458–8464 (1980).

34. Chen, I. W. & Charalampous, F. C. Biochemical studies on inositol: X. Partial purification of yeast inositol 1-phosphatase and its separation from glucose 6-phosphate cyclase. *Arch. Biochem. Biophys.* **117**, 154–157 (1966).

35. Loewus, M. W. & Loewus, F. A. *myo*-Inositol-1-Phosphatase from the Pollen of *Lilium longiflorum* Thunb. *Plant Physiol.* **70**, 765–770 (1982).

36. Kalujnaia, S. *et al.* Seawater acclimation and inositol monophosphatase isoform expression in the European eel (*Anguilla anguilla*) and Nile tilapia (*Orechromis niloticus*). *Am. J. Physiol. Regul. Integr. Comp. Physiol.* **305**, R369-384 (2013).

37. Sacchi, R., Li, J., Villarreal, F., Gardell, A. M. & Kültz, D. Salinity-induced regulation of the *myo*-inositol biosynthesis pathway in tilapia gill epithelium. *J. Exp. Biol.* **216**, 4626–4638 (2013).

38. Gardell, A. M., Qin, Q., Rice, R. H., Li, J. & Kültz, D. Derivation and osmotolerance characterization of three immortalized tilapia (*Oreochromis mossambicus*) cell lines. *PloS One* **9**, e95919 (2014).

39. Wang, X. & Kültz, D. Osmolality/salinity-responsive enhancers (OSREs) control induction of osmoprotective genes in euryhaline fish. *Proc. Natl. Acad. Sci. U. S. A.* **114**, E2729–E2738 (2017).

40. Jinek, M. *et al.* A programmable dual-RNA-guided DNA endonuclease in adaptive bacterial immunity. *Science* **337**, 816–821 (2012).

41. Cong, L. *et al.* Multiplex genome engineering using CRISPR/Cas systems. *Science* **339**, 819–823 (2013).

42. Mali, P. *et al.* RNA-guided human genome engineering via Cas9. *Science* **339**, 823–826 (2013).

43. Yasue, A. *et al.* Highly efficient targeted mutagenesis in one-cell mouse embryos mediated by the TALEN and CRISPR/Cas systems. *Sci. Rep.* **4**, 5705 (2014).

44. Gaj, T., Gersbach, C. A. & Barbas, C. F. 3rd. ZFN, TALEN, and CRISPR/Cas-based methods for genome engineering. *Trends Biotechnol.* **31**, 397–405 (2013).

45. Hamar, J. & Kültz, D. An efficient vector-based CRISPR/Cas9 system in an *Oreochromis mossambicus* cell line using endogenous promoters. *Sci. Rep.* **11**, 7854 (2021).

46. Li, C.-Y., Steighner, J. R., Sweatt, G., Thiele, T. R. & Juntti, S. A. Manipulation of the Tyrosinase gene permits improved CRISPR/Cas editing and neural imaging in cichlid fish. *Sci. Rep.* **11**, 15138 (2021).

47. Li, M. *et al.* Efficient and heritable gene targeting in tilapia by CRISPR/Cas9. *Genetics* **197**, 591–599 (2014).

48. Wu, Y. *et al.* Generation of fast growth Nile tilapia (*Oreochromis niloticus*) by myostatin gene mutation. *Aquaculture* **562**, 738762 (2023).

49. Concordet, J.-P. & Haeussler, M. CRISPOR: intuitive guide selection for CRISPR/Cas9 genome editing experiments and screens. *Nucleic Acids Res.* **46**, W242–W245 (2018).

50. Haeussler, M. *et al.* Evaluation of off-target and on-target scoring algorithms and integration into the guide RNA selection tool CRISPOR. *Genome Biol.* **17**, 148 (2016).

51. Hsu, P. D. *et al.* DNA targeting specificity of RNA-guided Cas9 nucleases. *Nat. Biotechnol.* **31**, 827–832 (2013).

52. Doench, J. G. *et al.* Rational design of highly active sgRNAs for CRISPR-Cas9–mediated gene inactivation. *Nat. Biotechnol.* **32**, 1262–1267 (2014).

53. Bloh, K. *et al.* Deconvolution of Complex DNA Repair (DECODR): Establishing a novel deconvolution algorithm for comprehensive analysis of CRISPR-Edited Sanger sequencing data. *CRISPR J.* **4**, 120–131 (2021).

54. Shirsat, N. *et al.* Revisiting Verhulst and Monod models: analysis of batch and fed-batch cultures. *Cytotechnology* **67**, 515–530 (2015).

55. Charlebois, D. A. & Balázsi, G. Modeling cell population dynamics. *In Silico Biol.* **13**, 21–39 (2019).

56. Polyak, K. *et al.* p27Kip1, a cyclin-Cdk inhibitor, links transforming growth factor-beta and contact inhibition to cell cycle arrest. *Genes Dev.* **8**, 9–22 (1994).

57. Roy, T., Ghosh, S., Saha, B. & Bhattacharya, S. A noble extended stochastic logistic model for cell proliferation with density-dependent parameters. *Sci. Rep.* **12**, 8998 (2022).

58. Duellman, S. J. *et al.* Bioluminescent, nonlytic, real-time cell viability assay and use in inhibitor screening. *Assay Drug Dev. Technol.* **13**, 456–465 (2015).

59. Sacchi, R., Gardell, A. M., Chang, N. & Kültz, D. Osmotic regulation and tissue localization of the myo-inositol biosynthesis pathway in tilapia (Oreochromis mossambicus) larvae. *J. Exp. Zool. Part Ecol. Genet. Physiol.* **321**, 457–466 (2014).

60. Roberts, M. F. Organic compatible solutes of halotolerant and halophilic microorganisms. *Saline Syst.* **1**, 5 (2005).

61. Rodionov, D. A. *et al.* Genomic identification and in vitro reconstitution of a complete biosynthetic pathway for the osmolyte di-*myo*-inositol-phosphate. *Proc. Natl. Acad. Sci. U. S. A.* **104**, 4279–4284 (2007).

62. Butzin, N. C. *et al.* Reconstructed ancestral *Myo*-inositol-3-phosphate synthases indicate that ancestors of the *Thermococcales* and *Thermotoga* species were more thermophilic than their descendants. *PloS One* **8**, e84300 (2013).

63. Dai, G., Yu, H., Kruse, M., Traynor-Kaplan, A. & Hille, B. Osmoregulatory inositol transporter SMIT1 modulates electrical activity by adjusting PI(4,5)P2 levels. *Proc. Natl. Acad. Sci. U. S. A.* **113**, E3290-3299 (2016).

64. Hager, K. *et al.* Kinetics and specificity of the renal Na+/*myo*-inositol cotransporter expressed in *Xenopus* oocytes. *J. Membr. Biol.* **143**, 103–113 (1995).

65. Adrian-Kalchhauser, I. *et al.* The round goby genome provides insights into mechanisms that may facilitate biological invasions. *BMC Biol.* **18**, 11 (2020).

66. Berry, G. T., Johanson, R. A., Prantner, J. E., States, B. & Yandrasitz, J. R. *myo*-inositol transport and metabolism in fetal-bovine aortic endothelial cells. *Biochem. J.* **295 (Pt 3)**, 863–869 (1993).

67. Wei, Y. *et al.* SLC5A3-dependent *myo*-inositol auxotrophy in acute myeloid leukemia. *Cancer Discov.* **12**, 450–467 (2022).

68. Pan, J. *et al.* A crucial role in osmoregulation against hyperosmotic stress: Carbohydrate and inositol metabolism in Nile tilapia (*Oreochromis niloticus*). *Aquac. Rep.* **28**, 101433 (2023).

69. Zhu, J. *et al.* New insights into the influence of *myo*-inositol on carbohydrate metabolism during osmoregulation in Nile tilapia (*Oreochromis niloticus*). *Anim. Nutr.* **10**, 86–98 (2022).

70. Foroutan, B. *et al. Myo*-inositol supplement helps the performance of seawater-acclimated Nile tilapia, *Oreochromis niloticus*. *Aquac. Fish.* (2022) doi:10.1016/j.aaf.2022.09.002.

71. Bu, X. *et al.* Growth, osmotic response and transcriptome response of the euryhaline teleost, *Oreochromis mossambicus* fed different *myo*-inositol levels under long-term salinity stress. *Aquaculture* **534**, 736294 (2021).

72. Kültz, D. Evolution of cellular stress response mechanisms. *J. Exp. Zool. Part Ecol. Integr. Physiol.* **333**, 359–378 (2020).

73. Yancey, P. H. Organic osmolytes as compatible, metabolic and counteracting cytoprotectants in high osmolarity and other stresses. *J. Exp. Biol.* **208**, 2819–2830 (2005).

74. Rhodes, J. D., Breck, O., Waagbo, R., Bjerkas, E. & Sanderson, J. N-acetylhistidine, a novel osmolyte in the lens of Atlantic salmon (*Salmo salar* L.). *Am. J. Physiol. Regul. Integr. Comp. Physiol.* **299**, R1075-1081 (2010).

75. Vislie, T. Cell volume regulation in fish heart ventricles with special reference to taurine. *Comp. Biochem. Physiol. A Physiol.* **76**, 507–514 (1983).

76. Tok, C. Y. *et al.* Glutamine accumulation and up-regulation of glutamine synthetase activity in the swamp eel, *Monopterus albus* (Zuiew), exposed to brackish water. *J. Exp. Biol.* **212**, 1248–1258 (2009).

77. Kültz, D. *et al.* Population-specific renal proteomes of marine and freshwater three-spined sticklebacks. *Proteomics Evol. Ecol.* **135**, 112–131 (2016).

78. Fiess, J. C. *et al.* Effects of environmental salinity and temperature on osmoregulatory ability, organic osmolytes, and plasma hormone profiles in the Mozambique tilapia (*Oreochromis mossambicus*). *Comp. Biochem. Physiol. A. Mol. Integr. Physiol.* **146**, 252–264 (2007).

79. Takeuchi, K., Toyohara, H., Kinoshita, M. & Sakaguchi, M. Ubiquitous increase in taurine transporter mRNA in tissues of tilapia (*Oreochromis mossambicus*) during high-salinity adaptation. *Fish Physiol. Biochem.* **23**, 173–182 (2000).

80. Kim, C. & Kültz, D. An osmolality/salinity-responsive enhancer 1 (OSRE1) in intron 1 promotes salinity induction of tilapia glutamine synthetase. *Sci. Rep.* **10**, 12103 (2020).

81. Charalampous, F. C. Biochemical studies on inositol. V. Purification and properties of the enzyme that cleaves inositol to D-glucuronic acid. *J. Biol. Chem.* **234**, 220–227 (1959).

82. Arner, R. J. *et al. myo*-Inositol oxygenase: molecular cloning and expression of a unique enzyme that oxidizes *myo*-inositol and d-*chiro*-inositol. *Biochem. J.* **360**, 313–320 (2001).

83. Root, L. *et al.* A data-independent acquisition (DIA) assay library for quantitation of environmental effects on the kidney proteome of *Oreochromis niloticus*. *Mol. Ecol. Resour.* **21**, 2486–2503 (2021).

84. Hankes, L. V., Politzer, W. M., Touster, O. & Anderson, L. *Myo*-inositol catabolism in human pentosurics: the predominant role of the glucuronate-xylulose-pentose phosphate pathway. *Ann. N. Y. Acad. Sci.* **165**, 564–576 (1969).

85. Sochor, M., Baquer, N. Z. & McLean, P. Regulation of pathways of glucose metabolism in kidney. The effect of experimental diabetes on the activity of the pentose phosphate pathway and the glucuronate-xylulose pathway. *Arch. Biochem. Biophys.* **198**, 632–646 (1979).

86. Novello, F. & McLean, P. The pentose phosphate pathway of glucose metabolism. Measurement of the non-oxidative reactions of the cycle. *Biochem. J.* **107**, 775–791 (1968).

87. Khosravi, S. *et al.* Dietary *myo*-inositol requirement of parrot fish, *Oplegnathus fasciatus*. *Aquaculture* **436**, 1–7 (2015).

88. Chen, X., Wang, J. & Zhao, W. Effects of dietary inositol supplementation on growth, digestive performance, antioxidant capacity, and body composition of golden pompano (*Trachinotus ovatus*). *Front. Physiol.* **13**, 850470 (2022).

89. Pan, S. *et al.* The positive effects of dietary inositol on juvenile hybrid grouper (♀ *Epinephelus fuscoguttatus* × ♂ *E. lanceolatu*) fed high-lipid diets: Growthperformance, antioxidant capacity and immunity. *Fish Shellfish Immunol.* **126**, 84–95 (2022).

90. Wang, C. *et al.* Effects of dietary *myo*-inositol on growth, antioxidative capacity, and nonspecific immunity in skin mucus of taimen *Hucho taimen* fry. *Fish Physiol. Biochem.* **46**, 1011–1018 (2020).

91. Eagle, H., Oyama, V. I., Levy, M. & Freeman, A. E. *Myo*-Inositol as an essential growth factor for normal and malignant human cells in tissue culture. *J. Biol. Chem.* **226**, 191–205 (1957).

92. Koguchi, T., Tanikawa, C., Mori, J., Kojima, Y. & Matsuda, K. Regulation of *myo*-inositol biosynthesis by p53-ISYNA1 pathway. *Int. J. Oncol.* **48**, 2415–2424 (2016).

93. Niwa, T., Sobue, G., Maeda, K. & Mitsuma, T. Myoinositol inhibits proliferation of cultured Schwann cells: evidence for neurotoxicity of myoinositol. *Nephrol. Dial. Transplant. Off. Publ. Eur. Dial. Transpl. Assoc. - Eur. Ren. Assoc.* **4**, 662–666 (1989).

94. Yang, L. *et al.* The *myo*-inositol biosynthesis rate-limiting enzyme ISYNA1 suppresses the stemness of ovarian cancer via Notch1 pathway. *Cell. Signal.* **107**, 110688 (2023).

95. Bizzarri, M., Dinicola, S., Bevilacqua, A. & Cucina, A. Broad spectrum anticancer activity of *myo*-inositol and inositol hexakisphosphate. *Int. J. Endocrinol.* **2016**, 5616807 (2016).

96. Vucenik, I. & Shamsuddin, A. M. Protection against cancer by dietary IP6 and inositol. *Nutr. Cancer* **55**, 109–125 (2006).

97. Gustafson, A. M. *et al.* Airway PI3K pathway activation is an early and reversible event in lung cancer development. *Sci. Transl. Med.* **2**, 26ra25 (2010).

98. Dinicola, S. *et al.* Inositol induces mesenchymal-epithelial reversion in breast cancer cells through cytoskeleton rearrangement. *Exp. Cell Res.* **345**, 37–50 (2016).

99. An, L. *et al.* Efficient generation of FVII gene knockout mice using CRISPR/Cas9 nuclease and truncated guided RNAs. *Sci. Rep.* **6**, 25199 (2016).

100. Fu, Y., Sander, J. D., Reyon, D., Cascio, V. M. & Joung, J. K. Improving CRISPR-Cas nuclease specificity using truncated guide RNAs. *Nat. Biotechnol.* **32**, 279–284 (2014).

This chapter is formatted for submission to the *American journal of physiology, Cell physiology*.

RESEARCH ARTICLE

Aim 3: Transcriptional up-regulation of the *myo*-Inositol biosynthesis pathway is enhanced by NFAT5 in hyper-osmotically stressed tilapia cells

Jens Hamar,[1] Avner Cnaani,[2] Dietmar Kültz[1]

[1]Department of Animal Sciences and Genome Center, University of California Davis, Davis, California, United States
[2] Department of Poultry and Aquaculture, Institute of Animal Sciences, Agricultural Research Organization, Rishon LeZion, Israel

Correspondence: Dietmar Kültz (dkueltz@ucdavis.edu).

ABSTRACT

Euryhaline fish experience variable osmotic environments requiring physiological adjustments to tolerate elevated salinity. Mozambique tilapia (*Oreochromis mossambicus*) possess one of the highest salinity tolerance limits of any fish. In tilapia and other euryhaline fish species the *myo*-inositol biosynthesis (MIB) pathway enzymes, *myo*-inositol phosphate synthase (MIPS) and inositol monophosphatase 1 (IMPA1.1), are among the most upregulated mRNAs and proteins indicating the high importance of this pathway for hyperosmotic (HO) stress tolerance. These abundance changes must be precluded by HO perception and signaling mechanism activation to regulate the expression of *MIPS* and *IMPA1.1* genes. In previous work using an *O. mossambicus* cell line (OmB), a reoccurring osmosensitive enhancer element (OSRE1) in both *MIPS* and *IMPA1.1* was shown to transcriptionally upregulate these enzymes in response to HO stress. The OSRE1 core consensus (5'-GGAAA-3') matches the core binding sequence of the predominant mammalian HO response transcription factor, nuclear factor of activated T-cells (NFAT5). HO challenged OmB cells showed an increase in *NFAT5* mRNA suggesting NFAT5 may contribute to MIB pathway regulation in euryhaline fish. Ectopic expression of wild-type NFAT5 induced an *IMPA1.1* promoter-driven reporter by 5.1-fold ($p < 0.01$). Moreover, expression of dominant negative NFAT5 in HO media resulted in a 47% suppression of the reporter signal ($p<0.005$). Furthermore, reductions of IMPA1.1 (37-49%) and MIPS (6-37%) mRNA abundance were observed in HO challenged NFAT5 knockout cells relative to control cells. Collectively, these multiple lines of experimental evidence establish NFAT5 as a tilapia transcription factor that contributes to the HO induced activation of the MIB pathway.

Keywords: NFAT5; Hyperosmolality; CRISPR/Cas9; dominant negative mutant; tilapia; synthetic biology

INTRODUCTION

Euryhaline fish acclimate to altered osmotic conditions by regulating their extracellular osmolality and, during severe salinity stress, activation of intracellular enzymes that promote accumulation of compatible organic osmolytes (1). Having one of the widest ranges of salinity tolerance of all fish, *O. mossambicus* represent an ideal species to study these mechanisms. Physiological stress responses include sensors (the molecules or proteins that perceive the stress condition), intermediate signal transducers (the molecules that relay the stress signal from the sensors to the effectors), and effector elements (the molecules that mediate the molecular changes allowing persistence during the stress condition). Accumulation of inert intracellular compatible osmolytes such as *myo*-inositol, represents a primary response to relieve osmotic stress caused by extracellular osmolality increases (2–5). Enzymes of the *myo*-inositol biosynthesis (MIB) pathway have been identified as primary proteins that increase in abundance during hyper-osmotic stress in multiple fish species including tilapia (3, 6) and European eel (7). In a tilapia cell line derived from *O. mossambicus* brain tissue (OmB) treated with hyper-osmotic (HO) media, MIB enzyme transcriptional upregulation paralleled that seen in whole animals subjected to HO challenge (8), demonstrating the utility of this model for investigating this pathway. The considerable abundance changes of the MIB pathway enzymes in salinity-stressed cells of tilapia and several species of euryhaline fish illustrates that the regulation of this pathway is a key event for the HO stress response in euryhaline fish. HO induced upregulation of the MIB pathway enzymes requires regulatory enhancer elements that respond to HO conditions. In OmB cells, an osmotic responsive enhancer element (OSRE1) recurs in many locations of the *MIPS* and *IMPA1.1* promoters and was found to be primarily responsible for transcriptional upregulation of these enzymes in HO media (9). Cloning of these OSRE1 enhancers into a minimal promoter expression vector also resulted in strong HO induction of a reporter gene (9).

The conserved OSRE1 core sequence of 5'-GGAAA-3' represents the core recognition sequence of the Rel homology domain (RHD) (10–13) included in transcription factors commonly associated with cellular stress response signaling, including the nuclear factor of activated T-cell (NFAT) (14) and NF-κB protein families (15, 16). Of the transcription factors belonging to these Rel protein families, NFAT5 is the strongest candidate as an OSRE1 interacting partner since this transcription factor has a well-established role as the primary transcriptional activator of HO responsive genes in mammalian cells (17–20). HO activation of NFAT5 in mammals is achieved by multiple mechanisms, including a localization change (21, 22), post-translational modification (23–25), and increased NFAT5 mRNA abundance (17, 21, 26–29). NFAT5 mRNA abundance increases were also observed in multiple tissues of Atlantic Salmon exposed to HO challenge (30), suggesting this role is phylogenetically conserved across lower and higher vertebrates.

Effective strategies to establish causal interactions between specific transcription factors and DNA regulatory elements in effector genes include *cis*-element reporter gene expression in combination with either *trans*-factor overexpression (23, 31) or *trans*-factor dominant negative mutant expression (32, 33). A third approach is to generate gene knock-out (KO) animals or cell lines, e.g., by CRISPR/Cas9 gene editing, which is an efficient method for establishing causality between signal transducers and effector mechanisms (34, 35). Disruption of any genetic locus encoding the protein of interest in tilapia cells can be proficiently achieved using a plasmid-based CRISPR/Cas9 system customized for *O. mossambicus* cells (36). In mammalian models NFAT5 KO is usually lethal at early stages of development (37, 38) but NFAT5 KO cell lines are viable, capable of proliferation, and have been used for mechanistic studies of NFAT5 interactions (39–41).

Using the tilapia OmB cell line, the objective of this study was to investigate the role of tilapia NFAT5 for transcriptional HO induction of genes that encode MIB pathway enzymes. The hypothesis tested was that NFAT5 is necessary for the induction of MIB pathway genes during HO stress.

MATERIALS AND METHODS

Cell lines and maintenance

O. mossambicus OmB wildtype (wt) cells and the engineered Cas9 expressing transgenic OmB cells (Cas9-OmB1) were propagated and maintained according to standard OmB cell culture conditions and protocols as documented in previous reports (8, 36) unless otherwise specified.

Primer design and sequence analysis

All primer design, sequence alignments, and other amino acid/DNA sequence analysis were performed using Geneious Prime software (Version 11.0.3, Biomatters Inc, https://www.geneious.com). All alignments were performed as global alignments with free end gaps.

O. mossambicus NFAT5 cds Sequence Assembly					
Amplicon	Forward Primer ID	Reverse Primer ID	Forward Primer Sequence (5'-3')	Reverse Primer Sequence (5'-3')	Expected bp size
1	NFAT5_F1	NFAT5X3_R1	ATGCCCTCTGACTTTATCTCCC	CTTCCTTTATGTCCTCCCTTG	806
2	NFAT5X2_F3	NFAT5X3_R1	GTCAAAAGAGCGGCGGAGA	CTTCCTTTATGTCCTCCCTTG	661
3	NFAT5X4_F1	NFAT5X8_R1	TCTGATGAACCTAGGACTACTAATC	GCTCCATGTCAATTTCAGCC	727
4	NFAT5X8_F1	NFAT5X12_R1	GGCTGAAATTGACATGGAGC	GCCCGCAACAATGTCCTG	520
5	NFAT5_F1	NFAT5X12_R1	ATGCCCTCTGACTTTATCTCCC	GCCCGCAACAATGTCCTG	1872
6	NFAT5X12_F1	NFAT5X13_R1	AGACTGGTGATCTGCGTCCA	TTAGTAGGAACGAGTTATGTTGCTG	2030
7	NFAT5X7_F3	NFAT5X12(XbaI)_R1	CCCCCAAGCTTGGTCTCAGAGGAGGTCTTCATC	CCCCCTCTAGAGCCCGCAACAATGTCCTG	576
8	NFAT5X12_F1b	NFAT5X12_R4	CCCCCCTCGAGAGACTGGTGATCTGCGTCCA	TGTTGAGGCTGAGATGGTTG	1168
9	NFAT5X12_F7b	NFAT5X13_R2b	CCCCCCTCGAGATTTCAGACCCAGATCTCCC	CCCCCCTCAGATTAGTAGGAACGAGTTATGTTGCTG	945
O. mossambicus NFAT5 mRNA quantitative RT-PCR					
Target Gene	Accession Number	Dilution	Forward Primer Sequence (5'-3')	Reverse Primer Sequence (5'-3')	Expected bp size
NFAT5	NC031965	1:10	GAAGATCCTCGTCCAGCCTG	GCCAACGAACACCTGCAAAA	151
β-actin	AB037865	1:10	CCACAGCCGAGAGGGAAAT	CCCATCTCCTGCTCGAAGT	104
18s Rrna	AF497908	1:10	CGATGCTCTTAGCTGAGTGT	ACGACGGTATCTGATCGTCT	260

Table 1. Primer pair sequence information associated with RT-PCR generated amplicons used in sequencing and cloning of the HO induced *O. mossambicus* NFAT5 cds (MW075269.1) and qRT-PCR quantification of NFAT5 mRNA in IO and HO conditions.

O. mossambicus NFAT5 mRNA quantitation

To characterize isoform-specific *O. mossambicus NFAT5* mRNA sequences and abundances, OmB cells were exposed to osmotic HO treatments (media adjusted using NaCl to 650 mOsm/kg for HO treatment or to 315 mOsm/kg for basal iso-osmotic (IO) control treatment) (9) for 6 hours followed by RNA extraction using Invitrogen PureLink RNA Mini Kit (cat# 12183018A). A Qiagen One-step RT-PCR kit (cat#

210210) and gene specific primer pairs for amplicons 1-4 listed in Table 1 were used for cDNA synthesis and PCR amplification of four different regions of the *O. mossambicus* NFAT5 cds. Primers were designed using the XM_005467029 NFAT5 isoform sequence from the *O. niloticus* (taxid: 8128) reference genome. Agarose gel electrophoresis was performed to detect *O. mossambicus* amplicons 1-4 from both HO and IO treatments.

In a separate experiment, osmotic treatments (HO and IO) and RNA isolation were performed as described above on six replicate 90% confluent 10 cm plates of OmB cells per treatment. Directly after harvesting cells RNA isolation and cDNA synthesis was performed using Invitrogen Superscript IV (cat.# 18090010) according to manufacturer protocol using 200 ng of template RNA and a 50:50 mix of Oligo-dT and random hexamer primers. Quantitative PCR was performed on 10x dilutions of each cDNA using Promega GoTaq qPCR Master Mix (cat# A6001) on an Applied Biosystems QuantStudio 3 Real-Time PCR system using qPCR primer pairs for *NFAT5* and both β-actin and 18s rRNA as reference genes (RG) as listed in Table 1. The primer pair targeting NFAT5 was designed to flank a 1035 bp intron using *O. niloticus* (taxid: 8128) *NFAT5* genomic sequence (gene ID # LOC100691255). The RG primer pair sequences were obtained from a previous study (8).

Sequencing and characterization of *O. mossambicus* NFAT5

Using RNA from the HO treated cells, Invitrogen Superscript III (cat.# 18080-044) was used for cDNA synthesis of longer sections of the *O. mossambicus* NFAT5 cds using gene specific primers (NFATX12_R1 for the 5' end of the mRNA transcript and NFATX13_R1 for the 3' end, Table 1). The cDNA reactions were treated with New England Biolabs RNAse H (cat. #M0297S) followed by PCR amplification to generate amplicons 5 and 6 (for primer pairs see Table 1). Amplicons 8 and 9 were PCR amplified from amplicon 6 as template DNA. DNA sequences for amplicons 1-4, 8, and 9 were obtained from the UC Davis core Sanger sequencing facility (amplicons 8 and 9 were cloned into pBluescript II SK+ first, then

sequenced from the plasmid). These sequences were assembled into the complete cds using Geneious software and submitted to the NCBI database.

In silico translation was performed on the constructed *O. mossambicus* NFAT5 cds followed by aa alignment with known functional NFAT5 domains in mammals to identify critical functional domains. These known domains included the nuclear export signal (NES) (22), auxiliary export domain (AED) (42), nuclear localization signal (NLS) (43), DNA binding Rel homology domain (RHD) (32), and transcriptional activation domains (AD1, AD2, and AD3) (23).

Construction of reporter and ectopic expression vectors

An IMPA1.1-EGFP reporter vector was constructed by PCR amplification of a 2700 bp fragment of the *IMPA1.1* promoter. The region of *O. mossambicus* genomic DNA starting at the endogenous start codon on the 3' end and extending to 1065 bp 5' of the predicted TSS (1635 bp between TSS and start codon consisting of exon 1, intron 1, exon 2, intron 2 and the first 36 bp of exon 3) was cloned upstream of the EGFP cds in an EGFP_SV40PA base vector reported previously (36). To confirm HO induced activity of the reporter, two 3.5 cm wells of a plate with 85% confluent OmB cells were transfected with 1 µg of IMPA1.1-EGFP vector. Medium was replaced with either IO (315 mOsm/kg) or HO (650 mOsm/kg) media 24 hours after transfection. Tile scan imaging of the center 10% of each well was performed 24 hours after application of osmotic treatments using a Leica DMi8 inverted microscope with a GFP filter.

To reduce overall plasmid size of the other vectors used in this study, additional truncated recombinant promoters were designed. OmAP(I-)2 and OmEF1a(I-)2 promoters were produced by using their full-length versions, *O. mossambicus* β actin (OmBAct) and elongation factor 1 α (OmEF1a), as PCR templates (36). A reverse primer spanning the 3' end of exon 1 and the 5' end of exon 2 was used for this purpose. This cloning strategy effectively removed intron 1 but maintained the same 5' UTR and the endogenous start codon. Moreover, the Kozak sequence was retained but modified to include a NotI

restriction site to provide more cloning options. OmEF1a(I-)2 was cloned into a reporter vector (OmEF1a(I-)2RFP containing the dtomato red fluorescent protein (RFP) cds. This plasmid was used for co-transfection with IMPA1.1-EGFP reporter plasmids to normalize for differences in transfection efficiency and cell density between wells. Another promoter (CMVIE-OmAP(I-)2) was constructed for expression of dominant negative proteins. The cytomegalo virus immediate early enhancer (CMVIE ~300 bp) was cloned upstream of the β-actin core promoter as in Hitoshi et al (45) of OmAP(I-)2 to improve expression strength. Fusion of the CMVIE enhancer with interspecies promoters has been demonstrated to be effective (44, 45), including in fish (46).

To generate a dominant negative (DN) NFAT5 cds (NFAT5DN) modeled after mammalian NFAT5DN (32), a truncated NFAT5 cds was PCR amplified using a reverse primer (NFAT5trunc_R; 5'-TTTAAGAAAGTTTTTTCCAATGATGAAGACC-3) designed 3' prime of the RHD but 5' of the AD1 and AD2 domains. This primer was paired with NFAT5_F1 forward primer to PCR amplify (from amplicon 5 as template DNA) a 1332 bp truncated NFAT5 cds including the DNA binding and nuclear localization domains but omitting the transcriptional activation domains. To generate a full wild-type NFAT5 cds (NFAT5WT) the NFAT5DN sequence, amplicon 7 (PCR amplified from amplicon 5, spanning exon 7 to exon 12), and the C-terminal fragments (amplicons 8 and 9 containing exons 12-13 subcloned from pBluescript II SK+ plasmid) were assembled into a new plasmid using standard restriction enzyme techniques. The NFAT5DN cds was cloned into a plasmid driven by the CMVIE-OmAP(I-)2 promoter generating the NFAT5DN vector. The full length wild-type (WT) cds was cloned into a plasmid driven by the OmAP(I-)2 promoter to generate the NFAT5WT vector. The first 1332 base pairs of Cas9 cds were also cloned into a plasmid driven by the CMVIE-OmAP(I-)2 promoter to be used as an overexpression vector (OE) that controls for non-specific deleterious effects caused by ectopic protein expression (47).

EGFP/RFP Reporter Assays

For the NFAT5DN inhibition experiments, transfection reactions consisted of 1000 ng expression vector, 100 ng IMPA1.1-EGFP reporter, and 100 ng RFP normalizer plasmids. Three variations of expression vector were used: 100% control vector, 50% OE control vector plus 50% NFAT5DN vector, and 100% NFAT5DN vector. Four replicates of these plasmid combinations were used for each HO (650 mOsm/kg) and IO (315 mOsm/kg) treatments. Plasmid transfections of cells were performed using Promega ViaFect (cat.# E4981) followed by 48 hour exposure to either HO or IO conditions after transfection. Tile scan imaging of the center 10% of each well was performed 24 hours after HO and IO treatments. For the NFAT5WT activation experiments, plasmid complexes were prepared consisting of 500 ng expression vector, 50 ng IMPA1.1-EGFP reporter, and 50 ng RFP normalizer plasmids. Two variations of expression vector were used: 100% OE control vector, and 100% NFAT5WT vector. Two replicates were used per treatment group with each replicate consisting of one 12-well plate of OmB cells. Tile scan imaging was performed on the center 20% of each well 24 hours after transfection. All images were generated using a 20X objective and both GFP (30 ms exposure) and TXR (20 ms exposure for RFP) filters as composite tile scans using a Leica DMi8 inverted microscope. Total fluorescence intensity per filter was quantified using the LASX Navigator analysis tool (Leica Application Suite X Version 3.0.4 software). Reporter activity is expressed as relative fluorescence intensity (RFI = total EGFP fluorescence intensity/ total RFP fluorescence intensity).

Generation of NFAT5 KO cell lines

The NFAT5 amino acid sequences for *O. niloticus* (XP_005467085), *Oryzias latipes* (XP_011487371), and *Fundulus heteroclitus* (XP_021177424.2) were aligned to find the most conserved regions within the first third of the coding sequence that would have the highest probability of gene product disruption by CRISPR/Cas9 targeting. The corresponding nucleotide sequences of these regions were entered into the

online CRISPOR gRNA selection algorithm (49) to find candidate gRNAs with the highest predicted specificity (lowest potential of off-target effects) and efficiency (highest potential to cleave target site) scores. Based on these scores, eight gRNAs were selected for *in vivo* empirical testing of mutational efficiency. Expression plasmids for each candidate gRNA were constructed and transfected into Cas9-OmB1 cells, followed by hygromycin B selection, direct PCR of test amplicons including the gRNA targeted region, Sanger sequencing, and INDEL% quantification of the resulting chromatogram using the online TIDE mutational efficiency algorithm (50). The top three INDEL% scoring guides were used to repeat CRISPR/Cas9 treatment of Cas9-OmB1 cells followed by low density seeding of hygromycin B selected cells into 96-well plates. Selected wells were genotyped by direct PCR and Sanger sequencing of the corresponding test amplicon followed by input of the chromatogram into the online DECODR algorithm (51). Selected genotypes showing a maximum of two alleles all with 100% frameshift mutation were propagated and genotyped again after multiple passages. For subsequent experiments, one genotype for each gRNA was selected based on maintenance of the original genotype and highest R^2 model fit for the DECOCDR algorithm. Three non-essential (NE) gene (NANOS3, MSTN T5, and TYR T1) control KO lines were also used and the gRNA selection process and methods for generation and genotyping of these KO cell lines were performed as described previously (48).

Quantitative PCR of IMPA1.1 and MIPS in NFAT5 KO cells

The three NFAT5 KO lines and three NE control KO lines were grown to ~90% confluency in 6 cm plates followed by acute replacement of media with either 650 mOsm/kg HO or control 315 mOsm/kg IO media. Cell harvest and RNA isolation was performed 24 hours after dosing followed by cDNA synthesis and quantitative PCR as described in the previous section except a 1000x dilution was used for 18s rRNA RG. The target gene primer pairs used were IMPA1 and MIPS-250 from a previous study (8). For each combination (target gene, RG, and osmotic treatment) the fold change between the NFAT5 KO and NE KO control groups was calculated using the $2^{-\Delta\Delta Ct}$ method (52, 53).

Statistical Analysis

All statistical analyses were performed using RStudio version 2021.09.1. One tailed Welch and two sample t-tests were performed on all relative mRNA abundance comparisons and for determining the effect of NFAT5WT activation on IMPA1.1-EGFP reporter induction. Linear regression was used to model the effect of NFAT5DN inhibition on HO induction of the IMPA1.1-EGFP reporter. All data reported and shown in figures are represented as means ± standard errors.

RESULTS

RT-PCR of NFAT5

Qualitative assessment of PCR amplicon images after gel electrophoresis of the different NFAT5 cds segments yielded consistently brighter bands from HO treated cells compared to IO controls across all segments (Figure 1A). Quantitative PCR of NFAT5 mRNA abundance confirms these visual approximations by yielding a statistically significant mean fold change of 3.87 (p value = 1.789e-05) in HO treated cells relative to iso-osmotic treated controls (Figure 1B).

Characterization of HO induced NFAT5

The assembled *O. mossambicus NFAT5* cds sequence from HO treated cells (NCBI accession # MW075269.1) was aligned with the predicted *O. niloticus NFAT5* isoform with all possible exons (XM_005467029) to identify the exon splicing pattern and any sequence differences between these two tilapia species (Figure 1C). When compared to the predicted *O. niloticus NFAT5* isoform XM_005467029, the predicted *O. mossambicus* HO induced *NFAT5* transcript (MW075269.1) is missing exon 2 and

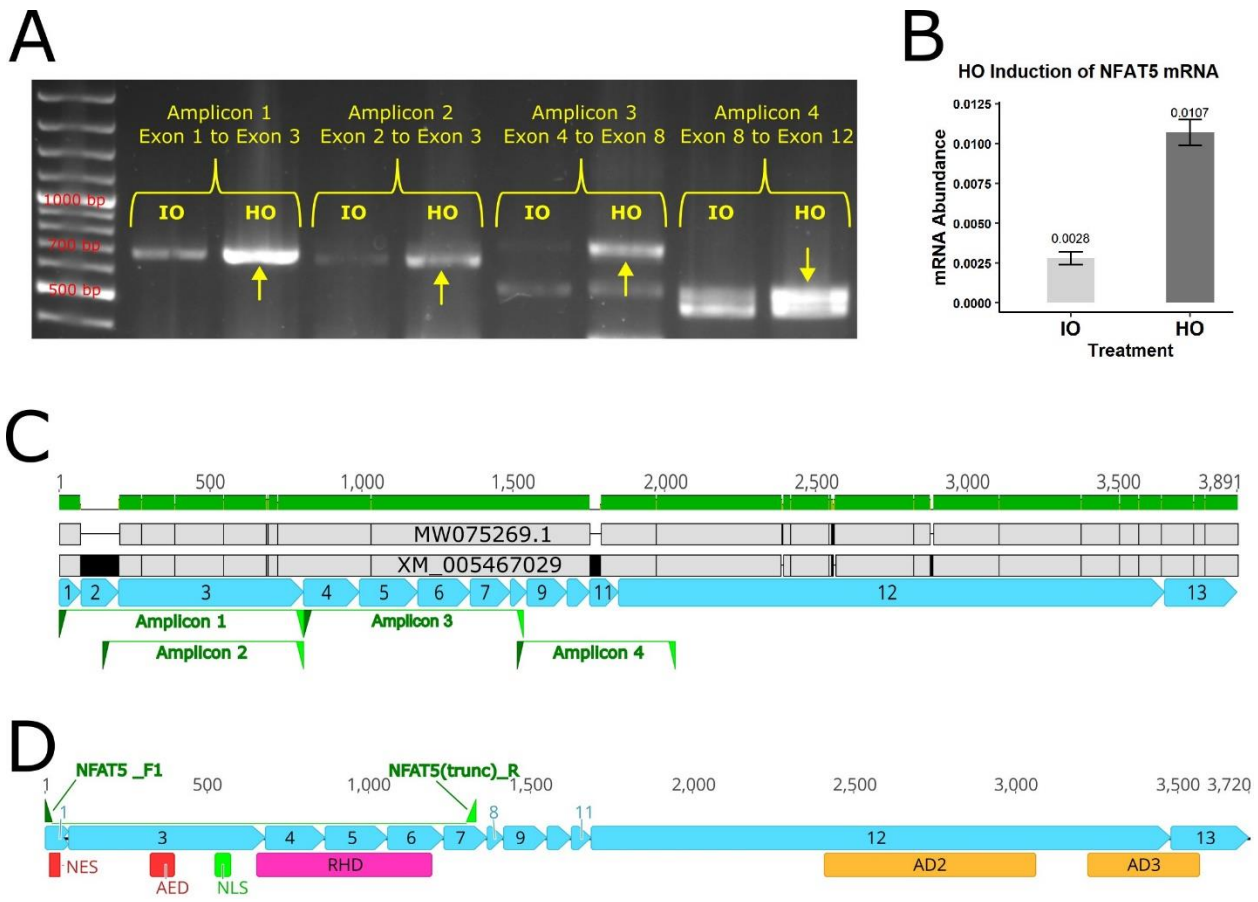

Figure 1. Characterization of NFAT5 mRNA isoform abundance patterns and sequences in isosmotic (IO) and hyperosmotic (HO) conditions. A: Agarose gel electrophoresis of different RT-PCR amplified regions of the NFAT5 cds from both IO and HO treatments showing greater abundance in all amplicons for HO treatments. Multiple bands of similar intensity from amplicon 4 indicate the presence of two variants of exon 11. A notably weaker intensity of amplicon 2 relative to amplicon 1 indicates that exon 2 is missing from most transcripts. A yellow arrow depicts the expected band for each amplicon. B: NFAT5 mRNA abundance relative to β-actin reference gene in IO and HO conditions. C: Assembled sequence of HO induced *O. mossambicus NFAT5* transcript (MW075269.1) aligned with the predicted *O. niloticus NFAT5* sequence containing all possible exons (XM_005467029). MW075269.1 is missing exon 2 and a 65 bp section of exon 11. Location of primers used to generate amplicons 1-4 in 1A also included. D: Critical protein domains identified in mammalian NFAT5 mapped to the *O. mossambicus* MW075269.1 cds based on alignment of individual domain amino acid sequence to predicted MW075269.1 amino acid sequence. Designed primer locations for PCR amplification of truncated NFAT5 cds for use as dominant negative mutant in subsequent experiments are indicated in green.

contains the shorter 65 bp version of exon 11 (Figure 1C). The mammalian NFAT5 domain aa sequences aligned to the MW075269.1 predicted aa sequence had pairwise % identities of NES = 81.8, AED = 76.9, NLS = 70.6, RHD = 82.2, AD2 = 32.1, and AD3 = 40.9. The AD1 domain was omitted from MW075269.1 along with exon 2 but aligned to *O. niloticus* NFAT5 isoform XP_005467085 with 60.7 pairwise % identity. All domains aligned in the same relative position as previously reported for mammals (23, 54) (Figure 1D).

Construction and validation of reporter plasmids

Based on the *O. niloticus* reference genome, the selected regulatory *IMPA1.1* promoter region should have been 4086 bp, however a 1386 bp section in the intron between exons 2 and 3 was omitted resulting in the 2700 bp region that was cloned into the EFGP_SV40 PA reporter vector (Figure 2A). HO responsiveness of the reporter vector was qualitatively confirmed from tile scan images post transfection and HO treatment with notably higher EGFP intensity of the HO treated cells (Figure 2B). The engineered OmEF1a(I-)2 promoter (Figure 2C) showed strong, stable RFP expression (Figure 2D).

Interaction between NFAT5DN or NFAT5WT with IMPA1.1 reporter

The engineered CMVIE-OmAP(I-)2 promoter (Figure 3A) was effective in producing sufficient NFAT5DN quantities as HO RFI induction of the IMPA1.1-EGFP reporter decreased linearly with increasing concentration of NFAT5DN (p-value = 0.00269) amounting to a 47% reduction from no NFAT5DN present to the highest NFAT5DN concentration (Figure 3B). In IO media, IMPA1.1-EGFP reporter RFI was significantly greater in NFAT5WT transfected cells (5.1 fold, $p < 0.01$) compared to cells transfected with the OE control vector (Figure 3C).

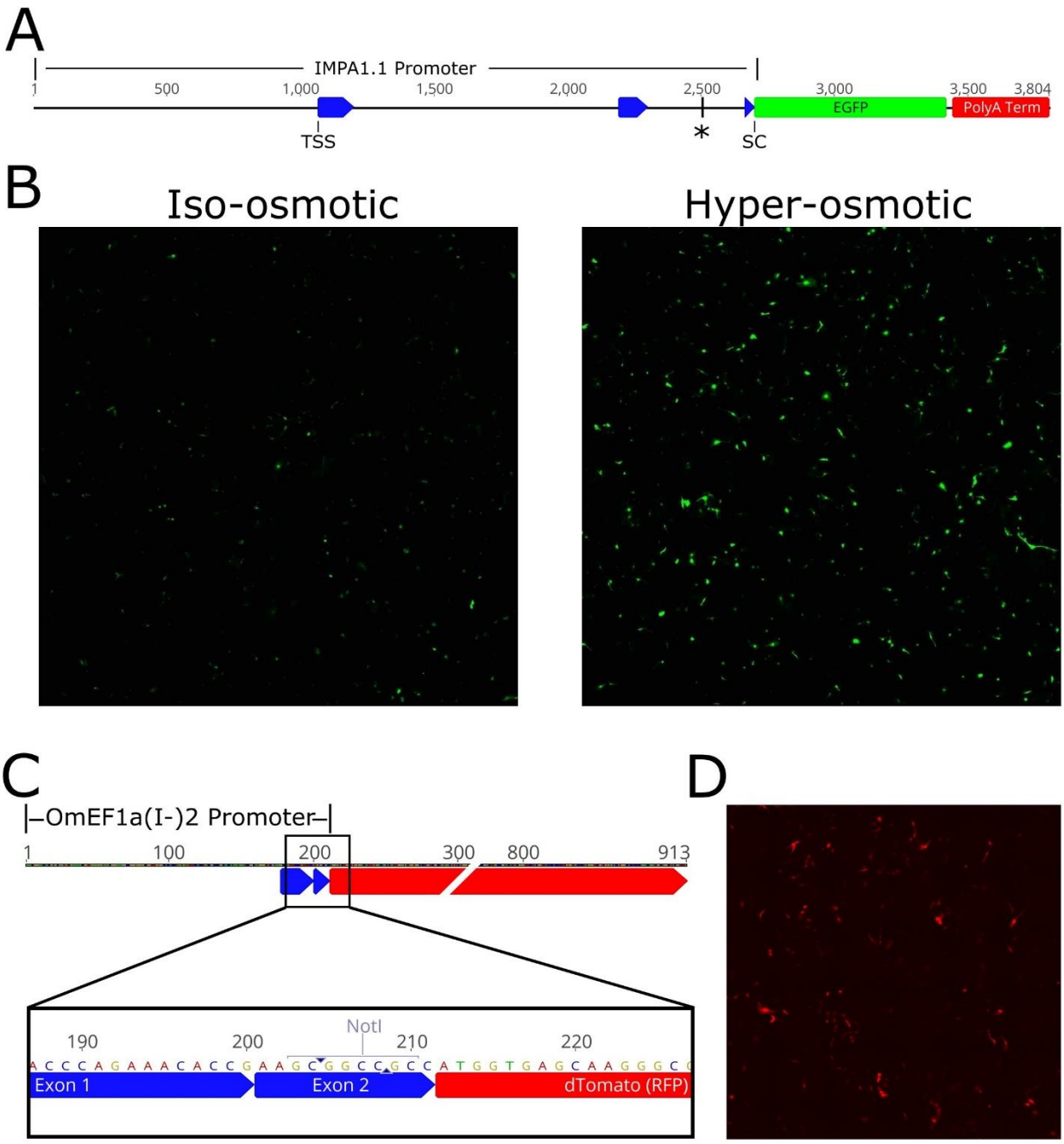

Figure 2. Construction and validation of the IMPA1.1-EGFP reporter. A: vector map of the IMPA1.1-EGFP reporter showing the boundaries of the IMPA1.1 regulatory region from 1065 5' of the transcription start site (TSS) to the endogenous start codon of exon 3 (*1386 bp were omitted by the PCR reaction). B: Validation of IMPA1.1-EGFP reporter showing strongly increased fluorescence after 24 hour HO treatment relative to IO controls. C: Engineered EF1a(I-)2 promoter from endogenous *O. mossambicus* OmEF1a showing inclusion of 5' UTR within the first two exons but deletion of the first intron and modified Kozak sequence to generate NotI restriction. D: Functional validation of EF1a(I-)2 promoter expressing RFP showing strong fluorescence.

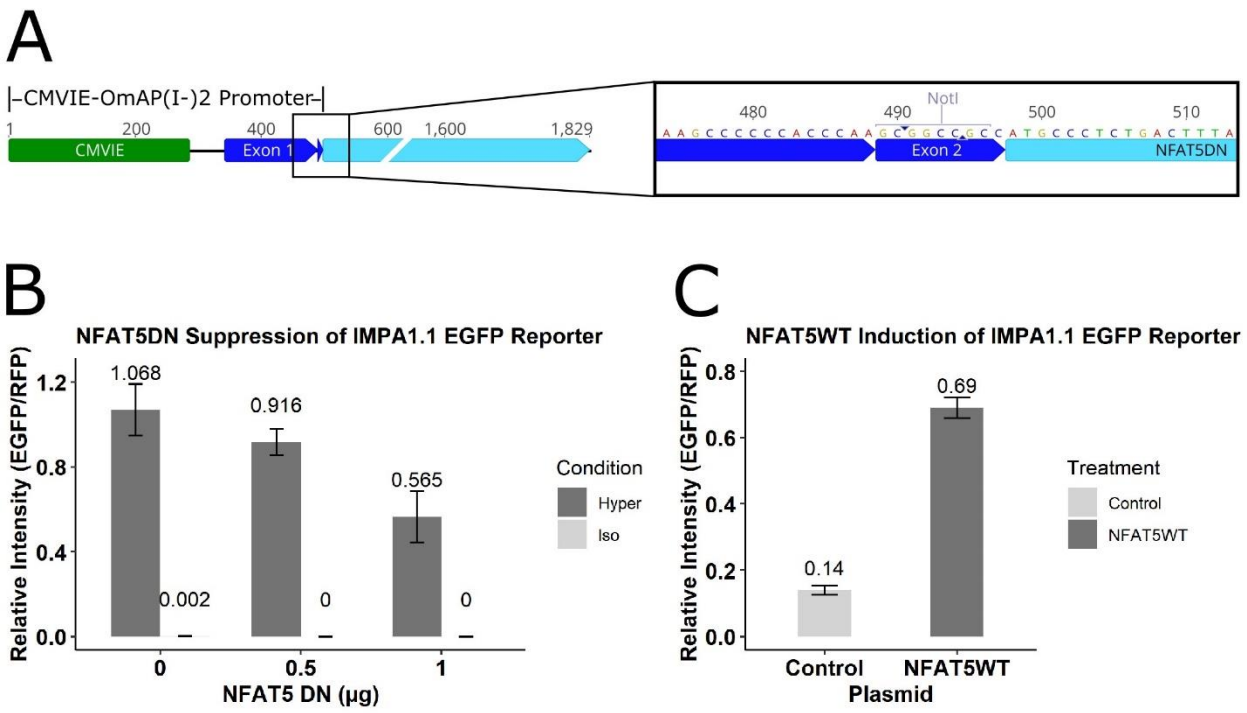

Figure 3. Interactions between different NFAT5 versions and the IMPA1.1 promoter. A: CMVIE-OmAP(I-)2 promoter engineered from endogenous *O. mossambicus* OmBact for NFAT5DN expression showing inclusion of 5' UTR within the first two exons but deletion of the first intron, modified Kozak sequence to generate NotI restriction site, and inclusion of the cytomegalovirus immediate early enhancer (CMVIE) at the 5' end. B&C: effect of different NFAT5 variants on relative fluorescence intensity (RFI) of the IMPA1.1 EGFP reporter. B: Suppression of HO induced RFI with increasing NFAT5DN. C: induction of RFI by NFAT5WT in IO conditions.

CRISPR/Cas9 gRNA design and testing

The interspecies NFAT5 aa sequence alignments identified the most highly conserved region as between aas 320 and 450 of the *O. niloticus* NFAT5 protein (XP_005467085) (Figure 4A). This region corresponded to exons 4 through 6 of the *O. niloticus NFAT5* genomic sequence (gene ID # LOC100691255) in which the candidate gRNAs were found by CRISPOR algorithm search (Figure 4B). The top eight selected candidate gRNAs all yielded high MIT (Massachusetts Institute of Technology) specificity (92 or greater) and Doench efficiency (45 or greater) scores (Table 2). The three gRNAs with the highest TIDE mutational efficiency scores from *in vivo* empirical testing were T3 (60.4%), T5 (51.9%), and T7 (56.1%).

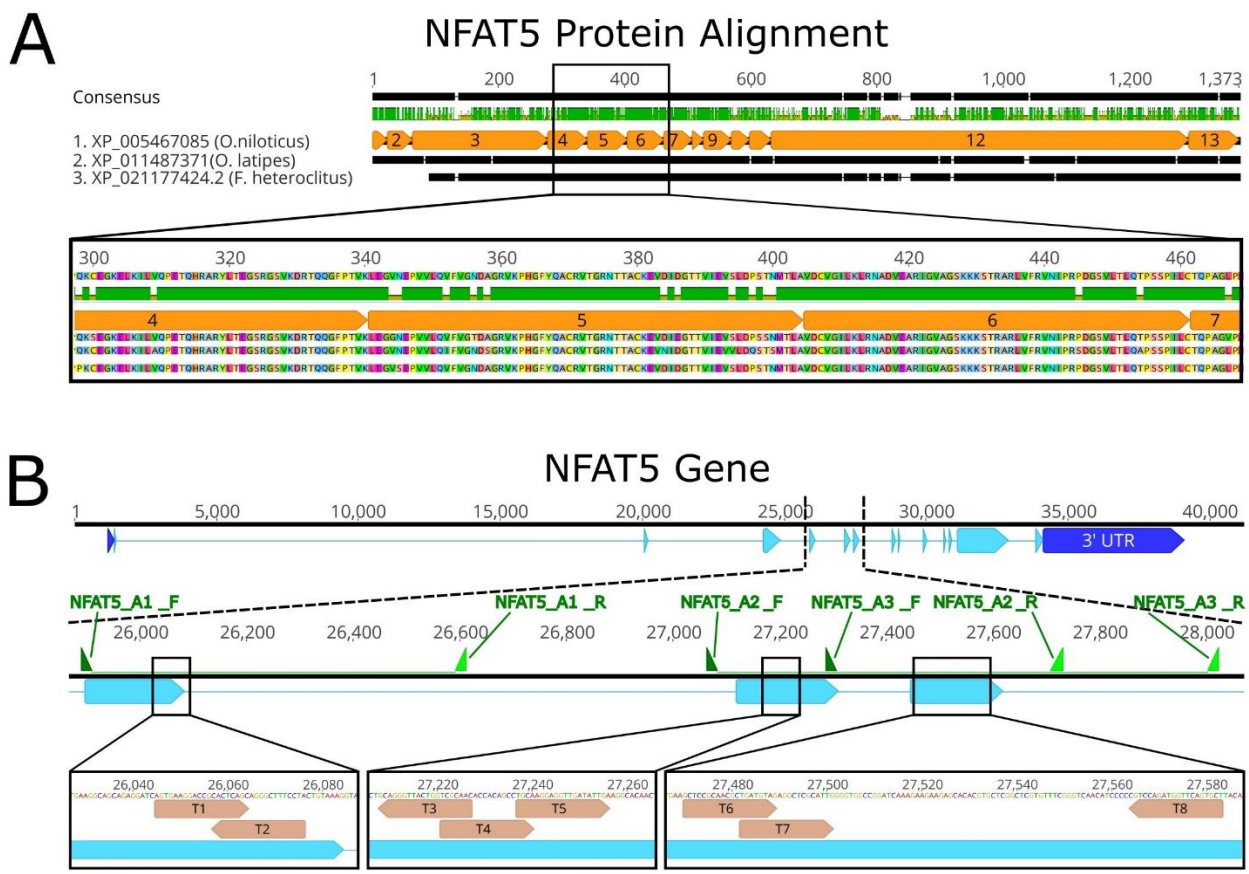

Figure 4. Selection of target regions for development of NFAT5 KO cell lines. A: amino acid (aa) sequence alignment of predicted NFAT5 proteins from three fish species (*Oreochromis niloticus*, *Oryzias latipes*, and *Fundulus heteroclitus*) to identify highly conserved regions assumed to be essential sequence for gRNA targeting. The corresponding nucleotide sequence of the conserved (boxed) region was loaded into the CRISPOR gRNA selection algorithm. B: NFAT5 genomic locations corresponding to conserved aa sequence region and selected gRNAs from the CRISPOR output for in vivo empirical testing. Includes locations of the primer pairs used to generate test amplicons for mutational efficiency and genotyping.

Target	gRNA	Test Amplicon (Primers and Length)			MIT Spec.	Doench	TIDE
#	Sequence	Forward Primer	Reverse Primer	Size (bp)	Score	Efficiency	INDEL%
T1	GTGAAGGACCGCACTCAGC	GCTGCAGCTCTGATGAACCT	CCTTAGAGCTTTGGTCCCCG	722	95	48	14.1
T2	GGAAAGCCCTGCTGAGTG	GCTGCAGCTCTGATGAACCT	CCTTAGAGCTTTGGTCCCCG	722	92	65	39.4
T3	GTTGCGACCAGTAACCCTGC	CAGCAGATCTACCAGGAGCG	CCTTGCTGGGTAATTTTCTGCA	667	94	61	60.4
T4	GCAACACCACAGCCTGCA	CAGCAGATCTACCAGGAGCG	CCTTGCTGGGTAATTTTCTGCA	667	90	60	8.8
T5	GCAAGGAGGTTGATATTGA	CAGCAGATCTACCAGGAGCG	CCTTGCTGGGTAATTTTCTGCA	667	92	45	51.9
T6	GCTCCGCAACGCTGATGTAG	TCCAAGCTCCAACATGACCC	GCCCTAAGCGTCTTTCCTGT	738	97	53	36.4
T7	GATGTAGAGGCTCGCATTG	TCCAAGCTCCAACATGACCC	GCCCTAAGCGTCTTTCCTGT	738	98	63	56.1
T8	GACTGAACCATCTGGACG	TCCAAGCTCCAACATGACCC	GCCCTAAGCGTCTTTCCTGT	738	95	60	0.1

Table 2. Candidate gRNA sequences selected for *in vivo* empirical testing of mutational efficiency including test amplicon sizes with associated primer pairs, CRISPOR MIT specificity scores, predicted efficiency (Doench) and *in vivo* empirically tested efficiency (TIDE INDEL%).

Generation of NFAT5 KO clonal lines

All gRNA targets yielded at least one clonal genotype with 100% frameshift mutation that remained constant from initial genotyping to the end of the experiment after multiple passages. The selected clones for subsequent experiments all maintained a high R^2 DECODR model fit of 0.94 or greater throughout the entire experiment (Figure 5).

Clone ID	INDEL IDs	Allele Sequence	Freq (%)	Model R^2
NFAT5 T3	**WT**	**CATGGGTTTTACCAAGCCTGCAGGGTTACTGGTCGCAACACCACAGCCTGCAAGGAGGTT**		
Init.	-1	CATGGGTTTTACCAAGCCTGCA-CTGTACTGGTCGCAACACCACAGCCTGCAAGGAGGTT	100.0	**1.00**
Post	-1	CATGGGTTTTACCAAGCCTGCA-CTGTACTGGTCGCAACACCACAGCCTGCAAGGAGGTT	100.0	**1.00**
NFAT5 T5	**WT**	**CTGGTCGCAACACCACAGCCTGCAAGGAGGTTGATATTGAAGGCACAACTGTTATCGAAG**		
Init.	-1	CTGGTCGCAACACCACAGCCTGCAAGGAGGTTGATA-TGAAGGCACAACTGTTATCGAAG	67.1	**0.98**
	+1	CTGGTCGCAACACCACAGCCTGCAAGGAGGTTGATATTTGAAGGCACAACTGTTATCGAA	32.9	
Post	-1	CTGGTCGCAACACCACAGCCTGCAAGGAGGTTGATA-TGAAGGCACAACTGTTATCGAAG	66.1	**0.96**
	+1	CTGGTCGCAACACCACAGCCTGCAAGGAGGTTGATATTTGAAGGCACAACTGTTATCGAA	33.9	
NFAT5 T7	**WT**	**GATCCTGAAGCTCCGCAACGCTGATGTAGAGGCTCGCATTGGGGTGGCCGGATCAAAGAA**		
Init.	-64	GATCCTGAA----------(-64)----------GCTCGGCTCG	57.1	**0.95**
	-1	GATCCTGAAGCTCCGCAACGCTGATGTAGAGGCTCGCA-TGGGGTGGCCGGATCAAAGAA	42.9	
Post	-64	GATCCTGAA----------(-64)----------GCTCGGCTCG	58.4	**0.94**
	-1	GATCCTGAAGCTCCGCAACGCTGATGTAGAGGCTCGCA-TGGGGTGGCCGGATCAAAGAA	41.6	

PAM Target Sequence Insertion – Deletion

Figure 5. Genotype sequence output from DECODR algorithm analysis of test amplicon chromatograms from both initial screening process (Init.) and at the end of the experiment after multiple passages (Post) on the selected clonal NFAT5 KO cell line for each gRNA (clone ID). For each INDEL (insertion/deletion mutation) the net bp change (INDEL ID), precise allele sequence at the targeted site relative to the wild-type sequence, the predicted relative frequency of each allele (Freq %), and the R2 model fit of each chromatogram input to the DECODR algorithm are shown.

IMPA1.1 and MIPS mRNA abundances in NFAT5 KO cells exposed to IO and HO conditions

Quantitative PCR was performed on the NFAT5 KO and NE KO control lines after 24 hours exposure to HO challenge (650 mOsm/kg) or IO control (315 mOsm/kg) media with primer pairs targeting IMPA1.1 and MIPS transcripts and using both β-actin and 18s ribosomal RNA as RG. In IO control cells, there was

no significant difference in MIPS (β-actin RG: 1.59 fold change, p-value= 0.7449 and 18s rRNA RG: 1.19 fold change, p-value= 0.6508) or IMPA1.1 relative abundance (β-actin RG: 0.81 fold change, p-value= 0.3845 and 18s rRNA RG: 0.69 fold change, p-value= 0.3204) using either reference gene (Figure 6). In HO media for both reference genes, there was a moderate non-significant reduction in MIPS mRNA abundance (β-actin RG: 0.94 fold change, p-value= 0.4404 and 18s rRNA RG: 0.63 fold change, p-value= 0.1677) (Figure 6A&B) and a near significant reduction in IMPA1.1 mRNA abundance with the β-actin RG (0.73 fold change, p-value= 0.1331) (Figure 6C) and a significant reduction with 18s rRNA RG (0.51 fold change, p-value= 0.02036) (Figure 6D) in NFAT5KO cells relative to NE KO control lines.

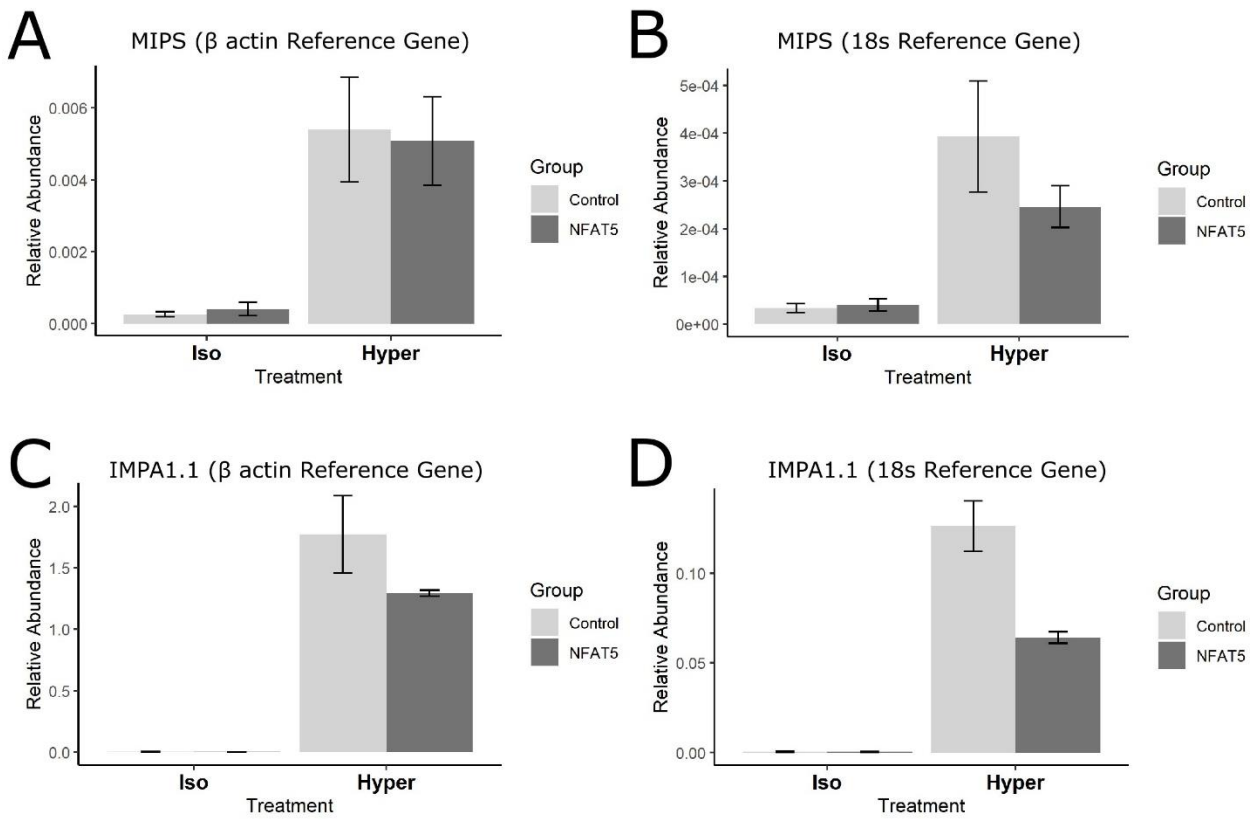

Figure 6. . Relative mRNA abundance of MIPS (A&B) and IMPA1.1 (C&D) genes quantified by qRT-PCR in NFAT5 KO cells lines compared to NE KO controls in both IO and HO conditions normalized using both β-actin and 18s rRNA as reference genes. Relative mRNA abundance of MIPS and IMPA1.1 transcripts are displayed as ($2^{-\Delta Ct}$) (52, 53).

DISCUSSION

Induction of NFAT5 in response to HO stress has been observed in all vertebrate classes investigated thus far, i.e., in mammals (55, 56), amphibians (57), and fish (30). Conservation of this role from even earlier in phylogenetic history is implied by HO responsiveness of NAFT5 from *Ciona robusta*, a primitive chordate, when expressed in a human cell line (58). In mammalian models, NFAT5 accounts for the majority of HO induced transcriptional changes (19, 55, 56, 59). Considering the phylogenetic conservation of HO responsive NFAT5 signaling, this regulatory mechanism was expected to be active in HO challenged cells from a euryhaline fish which was confirmed by the initial RT-PCR work of this study. The synthetic biology approaches that followed established the connection between NFAT5 and HO induced gene expression of the MIB pathway.

It is common for different gene suppression techniques to yield a different phenotype for the same target gene (60). Therefore, applying multiple strategies yields the most robust results. Ectopic expression of DN TFs, i.e., TFs in which the TAD is deleted but the DBD is maintained (33), is an effective strategy to evaluate interactions with DNA regulatory elements and has been a critical tool in deciphering the functions and interactions of other RHD transcription factors (32, 61, 62). However, DN proteins require precise engineering in order to function as intended and thus when using a new DN protein it may not be certain to what degree observations are due to endogenous interactions between the proteins in question or the effectiveness of the DN design. We used characterization of the predicted XM_005467029 aa sequence using domain information and validated NFATDN design from mammalian studies (32) to maximize the potential for *O. mossambicus* NFAT5DN intended functionality. Overexpression of TFs has been historically useful in elucidating protein function (31, 63). However, TFs can bind to DNA non-specifically (64, 65) and an abnormally high concentration can result in increased global transcription (66, 67) leading to erroneous transcriptionally induced phenotypes. This potential

confounding factor was accounted for by normalization through co-transfection of the IMPA1.1-EGFP reporter with the RFP vector which would also be affected by non-specific TF activity. CRISPR/Cas9 mediated editing is another efficient method for target gene disruption but careful interpretation of the effect is required due to the potential of cellular changes not relevant to the phenotype in question caused by unknown off target effects (68). Here, replication with multiple NFAT5 KO clones obtained from different gRNAs was used to control for this potential pitfall. Collectively, these approaches can provide compelling evidence in deciphering the interactions between NFAT5 and its target genes.

The capability of NFAT5 to induce the IMPA1.1 promoter was demonstrated by the statistically significant induction of the IMPA1.1-EGFP reporter by NFAT5WT in IO conditions. The HO induced upregulation of *NFAT5* mRNA abundance observed by qRT-PCR in tilapia OmB cells was also highly significant, consistent with the typical response of HO exposed mammalian cells (17, 55, 69). Collectively, this established high plausibility that NFAT5 is at least partially responsible for the HO induced increase in IMPA1.1 mRNA abundance that is consistently observed in tilapia cells (3, 6, 8, 70).

Here we used dominant negative and gene KO approaches to establish causality between NFAT5 and MIB enzyme regulation. The NFAT5DN and NFAT5KO results for HO regulation of IMPA1.1 are consistent with each other and the result of NFAT5WT overexpression in cells exposed to IO. The continuity of these results instill high confidence in the methodologies and the observed results. Collectively, our results indicate that tilapia NFAT5 is partly responsible for *IMPA1.1* (37 – 49%) and MIPS (6 - 37%) transcriptional induction during HO stress. Considering the magnitude at which these genes are HO induced there is still a very substantial amount of HO induced gene activation present despite disrupted NFAT5 signaling. This result suggests that in tilapia cells other osmoresponsive signaling networks are strongly induced by the HO stress. Since *O. mossambicus* and other euryhaline fishes encounter osmotic gradients in an aqueous ambient environment and can sustain more rapid and extreme changes in plasma osmolalities (3, 71, 72), a much wider range of tissues and cell types are subjected to a more

dynamic range of osmotic exposure. This may necessitate complementary signaling mechanisms to account for these more diverse osmotic challenges.

The *MIPS* and *IMPA1.1* promoter regions contain similar copy numbers of the OSRE1 enhancer (9), and yet a lesser relative impact of NFAT5KO on *MIPS* abundance was observed relative to *IMPA1.1*. Although the consensus OSRE1 core was present in all of these *cis*-elements, the overall enhancer sequence was highly variable. NFAT5 has the most stringent binding sequence of all the NFATs and it's binding affinity is highly affected by core adjacent sequence (73, 74). Consequently, the relative influence NFAT5 has on transcription is dependent on the collective sequence dependent binding affinity of all the OSRE1 elements present in the promoter. Although not generally associated with HO signaling, the calcineurin regulated NFAT1-4 proteins are possible additional interacting partners with OSRE1 as there is high overlap in binding sequence between all the NFATs and there have been other accounts of calcineurin based NFAT signaling in response to HO stress. In immortalized murine renal collecting duct cells calcineurin mediated regulation of aquaporin 2 expression was demonstrated in response to HO stress (75). This response would require an increase of intracellular Ca^{2+} which is commonly associated with hypo-osmotic response (1, 76), however, conflicting reports exist that it can also be a HO response (77, 78). Like most promoters which contain many different *cis* elements responsive to a variety of regulators, the *IMPA1.1* promoter contains several HO responsive regions lacking an OSRE1 (9) representing potential *cis* elements that interact with parallel NFAT independent HO signaling pathways. The ubiquitous c-Myc (79), osmotic stress transcription factor 1 (Ostf1) (80), and CCAAT/enhancer binding protein (C/EBP) (81) are among other transcription factors associated with the HO stress response in fish and may interact with NFAT5 to achieve full HO induction of MIB pathway genes.

Despite the evidence supporting NFAT5 is only responsible for approximately half of HO induced IMPA1.1 promoter activity, the effect size observed by ectopic NFAT5WT expression seems

comparatively low. HO treatment typically leads to IMPA1.1 mRNA abundance increases of several hundred-fold which is substantially higher than the 5.1-fold induction of the IMPA1.1-EGFP reporter by NFAT5WT. The disparity seems even more striking when considering the NFAT5WT was expressed from a β-actin promoter likely leading to NFAT5 levels in excess of what occurs naturally. This discrepancy can be reconciled by the post translational regulation of NFAT5. Since NFAT5WT overexpression in this study was performed in IO conditions, any localization or activity effects caused by HO conditions were not represented in this result.

In mammalian models subcellular distribution of NFAT5 is controlled by an N-terminal regulatory domain (NTD) containing a N-terminal NES, followed by AD1 (23), the hypo-osmotic responsive AED (42), and the potent HO responsive NLS (43). In basal IO conditions, mammalian NFAT5 has a constitutive distribution throughout both the cytoplasm and the nucleus held in equilibrium by this region (54, 74). HO conditions induce strong NFAT5 nuclear enrichment (42, 54, 82), which is mediated by HO activation of the NLS (43). Considering the highly conserved N-terminal NFAT5 domain, the mechanism of HO regulation of *O. mossambicus* NFAT5 is likely very similar to that observed in mammalian models. In addition to nuclear localization, transcriptional activity is also highly HO induced by multiple post translational modifications to the TADs (AD1, AD2, and AD3) and other accessory modulating domains (23–25). In HO treated NFAT5 TADs isolated from the NTD, activity increases of several magnitudes have been observed (23, 25). Interestingly, exon 2 which contains the AD1 activation domain is excised from the predominant HO induced NFAT5 isoform observed in this study. Although weaker than the other NFAT5 ADs, mammalian AD1 has demonstrated intrinsic transcriptional activity and an ability to synergistically enhance the activation strength of the other NFAT5 ADs up to two-fold (23). Excision of exon 2 from the HO induced form of *O. mossambicus* NFAT5 seems counterintuitive, especially considering the two nuclear export signals (NES and AED) flanking exon 2 are still maintained in the transcript. Conformational change leading to increased activity of mammalian

NFAT5 in response to elevated ions has been reported (83). This conformational change might have a suppressive effect on one or both of the export signals. Therefore it is possible omission of exon 2 in the HO induced NFAT5 isoform from this study results in a structural change that functionally replicates this effect. Collectively, these considerations support that full *O. mossambicus* NFAT5 HO influence is a combination of changes in NFAT5 abundance, localization, and activity.

Perspectives and Significance

Although a role of NFAT5 in fish salinity tolerance has been implicated, this study is the first to establish causality between NFAT5 and HO induced differential gene expression in fish cells. The work described here provides important new insights on the mechanisms of fish salinity tolerance, especially those influenced by NFAT5. This work has produced new valuable tools and methodologies such as dominant negative expression systems and NFAT5 KO cell lines to further evaluate the role of NFAT5 and other complimentary regulators in HO tolerance and for other physiological functions of euryhaline fishes.

By accounting for weaknesses of each method and using a very comprehensive multifaceted approach composed of distinct methods and numerous controls that all supported the same results, we have accumulated solid support for the following conclusions: *O. mossambicus* NFAT5 mRNA abundance is elevated during HO stress, specifically a predominant isoform that is missing the AD1 containing exon 2. This isoform is able to localize to the nucleus and induce transcription in the absence of HO induction indicating its capability for maintaining basal activity under IO conditions. In OmB cells, NFAT5 has a clear role in the regulation of the highly HO transcriptionally induced *IMPA1.1* and *MIPS* genes. Disruption of NFAT5 results in up to 49% and 37% reduction of HO induced mRNA abundance for IMPA1.1 and MIPS, respectively. This contribution of tilapia NFAT5 to HO target gene induction is less than what is typically observed in mammalian models. Therefore, euryhaline fish such as tilapia must

have a more elaborate HO response signaling network with other strongly induced signaling pathways that are activated jointly with NFAT5 signaling pathways during HO stress.

ACKNOWLEDGMENTS

The authors thank Leah MacNiven for assisting with fluorescent imaging and Amber Yiao for help in primer design of NFAT5 qRT-PCR primers.

GRANTS

National Science Foundation, Grant/Award Number: IOS- 2209383.

US-Israel Binational Agricultural Research and Development Fund, Grant/Award Number: IS-5358-21.

DISCLOSURES

The authors have no conflicts of interest to disclose.

AUTHOR CONTRIBUTIONS

J.H. and D.K. conceived and designed research, J.H. performed experiments, analyzed data, interpreted results of experiments, prepared figures, and drafted manuscript. J.H., D.K., and A.C. edited and revised manuscript. J.H., D.K., and A.C. approved final version of manuscript.

REFERENCES

1. **Kültz D**. The combinatorial nature of osmosensing in fishes. *Physiology (Bethesda)* 27: 259–275, 2012. doi: 10.1152/physiol.00014.2012.

2. **Bagnasco S**, **Balaban R**, **Fales HM**, **Yang YM**, **Burg M**. Predominant osmotically active organic solutes in rat and rabbit renal medullas. *J Biol Chem* 261: 5872–5877, 1986.

3. **Gardell AM**, **Yang J**, **Sacchi R**, **Fangue NA**, **Hammock BD**, **Kültz D**. Tilapia (*Oreochromis mossambicus*) brain cells respond to hyperosmotic challenge by inducing *myo*-inositol biosynthesis. *J Exp Biol* 216: 4615–4625, 2013. doi: 10.1242/jeb.088906.

4. **Yancey PH**, **Clark ME**, **Hand SC**, **Bowlus RD**, **Somero GN**. Living with water stress: evolution of osmolyte systems. *Science* 217: 1214–1222, 1982. doi: 10.1126/science.7112124.

5. **Michell RH**. Inositol derivatives: evolution and functions. *Nat Rev Mol Cell Biol* 9: 151–161, 2008. doi: 10.1038/nrm2334.

6. **Sacchi R**, **Li J**, **Villarreal F**, **Gardell AM**, **Kültz D**. Salinity-induced regulation of the *myo*-inositol biosynthesis pathway in tilapia gill epithelium. *J Exp Biol* 216: 4626–4638, 2013. doi: 10.1242/jeb.093823.

7. **Kalujnaia S**, **Gellatly SA**, **Hazon N**, **Villasenor A**, **Yancey PH**, **Cramb G**. Seawater acclimation and inositol monophosphatase isoform expression in the European eel (*Anguilla anguilla*) and Nile tilapia (*Orechromis niloticus*). *Am J Physiol Regul Integr Comp Physiol* 305: R369-384, 2013. doi: 10.1152/ajpregu.00044.2013.

8. **Gardell AM**, **Qin Q**, **Rice RH**, **Li J**, **Kültz D**. Derivation and osmotolerance characterization of three immortalized tilapia (*Oreochromis mossambicus*) cell lines. *PLoS One* 9: e95919, 2014. doi: 10.1371/journal.pone.0095919.

9. **Wang X**, **Kültz D**. Osmolality/salinity-responsive enhancers (OSREs) control induction of osmoprotective genes in euryhaline fish. *Proc Natl Acad Sci U S A* 114: E2729–E2738, 2017. doi: 10.1073/pnas.1614712114.

10. **Senger K**, **Armstrong GW**, **Rowell WJ**, **Kwan JM**, **Markstein M**, **Levine M**. Immunity regulatory DNAs share common organizational features in *Drosophila*. *Mol Cell* 13: 19–32, 2004. doi: 10.1016/s1097-2765(03)00500-8.

11. **Kunsch C**, **Ruben SM**, **Rosen CA**. Selection of optimal kappa B/Rel DNA-binding motifs: interaction of both subunits of NF-kappa B with DNA is required for transcriptional activation. *Mol Cell Biol* 12: 4412–4421, 1992. doi: 10.1128/mcb.12.10.4412-4421.1992.

12. **Ghosh S**, **May MJ**, **Kopp EB**. NF-kappa B and Rel proteins: evolutionarily conserved mediators of immune responses. *Annu Rev Immunol* 16: 225–260, 1998. doi: 10.1146/annurev.immunol.16.1.225.

13. **Northrop JP**, **Ho SN**, **Chen L**, **Thomas DJ**, **Timmerman LA**, **Nolan GP**, **Admon A**, **Crabtree GR**. NF-AT components define a family of transcription factors targeted in T-cell activation. *Nature* 369: 497–502, 1994. doi: 10.1038/369497a0.

14. **Rao A**, **Luo C**, **Hogan PG**. Transcription factors of the NFAT family: regulation and function. *Annu Rev Immunol* 15: 707–747, 1997. doi: 10.1146/annurev.immunol.15.1.707.

15. **Chen Y-Q**, **Sengchanthalangsy LL**, **Hackett A**, **Ghosh G**. NF-κB p65 (RelA) homodimer uses distinct mechanisms to recognize DNA targets. *Structure* 8: 419–428, 2000. doi: 10.1016/S0969-2126(00)00123-4.

16. **Ghosh G**, **Duyne GV**, **Ghosh S**, **Sigler PB**. Structure of NF-κB p50 homodimer bound to a κB site. *Nature* 373: 303–310, 1995. doi: 10.1038/373303a0.

17. **Kino T**, **Takatori H**, **Manoli I**, **Wang Y**, **Tiulpakov A**, **Blackman MR**, **Su YA**, **Chrousos GP**, **DeCherney AH**, **Segars JH**. Brx mediates the response of lymphocytes to osmotic stress through the activation of NFAT5. *Sci Signal* 2: ra5, 2009. doi: 10.1126/scisignal.2000081.

18. **Woo SK**, **Lee SD**, **Na KY**, **Park WK**, **Kwon HM**. TonEBP/NFAT5 stimulates transcription of HSP70 in response to hypertonicity. *Mol Cell Biol* 22: 5753–5760, 2002. doi: 10.1128/MCB.22.16.5753-5760.2002.

19. **López-Rodríguez C**, **Antos CL**, **Shelton JM**, **Richardson JA**, **Lin F**, **Novobrantseva TI**, **Bronson RT**, **Igarashi P**, **Rao A**, **Olson EN**. Loss of NFAT5 results in renal atrophy and lack of tonicity-responsive gene expression. *Proc Natl Acad Sci U S A* 101: 2392–2397, 2004. doi: 10.1073/pnas.0308703100.

20. **Ito T**, **Fujio Y**, **Hirata M**, **Takatani T**, **Matsuda T**, **Muraoka S**, **Takahashi K**, **Azuma J**. Expression of taurine transporter is regulated through the TonE (tonicity-responsive element)/TonEBP (TonE-binding protein) pathway and contributes to cytoprotection in HepG2 cells. *Biochem J* 382: 177–182, 2004. doi: 10.1042/BJ20031838.

21. **Woo SK**, **Dahl SC**, **Handler JS**, **Kwon HM**. Bidirectional regulation of tonicity-responsive enhancer binding protein in response to changes in tonicity. *Am J Physiol Renal Physiol* 278: F1006-1012, 2000. doi: 10.1152/ajprenal.2000.278.6.F1006.

22. **Tong EHY**, **Guo J-J**, **Huang A-L**, **Liu H**, **Hu C-D**, **Chung SSM**, **Ko BCB**. Regulation of nucleocytoplasmic trafficking of transcription factor OREBP/TonEBP/NFAT5. *J Biol Chem* 281: 23870–23879, 2006. doi: 10.1074/jbc.M602556200.

23. **Lee SD**, **Colla E**, **Sheen MR**, **Na KY**, **Kwon HM**. Multiple domains of TonEBP cooperate to stimulate transcription in response to hypertonicity. *J Biol Chem* 278: 47571–47577, 2003. doi: 10.1074/jbc.M308795200.

24. **Choi SY**, **Lee-Kwon W**, **Kwon HM**. The evolving role of TonEBP as an immunometabolic stress protein. *Nat Rev Nephrol* 16: 352–364, 2020. doi: 10.1038/s41581-020-0261-1.

25. **Ferraris JD**, **Williams CK**, **Persaud P**, **Zhang Z**, **Chen Y**, **Burg MB**. Activity of the TonEBP/OREBP transactivation domain varies directly with extracellular NaCl concentration. *Proc Natl Acad Sci U S A* 99: 739–744, 2002. doi: 10.1073/pnas.241637298.

26. **Ko BCB**, **Turck CW**, **Lee KWY**, **Yang Y**, **Chung SSM**. Purification, Identification, and Characterization of an Osmotic Response Element Binding Protein. *Biochem Biophys Res Commun* 270: 52–61, 2000. doi: 10.1006/bbrc.2000.2376.

27. **Navarro P**, **Chiong M**, **Volkwein K**, **Moraga F**, **Ocaranza MP**, **Jalil JE**, **Lim SW**, **Kim J-A**, **Kwon HM**, **Lavandero S**. Osmotically-induced genes are controlled by the transcription factor TonEBP in cultured cardiomyocytes. *Biochem Biophys Res Commun* 372: 326–330, 2008. doi: 10.1016/j.bbrc.2008.05.067.

28. **Tsai T-T**, **Guttapalli A**, **Agrawal A**, **Albert TJ**, **Shapiro IM**, **Risbud MV**. MEK/ERK signaling controls osmoregulation of nucleus pulposus cells of the intervertebral disc by transactivation of TonEBP/OREBP. *J Bone Miner Res* 22: 965–974, 2007. doi: 10.1359/jbmr.070322.

29. **Lee JH**, **Kim M**, **Im YS**, **Choi W**, **Byeon SH**, **Lee HK**. NFAT5 induction and its role in hyperosmolar stressed human limbal epithelial cells. *Invest Ophthalmol Vis Sci* 49: 1827–1835, 2008. doi: 10.1167/iovs.07-1142.

30. **Lorgen M**, **Jorgensen EH**, **Jordan WC**, **Martin SAM**, **Hazlerigg DG**. NFAT5 genes are part of the osmotic regulatory system in Atlantic salmon (*Salmo salar*). *Mar Genomics* 31: 25–31, 2017. doi: 10.1016/j.margen.2016.06.004.

31. **Prelich G**. Gene overexpression: uses, mechanisms, and interpretation. *Genetics* 190: 841–854, 2012. doi: 10.1534/genetics.111.136911.

32. **Miyakawa H**, **Woo SK**, **Dahl SC**, **Handler JS**, **Kwon HM**. Tonicity-responsive enhancer binding protein, a rel-like protein that stimulates transcription in response to hypertonicity. *Proc Natl Acad Sci U S A* 96: 2538–2542, 1999. doi: 10.1073/pnas.96.5.2538.

33. **Brown PH**, **Alani R**, **Preis LH**, **Szabo E**, **Birrer MJ**. Suppression of oncogene-induced transformation by a deletion mutant of c-jun. *Oncogene* 8: 877–886, 1993.

34. **Cortez JT**, **Montauti E**, **Shifrut E**, **Gatchalian J**, **Zhang Y**, **Shaked O**, **Xu Y**, **Roth TL**, **Simeonov DR**, **Zhang Y**, **Chen S**, **Li Z**, **Woo JM**, **Ho J**, **Vogel IA**, **Prator GY**, **Zhang B**, **Lee Y**, **Sun Z**, **Ifergan I**, **Van Gool F**, **Hargreaves DC**, **Bluestone JA**, **Marson A**, **Fang D**. CRISPR screen in regulatory T cells reveals modulators of Foxp3. *Nature* 582: 416–420, 2020. doi: 10.1038/s41586-020-2246-4.

35. **de Almeida M**, **Hinterndorfer M**, **Brunner H**, **Grishkovskaya I**, **Singh K**, **Schleiffer A**, **Jude J**, **Deswal S**, **Kalis R**, **Vunjak M**, **Lendl T**, **Imre R**, **Roitinger E**, **Neumann T**, **Kandolf S**, **Schutzbier M**, **Mechtler K**, **Versteeg GA**, **Haselbach D**, **Zuber J**. AKIRIN2 controls the nuclear import of proteasomes in vertebrates. *Nature* 599: 491–496, 2021. doi: 10.1038/s41586-021-04035-8.

36. **Hamar J**, **Kültz D**. An efficient vector-based CRISPR/Cas9 system in an *Oreochromis mossambicus* cell line using endogenous promoters. *Sci Rep* 11: 7854, 2021. doi: 10.1038/s41598-021-87068-3.

37. **Mak MC**, **Lam KM**, **Chan PK**, **Lau YB**, **Tang WH**, **Yeung PKK**, **Ko BCB**, **Chung SMS**, **Chung SK**. Embryonic Lethality in Mice Lacking the Nuclear Factor of Activated T Cells 5 Protein Due to Impaired Cardiac Development and Function. *PLOS ONE* 6: e19186, 2011. doi: 10.1371/journal.pone.0019186.

38. **Go WY**, **Liu X**, **Roti MA**, **Liu F**, **Ho SN**. NFAT5/TonEBP mutant mice define osmotic stress as a critical feature of the lymphoid microenvironment. *Proc Natl Acad Sci U S A* 101: 10673–10678, 2004. doi: 10.1073/pnas.0403139101.

39. **Chernyakov D**, **Groß A**, **Fischer A**, **Bornkessel N**, **Schultheiss C**, **Gerloff D**, **Edemir B**. Loss of RANBP3L leads to transformation of renal epithelial cells towards a renal clear cell carcinoma like phenotype. *J Exp Clin Cancer Res* 40: 226, 2021. doi: 10.1186/s13046-021-01982-y.

40. **Kim G-N**, **Hah Y-S**, **Seong H**, **Yoo W-S**, **Choi M-Y**, **Cho H-Y**, **Yun SP**, **Kim S-J**. The Role of Nuclear Factor of Activated T Cells 5 in Hyperosmotic Stress-Exposed Human Lens Epithelial Cells. *Int J Mol Sci* 22, 2021. doi: 10.3390/ijms22126296.

41. **Kang K**, **Huang L**, **Li Q**, **Liao X**, **Dang Q**, **Yang Y**, **Luo J**, **Zeng Y**, **Li L**, **Gou D**. An improved Tet-on system in microRNA overexpression and CRISPR/Cas9-mediated gene editing. *J Anim Sci Biotechnol* 10: 43, 2019. doi: 10.1186/s40104-019-0354-5.

42. **Xu S**, **Wong CCL**, **Tong EHY**, **Chung SSM**, **Yates JR III**, **Yin Y**, **Ko BCB**. Phosphorylation by Casein Kinase 1 Regulates Tonicity-induced Osmotic Response Element-binding Protein/Tonicity Enhancer-binding Protein Nucleocytoplasmic Trafficking *. *J Biol Chem* 283: 17624–17634, 2008. doi: 10.1074/jbc.M800281200.

43. **Kwon MS**, **Lee SD**, **Kim J-A**, **Colla E**, **Choi YJ**, **Suh P-G**, **Kwon HM**. Novel nuclear localization signal regulated by ambient tonicity in vertebrates. *J Biol Chem* 283: 22400–22409, 2008. doi: 10.1074/jbc.M710550200.

44. **Zúñiga RA**, **Gutiérrez-González M**, **Collazo N**, **Sotelo PH**, **Ribeiro CH**, **Altamirano C**, **Lorenzo C**, **Aguillón JC**, **Molina MC**. Development of a new promoter to avoid the silencing of genes in the production of recombinant antibodies in chinese hamster ovary cells. *J of Biol Eng* 13: 59, 2019. doi: 10.1186/s13036-019-0187-y.

45. **Hitoshi N**, **Ken-ichi Y**, **Jun-ichi M**. Efficient selection for high-expression transfectants with a novel eukaryotic vector. *Gene* 108: 193–199, 1991. doi: 10.1016/0378-1119(91)90434-D.

46. **Su J**, **Zhu Z**, **Xiong F**, **Wang Y**. Hybrid Cytomegalovirus-U6 Promoter-based Plasmid Vectors Improve Efficiency of RNA Interference in Zebrafish. *Mar Biotechnol* 10: 511–517, 2008. doi: 10.1007/s10126-008-9087-8.

47. **Moriya H**. Quantitative nature of overexpression experiments. *Mol Biol Cell* 26: 3932–3939, 2015. doi: 10.1091/mbc.E15-07-0512.

48. **Hamar J**, **Cnaani A**, **Kültz D**. Effects of CRISPR/Cas9 targeting of the *myo*-inositol biosynthesis pathway on hyper-osmotic tolerance of tilapia cells. *Genomics* Submitted, in review, [date unknown].

49. **Concordet J-P**, **Haeussler M**. CRISPOR: intuitive guide selection for CRISPR/Cas9 genome editing experiments and screens. *Nucleic Acids Res* 46: W242–W245, 2018. doi: 10.1093/nar/gky354.

50. **Brinkman EK**, **Chen T**, **Amendola M**, **van Steensel B**. Easy quantitative assessment of genome editing by sequence trace decomposition. *Nucleic Acids Res* 42: e168, 2014. doi: 10.1093/nar/gku936.

51. **Bloh K**, **Kanchana R**, **Bialk P**, **Banas K**, **Zhang Z**, **Yoo B-C**, **Kmiec EB**. Deconvolution of Complex DNA Repair (DECODR): Establishing a Novel Deconvolution Algorithm for Comprehensive Analysis of CRISPR-Edited Sanger Sequencing Data. *CRISPR J* 4: 120–131, 2021. doi: 10.1089/crispr.2020.0022.

52. **Livak KJ**, **Schmittgen TD**. Analysis of Relative Gene Expression Data Using Real-Time Quantitative PCR and the 2−ΔΔCT Method. *Methods* 25: 402–408, 2001. doi: 10.1006/meth.2001.1262.

53. **Schmittgen TD**, **Livak KJ**. Analyzing real-time PCR data by the comparative CT method. *Nat Protoc* 3: 1101–1108, 2008. doi: 10.1038/nprot.2008.73.

54. **Cheung CY**, **Huang T-T**, **Chow N**, **Zhang S**, **Zhao Y**, **Chau MP**, **Chan WC**, **Wong CCL**, **Boassa D**, **Phan S**, **Ellisman MH**, **Yates JR**, **Xu S**, **Yu Z**, **Zhang Y**, **Zhang R**, **Ng LL**, **Ko BCB**. Unconventional tonicity-regulated nuclear trafficking of NFAT5 mediated by KPNB1, XPOT and RUVBL2. *J Cell Sci* 135, 2022. doi: 10.1242/jcs.259280.

55. **Cheung CYK**, **Ko BCB**. NFAT5 in cellular adaptation to hypertonic stress – regulations and functional significance. *J Mol Signal* 8, 2013. doi: 10.1186/1750-2187-8-5.

56. **Kwon MS**, **Lim SW**, **Kwon HM**. Hypertonic Stress in the Kidney: A Necessary Evil. *Physiology* 24: 186–191, 2009. doi: 10.1152/physiol.00005.2009.

57. **Li J**, **Wang X**, **Lan T**, **Lu Y**, **Hong M**, **Ding L**, **Wang L**. CDK5/NFAT5-Regulated Transporters Involved in Osmoregulation in *Fejervarya cancrivora*. *Biology (Basel)* 11, 2022. doi: 10.3390/biology11060858.

58. **He M**, **Wei J**, **Li Y**, **Dong B**. Nuclear Factor of Activated T Cells-5 Regulates Notochord Lumenogenesis in Chordate Larval Development. *Int J Mol Sci* 23, 2022. doi: 10.3390/ijms232214407.

59. **Chernyakov D**, **Fischer A**, **Brandau M**, **Petrillo F**, **Fenton RA**, **Edemir B**. The nuclear factor of activated T cells 5 (NFAT5) contributes to the renal corticomedullary differences in gene expression. *Sci Rep* 12: 20304, 2022. doi: 10.1038/s41598-022-24237-y.

60. **Kok FO**, **Shin M**, **Ni C-W**, **Gupta A**, **Grosse AS**, **van Impel A**, **Kirchmaier BC**, **Peterson-Maduro J**, **Kourkoulis G**, **Male I**, **DeSantis DF**, **Sheppard-Tindell S**, **Ebarasi L**, **Betsholtz C**, **Schulte-Merker S**, **Wolfe SA**, **Lawson ND**. Reverse genetic screening reveals poor correlation between morpholino-induced and mutant phenotypes in zebrafish. *Dev Cell* 32: 97–108, 2015. doi: 10.1016/j.devcel.2014.11.018.

61. **Anrather J**, **Csizmadia V**, **Brostjan C**, **Soares MP**, **Bach FH**, **Winkler H**. Inhibition of bovine endothelial cell activation in vitro by regulated expression of a transdominant inhibitor of NF-kappa B. *J Clin Invest* 99: 763–772, 1997. doi: 10.1172/JCI119222.

62. **Macián F**, **García-Rodríguez C**, **Rao A**. Gene expression elicited by NFAT in the presence or absence of cooperative recruitment of Fos and Jun. *EMBO J* 19: 4783–4795, 2000. doi: 10.1093/emboj/19.17.4783.

63. **Takahashi K**, **Tanabe K**, **Ohnuki M**, **Narita M**, **Ichisaka T**, **Tomoda K**, **Yamanaka S**. Induction of Pluripotent Stem Cells from Adult Human Fibroblasts by Defined Factors. *Cell* 131: 861–872, 2007. doi: 10.1016/j.cell.2007.11.019.

64. **Baughman HER**, **Narang D**, **Chen W**, **Villagrán Suárez AC**, **Lee J**, **Bachochin MJ**, **Gunther TR**, **Wolynes PG**, **Komives EA**. An intrinsically disordered transcription activation domain increases the DNA binding affinity and reduces the specificity of NFκB p50/RelA. *J Biol Chem* 298: 102349, 2022. doi: 10.1016/j.jbc.2022.102349.

65. **Afek A**, **Schipper JL**, **Horton J**, **Gordân R**, **Lukatsky DB**. Protein−DNA binding in the absence of specific base-pair recognition. *Proc Natl Acad Sci U S A* 111: 17140–17145, 2014. doi: 10.1073/pnas.1410569111.

66. **Lin CY**, **Lovén J**, **Rahl PB**, **Paranal RM**, **Burge CB**, **Bradner JE**, **Lee TI**, **Young RA**. Transcriptional amplification in tumor cells with elevated c-Myc. *Cell* 151: 56–67, 2012. doi: 10.1016/j.cell.2012.08.026.

67. **Banks CAS**, **Lee ZT**, **Boanca G**, **Lakshminarasimhan M**, **Groppe BD**, **Wen Z**, **Hattem GL**, **Seidel CW**, **Florens L**, **Washburn MP**. Controlling for gene expression changes in transcription factor protein networks. *Mol Cell Proteomics* 13: 1510–1522, 2014. doi: 10.1074/mcp.M113.033902.

68. **Kimberland ML**, **Hou W**, **Alfonso-Pecchio A**, **Wilson S**, **Rao Y**, **Zhang S**, **Lu Q**. Strategies for controlling CRISPR/Cas9 off-target effects and biological variations in mammalian genome editing experiments. *J Biotech* 284: 91–101, 2018. doi: 10.1016/j.jbiotec.2018.08.007.

69. **Cai Q**, **Ferraris JD**, **Burg MB**. High NaCl increases TonEBP/OREBP mRNA and protein by stabilizing its mRNA. *Am J Physiol Renal Physiol* 289: F803-807, 2005. doi: 10.1152/ajprenal.00448.2004.

70. **Sacchi R**, **Gardell AM**, **Chang N**, **Kültz D**. Osmotic regulation and tissue localization of the *myo*-inositol biosynthesis pathway in tilapia (*Oreochromis mossambicus*) larvae. *J Exp Zool A Ecol Genet Physiol* 321: 457–466, 2014. doi: 10.1002/jez.1878.

71. **Lema SC**, **Carvalho PG**, **Egelston JN**, **Kelly JT**, **McCormick SD**. Dynamics of Gene Expression Responses for Ion Transport Proteins and Aquaporins in the Gill of a Euryhaline Pupfish during Freshwater and High-Salinity Acclimation. *Physiol Biochem Zool* 91: 1148–1171, 2018. doi: 10.1086/700432.

72. **Yamaguchi Y**, **Breves JP**, **Haws MC**, **Lerner DT**, **Grau EG**, **Seale AP**. Acute salinity tolerance and the control of two prolactins and their receptors in the Nile tilapia (*Oreochromis niloticus*) and Mozambique tilapia (*O. mossambicus*): A comparative study. *Gen Comp Endocrinol* 257: 168–176, 2018. doi: 10.1016/j.ygcen.2017.06.018.

73. **Esensten JH**, **Tsytsykova AV**, **Lopez-Rodriguez C**, **Ligeiro FA**, **Rao A**, **Goldfeld AE**. NFAT5 binds to the TNF promoter distinctly from NFATp, c, 3 and 4, and activates TNF transcription during hypertonic stress alone. *Nucleic Acids Res* 33: 3845–3854, 2005. doi: 10.1093/nar/gki701.

74. **Lopez-Rodríguez C**, **Aramburu J**, **Rakeman AS**, **Rao A**. NFAT5, a constitutively nuclear NFAT protein that does not cooperate with Fos and Jun. *Proc Natl Acad Sci U S A* 96: 7214–7219, 1999. doi: 10.1073/pnas.96.13.7214.

75. **Li S-Z**, **McDill BW**, **Kovach PA**, **Ding L**, **Go WY**, **Ho SN**, **Chen F**. Calcineurin-NFATc signaling pathway regulates AQP2 expression in response to calcium signals and osmotic stress. *Am J Physiol Cell Physiol* 292: C1606-1616, 2007. doi: 10.1152/ajpcell.00588.2005.

76. **Raat NJ**, **van Os CH**, **Bindels RJ**. Effects of osmotic perturbation on [Ca2+]i and pHi in rabbit proximal tubular cells in primary culture. *Am J Physiol* 269: F205-211, 1995. doi: 10.1152/ajprenal.1995.269.2.F205.

77. **Erickson GR**, **Alexopoulos LG**, **Guilak F**. Hyper-osmotic stress induces volume change and calcium transients in chondrocytes by transmembrane, phospholipid, and G-protein pathways. *J Biomech* 34: 1527–1535, 2001. doi: 10.1016/S0021-9290(01)00156-7.

78. **Apostol S**, **Ursu D**, **Lehmann-Horn F**, **Melzer W**. Local calcium signals induced by hyper-osmotic stress in mammalian skeletal muscle cells. *J Muscle Res Cell Motil* 30: 97–109, 2009. doi: 10.1007/s10974-009-9179-8.

79. **Ma A**, **Cui W**, **Wang X**, **Zhang W**, **Liu Z**, **Zhang J**, **Zhao T**. Osmoregulation by the myo-inositol biosynthesis pathway in turbot Scophthalmus maximus and its regulation by anabolite and c-Myc. *Comp Biochem Physiol A Mol Integr Physiol* 242: 110636, 2020. doi: 10.1016/j.cbpa.2019.110636.

80. **Fiol DF**, **Chan SY**, **Kültz D**. Regulation of osmotic stress transcription factor 1 (Ostf1) in tilapia(*Oreochromis mossambicus*) gill epithelium during salinity stress. *J Exp Biol* 209: 3257–3265, 2006. doi: 10.1242/jeb.02352.

81. **Wong MK-S**, **Ozaki H**, **Suzuki Y**, **Iwasaki W**, **Takei Y**. Discovery of osmotic sensitive transcription factors in fish intestine via a transcriptomic approach. *BMC Genom* 15: 1134, 2014. doi: 10.1186/1471-2164-15-1134.

82. **Herbelet S**, **De Vlieghere E**, **Gonçalves A**, **De Paepe B**, **Schmidt K**, **Nys E**, **Weynants L**, **Weis J**, **Van Peer G**, **Vandesompele J**, **Schmidt J**, **De Wever O**, **De Bleecker JL**. Localization and Expression of Nuclear Factor of Activated T-Cells 5 in Myoblasts Exposed to Pro-inflammatory Cytokines or

Hyperosmolar Stress and in Biopsies from Myositis Patients. *Front Physiol* 9: 126, 2018. doi: 10.3389/fphys.2018.00126.

83. **Kumar R**, **DuMond JF**, **Khan SH**, **Thompson EB**, **He Y**, **Burg MB**, **Ferraris JD**. NFAT5, which protects against hypertonicity, is activated by that stress via structuring of its intrinsically disordered domain. *Proc Natl Acad Sci U S A* 117: 20292–20297, 2020. doi: 10.1073/pnas.1911680117.

General Conclusions

In summary, the objective of this work was to further characterize mechanisms of euryhaline fish salinity tolerance using an *O. mossamicus* tilapia cell line model. The *myo*-inositol biosynthesis (MIB) pathway enzymes (MIPS and IMPA1.1) and NFAT5 transcription factor were targeted based on previous work indicating these proteins as having high importance in salinity tolerance phenotypes. The chosen methodology to perform these evaluations was molecular manipulations, predominantly using CRISPR/Cas9, to alter the abundance or function of these proteins. In combination with subsequent phenotyping assays, establishing causality between the genes encoding the proteins and salinity tolerance related phenotypes was pursued. Execution of this objective was achieved through three aims: Aim 1) development of a CRISPR/Cas9 system that functions proficiently in tilapia cells to generate gene knockout versions of the OmB cell line for MIPS, IMPA1.1, and NFAT5; Aim 2) perform assays quantifying physiological performance of MIPS and IMPA1.1 KO lines under hyper-osmotic (HO) challenge; and Aim 3) perform assays quantifying regulation and abundance of HO responsive gene products, in this case MIPS and IMPA1.1, in NFAT5 KO lines.

The overriding conclusion from aim 1 is that vector-based platforms for CRISPR/Cas9 delivery can be highly proficient in non-model organism cells such as *O. mossambicus* tilapia when using species specific endogenous strong promoters for expression of the components. This is especially important when using a polymerase III promoter such as a U6 for gRNA production, as human and zebrafish U6 promoters used in other validated CRISPR/Cas9 systems showed negligible editing in the tilapia OmB cell line. The CRISPR/Cas9 system developed in this work using constitutive Cas9 and transient gRNA expression by the *O. mossambicus* EF1 alpha and U6 promoters respectively combined with hygromycin selection achieved very high editing efficiencies with the majority of alleles receiving mutations. This allowed proficient generation of target gene edited cells. A potential consequence of such high

efficiency is occurrence of unintended off-target genome altering events. Notable variability in phenotype assessments were observed in isolated KO cell lines of the same target gene. However, anticipation of this potential using a robust experimental design including replicate clonal lines obtained from different gRNAs for both target and control genes, allowed phenotypes consistent to the target gene to be quantified.

This CRISPR/Cas9 system and experimental design was applied to the MIB pathway enzymes and their hypothesized transcriptional regulator NFAT5 generating multiple KO cell lines for all genes. Relative to control lines, disruption if both MIPS and IMPA1.1 genes resulted in notably increased growth rates in basal iso-osmotic media. In HO conditions, significantly decreased metabolic activity but a moderate non-significant trend of reduced survival was observed for both MIB KO groups with the lowest survival rate observed in MIPS KO lines. It is the conventional belief that the end product of these enzymes, myo-inositol (MI), primarily serves as an inert osmolyte to relieve osmotic pressure by balancing osmolarity across the cell membrane in conditions of elevated extra cellular fluid osmolarity. However these results lead to the conclusions that MI plays an equal or greater role in metabolic processing and as a negative growth regulator in conditions of cellular HO stress. Furthermore, survival of the HO experimental condition is supported by multiple concerted mechanisms.

The NFAT5 KO lines were generated to test the contribution of NFAT5 in transcriptional regulation of the MIB pathway. Quantification of HO induced MIPS and IMPA1.1 transcription by qRT-PCR showed a reduction close to half for IMPA1.1 but a more moderate effect for MIPS. This evidence was reinforced with supplementary experiments using ectopic expression of dominant negative and wild-type versions of NFAT5 which both demonstrated clear interaction with the IMPA1.1 promoter but again an effect of less than 50% was observed. Although a contribution of NFAT5 seems clear, significant transcription of both IMPA1.1 and MIPS is evident despite disrupted NFAT5 indicating the presence of other strong HO regulators.

This work has extended understanding MI's role in cellular HO stress, but this was potentially limited by compensation with alternative osmolytes and exogenous MI sources. Increased understanding of this mechanism can be achieved in future studies manipulating the pathways that produce these other osmolytes, MI transporters, or the media composition of MI and other osmolytes. The work with NFAT5 confirmed suspicions it was an MIB pathway HO regulator, but the results indicate a much more extensive HO regulatory network exists. With the newly developed cell lines and MIB reporters, there is great opportunity for more extensive exploration of HO signaling in euryhaline fish including transcriptomic or proteomic screens for other NFAT5 regulated genes, targeting of candidate upstream regulators of NFAT5, and examination of other regulators interacting with MIB enzyme promoters. Although the cell line work has provided important mechanistic insights on the functional roles of these proteins, the studied cells are removed from the complete complex system representing their natural state. This puts limitations on interpretation outside the context of the whole organism. Future work should include repeating these genomic manipulations in tilapia embryos to provide a better picture of how these proteins function in the complete systemic physiology of adult animals.

Overall, this work has generated new gene molecular tools for use in tilapia cells and provided insights to important biological questions related to osmoregulation in euryhaline fish. Tilapia customized genetic manipulation systems were developed, critical elements to consider when developing such tools in a non-model organism were identified, and appropriate experimental design to achieve findings specific to the target genes in question were established. This work strongly indicates involvement of MI and the MIB pathway in metabolic processes and cell cycle regulation during HO stress, but the pathway is not critical for survival of cultured tilapia cells in the experimental HO challenge condition. Activation of NFAT5 signaling has been demonstrated in HO conditions with a clear but partial role in regulation of at least IMPA1.1 of the MIB pathway. These results uphold a combinatorial nature of both effector (MIB enzymes) and regulatory (NFAT5) mechanisms of HO stress response in tilapia cells.

Although the MIB pathway and NFAT5 have been validated as major components of tilapia cell HO response, other parallel and compensatory mechanisms exist supporting survival and signaling in HO stress.